

**Studying fast dynamics in biological complexes:  
From photosynthesis *in vivo* to single DNA  
molecules *in vitro***

***Shazia Farooq***

## **Thesis committee**

### **Promotors**

Prof. Dr H. van Amerongen  
Professor of Biophysics  
Wageningen University & Research

### **Co-promotor**

Dr J. Hohlbein  
Assistant professor, Laboratory of Biophysics  
Wageningen University & Research

### **Other members**

Prof. Dr S. de Vries, Wageningen University & Research  
Prof. Dr T. M. Cordes, University of Groningen  
Prof. Dr T. J. Aartsma, Leiden University  
Dr C. Duffy, Queen Mary University of London, UK

This research was conducted under the auspices of the Graduate School  
Experimental Plant Science.

**Studying fast dynamics in biological complexes:  
From photosynthesis *in vivo* to single DNA  
molecules *in vitro***

***Shazia Farooq***

**Thesis**

submitted in fulfilment of the requirements for the degree of doctor  
at Wageningen University

by the authority of the Rector Magnificus,

Prof. Dr A.P.J. Mol,

in the presence of the

Thesis Committee appointed by the Academic Board

to be defended in public

on Tuesday 14 March 2017

at 4 p.m. in the Aula.

Shazia Farooq

Studying fast dynamics in biological complexes: From photosynthesis *in vivo* to  
single DNA molecules *in vitro*,

149 pages.

PhD thesis, Wageningen University, Wageningen, the Netherlands (2017)

With references, with summary in English

ISBN: 978-94-6343-100-2

DOI: 10.18174/406016

The research described in this thesis was financially supported by Foundation for Fundamental Research on Matter (**FOM**).



# Table of Contents

<b>CHAPTER 1</b>	<b>1</b>
<i>Introduction</i>	<i>1</i>
 <b>CHAPTER 2</b>	 <b>27</b>
<i>Studying DNA–protein interactions with single-molecule Förster resonance energy transfer</i>	<i>27</i>
 <b>CHAPTER 3</b>	 <b>61</b>
<i>Improving the time resolution in single-molecule FRET TIRF microscopy by combining stroboscopic alternating-laser excitation with dynamic probability distribution analysis</i>	<i>61</i>
 <b>CHAPTER 4</b>	 <b>91</b>
<i>Is there Excitation Energy Transfer between Different Layers of Stacked Photosystem-II-containing Thylakoid membranes?</i>	<i>91</i>
 <b>CHAPTER 5</b>	 <b>105</b>
<i>Monitoring non-photochemical quenching in leaves with ultrafast fluorescence measurements</i>	<i>105</i>
 <b>CHAPTER 6</b>	 <b>129</b>
<i>General Discussion</i>	<i>129</i>
 <b>CHAPTER 7</b>	 <b>143</b>
<i>Summary</i>	<i>143</i>





# **CHAPTER 1**

## **Introduction**

### **Background and aim**

During the last decades, fluorescence spectroscopy has emerged as a powerful tool in the fields of biophysics, biotechnology, biochemistry, cellular biology and the medical sciences. These techniques are highly sensitive, and allow us to study the structure and dynamics of (bio)molecular systems (Valeur 2001). A significant advantage of fluorescence techniques is that they can often be non-invasive and measurements can be performed in real time. In this thesis different advanced fluorescence methods will be used to study two important biological processes: (1) DNA dynamics and (2) plant photosynthesis. In the first part, conformational changes in DNA were investigated using single-molecule Förster Resonance Energy Transfer (smFRET). A new excitation and data analysis framework is introduced allowing the detection of single-molecule fluorescence with unprecedented throughput and time resolution. In the second part, picosecond time-resolved fluorescence spectroscopy was used to study ultrafast processes in photosynthesis such as excitation energy transfer and non-photochemical quenching (NPQ) on the ensemble level.

Photosynthesis is a process in which light energy is captured by a network of pigment-protein complexes and converted into chemical energy (Blankenship 2002, Govindjee. 2005). This energy conversion process requires interaction between different pigment proteins. The crystal structures of many of these photosynthetic pigment-protein complexes have been resolved and investigated (Guskov et al. 2009, Liu et al. 2004, Wei et al. 2016, Yan et al. 2007). Taken together with experimental results using ultrafast spectroscopic techniques, extensive knowledge about the organization and composition of these pigments in thylakoid membranes has been gained highlighting where light absorption, energy transfer and charge separation takes place. Ultrafast spectroscopy is an important experimental technique to characterize these highly efficient processes and identify the important constituents of photosynthetic machinery (Miloslavina et al. 2009, van Oort et al. 2009, Wientjes et al. 2013). In Chapter 4 and 5, we investigated in great detail the ultrafast processes in photosynthetic complexes such as excitation energy transfer (EET) and non-photochemical quenching (NPQ) by using picosecond time-resolved spectroscopy.

Even though conventional spectroscopic techniques are useful in following ultrafast photoinduced events in photosynthesis, they are typically performed on bulk samples. Thus, when structural inhomogeneity of the sample is involved, the information of individual species is lost due to the inevitable ensemble- and time-averaging effects. With the advent of single-molecule techniques, researchers are

enabling to characterize the individual pigment–protein complexes to build up the distribution of behaviors. In recent years, several photosynthetic antenna complexes including major light-harvesting complex II (LHCII) (Tietz et al. 2001) of higher plants and light-harvesting complex 2 (LH2) (Bopp et al. 1997, Richter et al. 2007) from purple bacteria have been studied at a single molecular level to explore the structural heterogeneity. In the case of LHCII, many interesting effects have been observed such as the fluorescence intermittency, spectral diffusion, rapid shifting of the fluorescence emission characteristics (Krüger et al. 2012, Krüger et al. 2011, Krüger et al. 2010, Tietz et al. 2001). In many cases fluorescence intermittency (blinking) was also observed which could be connected to regulated energy dissipation, i.e. non-photochemical quenching (NPQ) (Krüger et al. 2011). After introducing single-molecule fluorescence techniques to study DNA-protein interactions in Chapter 2, Chapter 3 continues with work on technical aspect of improving the time resolution of camera-based single molecule FRET technique by combining the concept of *alternating-laser excitation* (ALEX) (Hohlbein et al. 2014b, Kapanidis et al. 2004, Laurence et al. 2005, Lee et al. 2005, Muller et al. 2005) with *stroboscopic illumination* (Blumberg et al. 2005, Elf et al. 2007, Flors et al. 2007). The potential of stroboscopic alternating-laser excitation (sALEX) is then experimentally demonstrated by studying the dynamic system of an interconverting doubly labeled DNA hairpin at different salt concentrations (0-1 M). In future, this system might be suitable to study how molecular conformation affects the photophysics of individual pigment-protein complex with high throughput and high time resolution.

This chapter will provide an introduction to fluorescence spectroscopy, including some basic theory of fluorescence and various detection techniques as well as the general mechanism of photosynthesis. However, a detailed introduction to the single-molecule FRET technique and the underlying biology relevant for the work on DNA can be found in Chapter 2.

## Introduction

### The physical basis of fluorescence

A schematic description of the electronic states of a molecule and the transitions between them is often provided in the form of a Jablonski diagram (Figure 1) (Jabłoński 1935).

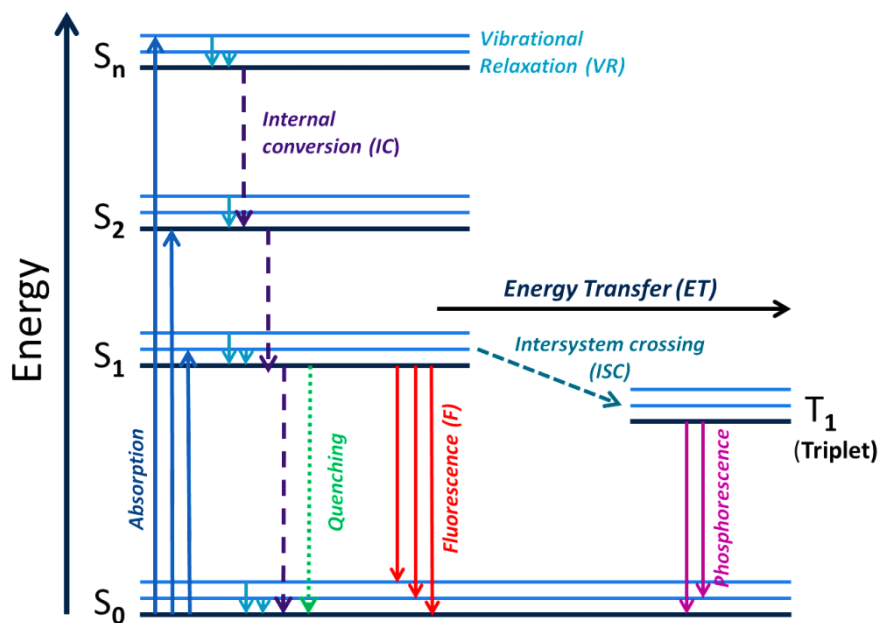


Figure 1: The Jablonski energy diagram illustrating different processes that can occur after excitation of a molecule. Light absorption and emission are represented by solid arrows whereas vibrational relaxation (VR), quenching, internal conversion (IC) and intersystem crossing (ISC) is given by dashed arrows.

If a photon has the energy that corresponds to the energy difference between the ground state and an excited state of the molecule, it might be absorbed and it leads to a transition from the ground state ( $S_0$ ) to the excited state ( $S_n$ ). This excited state typically exists for 1-10 nanoseconds. During this time the excited molecule rapidly ( $10^{-13}$ s) relaxes down non-radiatively to the lowest excited state level ( $S_1$ ) by several vibrational relaxations (VR) and internal conversion (IC) processes. From here, the de-excitation of the molecule to the  $S_0$  ground state can occur through the emission of a photon fluorescence. Because of the rapid relaxation to the  $S_1$  state fluorescence emission spectra are usually independent of the excitation wavelength. This is known as Kasha's rule (Kasha 1950). Since the molecule loses some energy in the

non-radiative relaxation process, the fluorescence will have a lower energy i.e. longer wavelength than the incoming photon.

Other de-excitation pathways from the  $S_1$  state are a transition to a triplet state by intersystem crossing (ISC). From the triplet state, the molecule can return to the ground state through internal conversion (non-radiatively) or by the emission of a photon (phosphorescence).

If there is another molecule nearby then there may be another relaxation pathway. The excited state energy of a donor fluorophore can be transferred to an acceptor molecule non-radiatively via dipole-dipole interaction. This process is called Förster resonance energy transfer (FRET) (Förster 1948). This path is not shown in the figure. For FRET the extent of energy transfer depends on the distance between the donor and acceptor (1-10nm) fluorophore and the spectral overlap of donor emission spectra and acceptor absorption spectra. This topic will be discussed in detail in chapter 2.

## Fluorescence lifetime and quantum yield

The fluorescence lifetime and quantum yield are important characteristics of a fluorophore. The quantum yield is defined as the number of photons emitted divided by the number of photons absorbed and is given as:

$\Phi_F = \# \text{ photons emitted} / \# \text{ photons absorbed}$ , or given as a function of radiative ( $k_r$ ), non-radiative ( $k_{nr}$ ) and energy transfer ( $k_{ET}$ ) rate constants:

$$\Phi_F = \frac{k_r}{k_r + k_{nr} + k_{ET}} = k_r * \tau$$

where the lifetime ( $\tau$ ), the average time a molecule spends in the excited state before it returns to the ground state, is given as:

$$\tau = \frac{1}{k_r + k_{nr} + k_{ET}}$$

The fluorescence lifetime (which is an exponential decay time) of a molecule is strongly affected by the environment, for example, the solvent polarity, refractive index, the proximity or the concentration of quenching species (Borst et al. 2005, Lakowicz 2006, Valeur 2001). Time-resolved fluorescence spectroscopy can be used to provide the information on rate constants of various processes in complex systems as (Jameson et al. 2003, van Oort et al. 2009, Visser et al. 2005) shown in figure 1.

### **Steady-state and time-resolved Fluorescence**

Fluorescence measurements can be categorized into two types: steady state and time resolved. In steady state experiments the sample is illuminated continuously with a light source, and the emission spectrum or intensity is recorded. In time-resolved measurements the sample is exposed to a short laser pulse, where the pulse width is shorter than the decay time of the sample. Time-resolve measurements are usually used to measure intensity and anisotropy decay as a function of time. Since steady state provides an average of time resolved measurements over the intensity decay, most of the information of kinetics is lost during the temporal averaging process. In photosynthetic complexes, processes like charge separation, energy transfer and non-photochemical quenching (NPQ) occurs very fast (on the ps to ns time scale). Thus, in this thesis, time-resolve fluorescence techniques are used to provide functional and quantitative information about these fast processes within photosynthetic complexes. The steady state single molecule technique to study conformational changes in DNA will be discussed in chapter 2.

### **Single-molecule Detection**

Single-molecule detection (SMD) methods allow studying the properties of single molecules and providing information about their molecular dynamics, interactions, and fluctuations over time and space. The main advantage of SMD over other detection techniques is that it avoids ensemble averaging, where most of the kinetic information is lost due to sample heterogeneity. Typical instruments for SMD consist of (1) a laser excitation source passing through a microscope objective, (2) a scanning stage to move the sample and (3) a total internal reflection (TIR) or confocal optics to reject unwanted signals. This technique becomes more powerful when combined with the Förster resonance energy transfer (FRET) technique. For more detail about this topic see chapter 2.

### **Methods and Instruments for Time-resolved Fluorescence**

There are two main approaches for measuring time-resolved fluorescence, frequency-domain and time-domain fluorescence.

In the frequency-domain method, the sample is excited by an intensity-modulated source of light. The emission is measured at the same modulation frequency as the excitation. The emission is delayed in time relative to the excitation time and this delay is measured as a phase shift, which can be used to calculate the lifetime.

Because only time-domain methods were used for the work described in this thesis, no further description of frequency domain method will be discussed here.

In the time-domain method, the sample is excited by a short pulse of light. The width of the excitation pulse is much shorter than the lifetime ( $\tau$ ) of the fluorophore. The fluorescence intensity is then recorded as a function of time, on a picosecond to nanosecond timescale.

For further principles, applications and details on time-domain and frequency-domain methods see (Lakowicz 1999, Valeur 2001). Data described in this thesis were obtained by using a streak camera and time-correlated single-photon counting (TCSPC). Both methods are time-domain techniques and require excitation of the sample with a short light pulse followed by measuring the fluorescence intensity as a function of time.

## **Time-Correlated Single Photon Counting (TCSPC)**

Time-correlated single-photon counting (TCSPC) (Birch and Imhof 1999, Lakowicz 1999, O'Connor and Phillips 1984, Valeur 2001) is based on measuring the time delay between a reference signal and a photon arriving at a detector (figure). A TCSPC measurement requires several repetitive excitations to detect single photons. The repetitive measurements allow to buildup a histogram of the measured time delay (Karolczak et al. 2001, Lakowicz 2006). In the TCSPC setup that has been used for this thesis, the excitation pulses were generated by a mode locked Ti:Sapphire laser, which was tuned to 800nm. The pump laser was a continuous wave (CW) diode pumped, frequency doubled Nd:YVO<sub>4</sub> laser. The laser repetition rate of 76 MHz was decreased to 3.8 MHz with a pulse picker and the pulses were frequency doubled, leading to vertically polarized 400 nm excitation pulses. The fluorescence was detected at 90° with respect to excitation light via band-pass filters using parallel or perpendicular polarization orientations. To detect decay traces at various detection wavelengths, different interference filters were used. The samples were measured in a 3 mm quartz cuvette, placed in a temperature controlled sample holder.

A short laser pulse excites the sample, one small part of this excitation pulse energy is sent to a fast photodiode, whose output is sent to one channel of a constant fraction discriminator (CFD) to generate an electronic pulse to stop a time-to-amplitude converter (TAC). The excitation pulse is fed via a microchannel plate photomultiplier tube (MC-PMT) into another channel of the CFD, which sends a start signal to the TAC. After a “start” signal due to the photon detection, the “stop” signal will arrive with a fixed delay after the excitation pulse. The output

## Introduction

pulse of the TAC is converted to a numerical value by an analogue to digital converter (ADC). The channel time spacing was typically set to 2.0 or 5.0 ps.

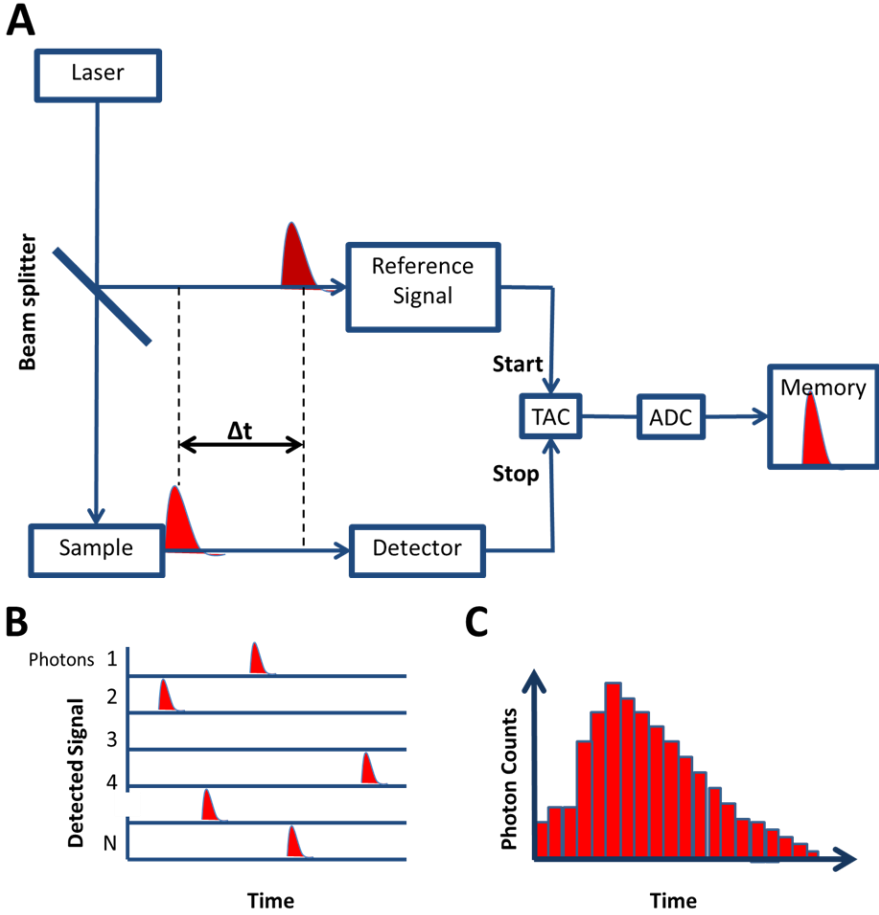


Figure 2: The schematics for the Time-correlated single photon counting (TCSPC). (A) The time-to-amplitude converter (TAC) measures the time delay  $\Delta t$  between a reference signal and a photon arriving at a detector. The time is converted to voltage which is sent to multi-channel analyser (MCA) where it is converted from an analogue to a digital signal. (B) Represent the output from the constant fraction discriminator (CFD). (C) The histogram of the photon arrival time represents the fluorescence decay curve.

To avoid “pile up error” due to multi-photon detection, the probability of detecting a photon per laser pulse should be kept below 1%. In our setup, this criterion was achieved by reducing the energy of the excitation pulses with neutral density filters to obtain a detection count rate of 30,000 per second (<1% of 3.8 MHz) (Vos



et al. 1987). Also, other instrumental sources for distortion of data such as TAC and ADC (non-)linearity, laser mode locking were minimized (van Hoek and Visser 1985). The instrument response function (IRF) of the setup is measured via the fast exponential decay of a fluorescent dye. Data was analysed with home built software (Digris et al 1999).

## **Streak Camera**

Another method to measure time resolve fluorescence applied in this thesis uses detection with a synchroscan streak camera system. The main advantage of this method compared to TCSPC is its ability to record simultaneously the photon's wavelength and its arrival time, allowing to measure the temporal evolution of entire fluorescence spectrum on the ps to ns time scale rather than measuring the fluorescence decay at a single wavelength (Schiller and Alfano 1980). This method is very useful when studying samples such as photosynthetic complexes, which usually contain fluorophores emitting at different wavelengths. Moreover, it has a better time resolution than that of TCSPC, as the width of the instrument response function (IRF) of the streak camera is typically 10-15 ps instead of 50-60 ps of the TCSPC setup. On the other hand, the disadvantage of streak camera is the relatively low sensitivity.

The laser excitation induces fluorescence photons which are focused by an objective into a spectrograph, where they are deflected in the horizontal direction by the grating. Then the photons hit the photocathode, producing photo-electrons. The photo-electrons are then accelerated by an electrostatic field and then deflected in the vertical direction by a periodical sweep field. These photo-electrons are then imaged by a 2D detector which consists of a micro channel plate (MCP), a phosphor screen and a CCD detector. The photo electron generated at different time experience different deflection fields and hits the MCP at different vertical positions.

We have used a photon counting streak camera (PCSC) for our experiments. PCSC works similar to streak camera as described above except for the detection part. PCSC counts the pulses which are recorded by a CCD camera on the phosphor screen. The software examines the size of the pulse and accept only those pulses that are above defined threshold. There is no "dead time" because the photons are spread in space across the photocathode. This means more than one photon can be detected for each laser pulse. Inaccuracy in measurement occurs only if the photons overlap in space and time on the phosphor screen.

## Introduction

In the streak camera (PCSC) setup that has been used in this thesis, the short laser pulses of about 200 fs duration were generated by a mode locked Ti:Sapphire laser, which was tuned to 800nm at a repetition rate of 76MHz. A small portion of the laser output was used for synchronization with the sweep field of the streak camera; while the major part was sent to the regenerative amplifier (RegA), where the repetition rate was decreased to 4 MHz. The laser pulse was then directed to an

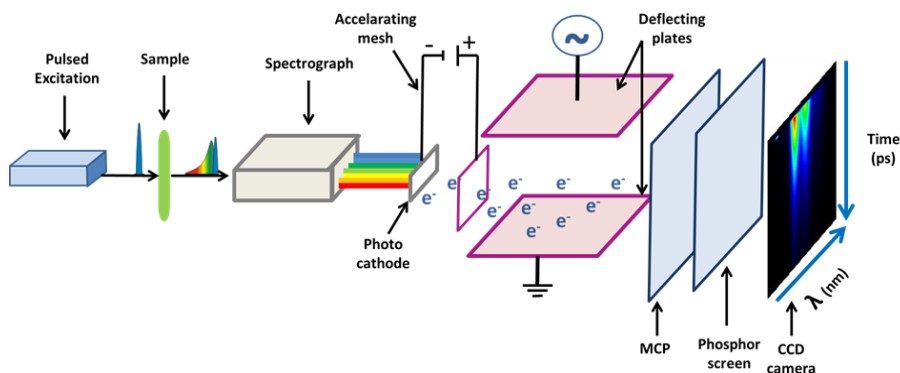


Figure 3: The schematics representation of a streak camera setup, consisting of a spectrograph, photocathode, accelerating mesh, sweep circuit, micro-channel plate (MCP), phosphor screen and CCD camera.

optical parameter amplifier (OPA), where the beam was split into two parts. The first part of it was frequency doubled, which was used for creating vertically polarized 400nm excitation, while the second part was used to generate white light source. For more details see (Van Stokkum et al. 2008).

## PHOTOSYNTHESIS

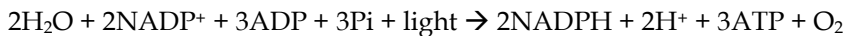
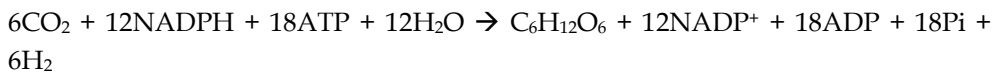
In this thesis, ultrafast fluorescence spectroscopy is used to study the first steps of photosynthesis. Photosynthesis is the process of transformation of solar light energy into chemical energy in many living organisms (Govindjee. 2005, Blankenship 2002). Photosynthesis is one of the fundamentally required processes for the existence of life on earth. It not only provides us with oxygen and fossil fuels but it is also responsible for feeding life on earth (Nelson and Ben-Shem 2004), For a better utilization of solar energy in photosynthesis, one must have a better understanding regarding structure, organization, and functioning of the photosynthetic apparatus and its inherent processes.

In this section, I will briefly explain the process of photosynthesis, the main machinery involved in oxygenic photosynthesis (i.e. light-harvesting and other

pigment-protein complexes) and the photoprotective mechanism called non-photochemical quenching employed by plants.

In most plants and algae, photosynthetic organisms are located in special cell compartments (organelles) called chloroplasts. Chloroplasts in land plants are usually 5-8  $\mu\text{m}$  in diameter and 1-3  $\mu\text{m}$  thick (Wise and Hooper 2007). The chloroplast is filled with a highly structured network of an interconnected membrane called the “thylakoid membrane”.

In general, two types of photosynthetic reactions occur in chloroplasts, the *light reactions* (light driven) and the *dark reactions*. Light reactions mainly take place inside the thylakoid membrane and lead to the production of NADPH and ATP which are both required to drive the *dark reactions* of the Calvin-Benson-Basham-cycle (Benson and Calvin 1950), which is responsible for the  $\text{CO}_2$  reduction into sugar. These reactions can be summarized (Raven et al. 2005) as follows:

**Light reactions:****Dark reactions:**

There are four main pigment-protein complexes involved in the light reactions that are embedded in the thylakoid membrane: (1) photosystem II (PSII), causing water splitting; (2) photosystem I (PSI), causing  $\text{NADP}^+$  reduction; (3) ATP synthase that produces ATP; (4) and the cytochrome (cyt) *b<sub>6</sub>f* complex, which mediates electron transport between PS II and PS I (Dekker and Boekema 2005, Nelson and Ben-Shem 2004, Staehelin 2003)

The thylakoid consists of stacked and unstacked regions, known as *grana* and *stroma lamellae*, respectively. In the thylakoid membranes, the pigment-protein complexes are distributed unevenly. PS I and ATP synthase reside mainly in the stroma lamellae whereas PS II is found in the stacked grana, and the cyt *b<sub>6</sub>f* complex is suggested to be located both in grana and stroma lamellae (Albertsson 2001, Dekker and Boekema 2005, Nelson and Ben-Shem 2004, Staehelin 2003, Trissl and Wilhelm 1993).

The light reactions of photosynthesis occur when sunlight is absorbed by the chlorophylls, mainly located in the light-harvesting antennas of PSI and PSII,

## Introduction

which are also involved in photo-protection in high-light conditions (Horton et al. 1996). Part of the absorbed energy is then transferred to the PSI and PSII core, where charge separation (CS) takes place in the reaction centres of PSI and PSII. The electron released from PSII is replaced by electrons that become available during water splitting. These electrons are then shuttled to PSI via an electron transfer chain (plastoquinone, plastoquinol, cyt  $b_6f$ , and plastocyanin) as shown in Figure 4.

The water splitting, which takes place in the oxygen evolving complex (OEC), produces oxygen as by-product and protons, which are accumulated on the luminal side of the thylakoid, thus creating a proton gradient across the membrane. This gradient drives ATP production by the ATP-synthase. Meanwhile, the electrons that are released by the PSI reaction centre due to light driven charge separation are used to reduce  $\text{NADP}^+$  into NADPH through ferredoxin (Fd) and ferredoxin-NADP $^+$ -reductase (FNR).

## Light-Harvesting Pigments

The two main types of photosynthetic pigments in higher plants are chlorophylls and carotenoids. The main function of these pigments is the absorption of light, excitation energy transfer between the pigments, the first charge-separation steps and protection in high-light conditions.

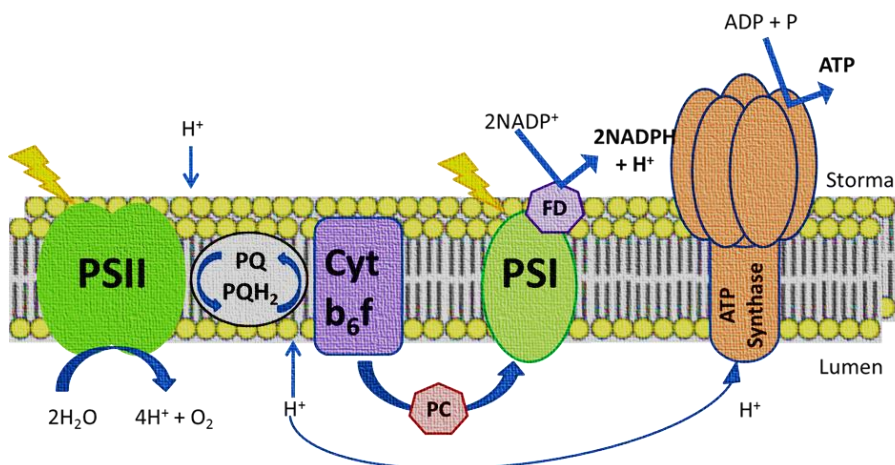


Figure 4: Simplified model of the electron transfer pathway in oxygenic photosynthesis, with main photosynthetic complexes, including Photosystem II (PSII), Photosystem I (PSI), cytochrome (Cyt  $b_6f$ ), ATP synthase, plastocyanin (PC), ferredoxin (FD). Whereas, electron and proton flows are indicated by arrows.

## Chlorophylls

A chlorophyll (Chl) consists of a porphyrin (cyclic tetrapyrrole) ring, that binds a magnesium (Mg) atom in the centre (see Figure 5). A fifth ring and a long phytol chain are responsible for binding to a protein via hydrophobic interactions. Chls are capable of absorbing light in the visible region due to a network of conjugated double bonds. There are several different forms of Chl present in nature, that can be distinguished from their substitutions. In higher plants two type of chlorophyll are present: Chl *a* and Chl *b*. Chl *a* and Chl *b* differ only in a substituent in the second pyrrole ring i.e. methyl in Chl *a* and an aldehyde for Chl *b*. Chl *a* and Chl *b* have two strong absorption bands: the Soret [B] and Q band, with high extinction coefficient ( $\sim 10^5 \text{ cm}^{-1} \text{ M}^{-1}$ ) in the visible region of the spectrum. In the higher energy (blue) region of the spectrum, an absorption band appears due to the Soret transitions.

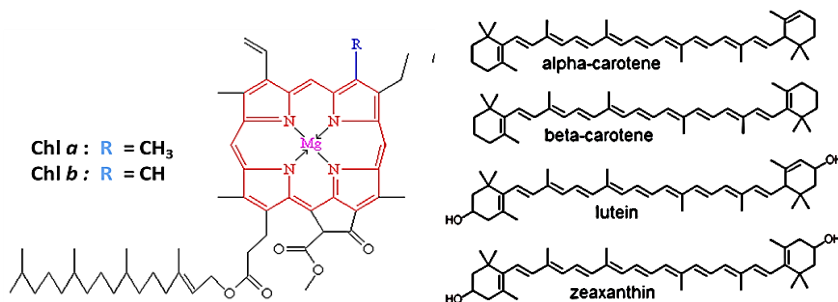


Figure 5: Chemical structure of photosynthetic pigments: chlorophyll *a* and *b*(left) and carotenoid (right). The porphyrin ring in chlorophylls is shown in red.

The maxima of the Soret band is around 430 nm for Chl *a* and 460 nm for Chl *b*. The red-most band represents the Q<sub>y</sub> transition to the lowest energy region of the absorption spectra, and peaks are observed around 670 nm for Chl *a* and 640 nm for Chl *b*. A weak Q<sub>x</sub> transition which appears around 580-640 nm is masked by the Q<sub>y</sub> vibronic bands. The strong absorption of both the red and blue but not the green region of the visible spectrum by Chls is the reason for the green colour of many plants. The absorption spectra of Chl *a* and Chl *b* do not completely overlap, and therefore light is absorbed over a wider spectral range when compared to for instance Chl *a*, which increases the efficiency of light-harvesting.

## Carotenoids

## **Introduction**

Carotenoids (Cars) are pigments that occur in many photosynthetic organisms. Carotenoids are isoprenoid molecules that belong to the tetraterpenoids (i.e. contain 40 carbon atoms) group. They can be different in length, ring type, and isomeric form. Cars are divided into two groups: **Xanthophylls** contain oxygen (e.g. lutein, neoxanthin, violaxanthin and zeaxanthin), and are mostly found in light-harvesting antenna complexes. **Carotenes** are oxygen free and only consist of carbon and hydrogen atoms (e.g.  $\alpha$  or  $\beta$ -carotenes). They are mostly bound to core complexes of PSI and PSII.

Cars play multiple important roles in the photosynthesis. They can absorb light energy in the spectral region in which Chls do not absorb and then transfer this energy to the Chls (Mimuro and Katoh 1991). They also play an essential role in structural stabilization and assembly of photosynthetic protein complexes (Paulsen et al. 1993, Plumley and Schmidt 1987). However, their most important role is protecting photosynthetic systems against oxygenic photodamage, as they are able to quench the Chl triplets state directly due to their very low triplet energy levels and can deactivate the resulting reactive oxygen species, i.e. singlet oxygen (Peterman et al. 1997), by converting the excess energy into heat.

## **Pigment-Protein Complexes**

PSI and PSII are two large pigment-protein complexes, where light absorption and charge separation occur (Croce and van Amerongen 2013, van Amerongen and Croce 2013, van Amerongen and Dekker 2003). Photosystems I and II are different in structure, function and compositions, but they both consist of a core complex that is responsible for charge separation and peripheral light-harvesting antenna complexes (containing Chls and Cars) that are responsible for absorption of light and transferring excitation energy to the reaction centres.

## **PHOTOSYSTEM I**

In higher plants, Photosystem I (PSI) is present as a monomeric supramolecular pigment-protein complex. The PSI core and outer light-harvesting antennae (LHCI) create two distinct moieties. Four LHCI (Lhca1-4) which are major components of the PSI antenna complex are arranged as two heterodimers organised in a form of a half-moon-shaped belt (Amunts et al. 2007, Mazor et al. 2015, Morosinotto et al. 2005). The PSI core complex contains 168 Chls, 2 phylloquinones, 3 Fe4S4 clusters and approx. 20 Cars (Amunts et al. 2007, Amunts et al. 2010). PSI complexes are extremely efficient as they exhibit a quantum yield of near unity (Trissl and Wilhelm 1993). That means almost every single photon absorbed by the PSI

complex is used to drive electron transport. The electron transport chain of the RC is coordinated by the two major protein subunits of the PSI core, PsaA and PsaB. They bind the primary electron donor P700 of PSI, the primary electron acceptor A<sub>0</sub> (also Chl *a*), the secondary acceptor A<sub>1</sub>, (a phylloquinone) and 4Fe-4S clusters.

Additional to the bulk antenna Chls PSI also contains long-wavelength “red” Chl *a* molecules (Morosinotto et al. 2005, Wientjes et al. 2012). These red pigments affect the trapping rate in PSI, thus affecting PSI spectral properties (Slavov et al. 2008). These red Chls are present in both core and LHCI but in plants, they are mainly found in the antenna complexes (Mullet et al. 1980, Slavov et al. 2008).

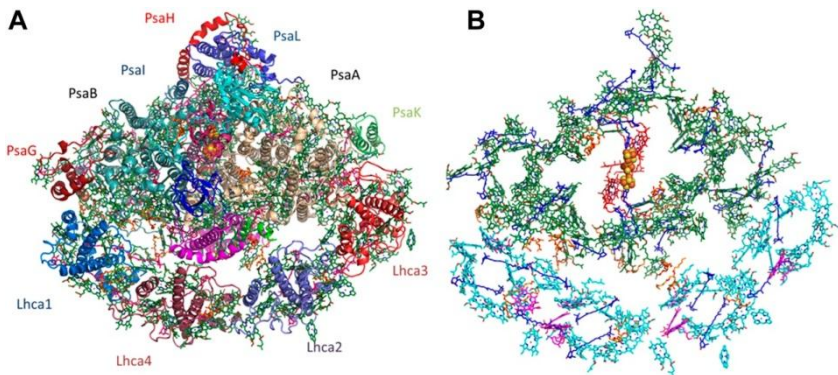


*Figure 6. Overall structure and organization of the plant PSI-LHCI supercomplex (Mazor et al. 2015). (A) A view from the stromal side of the membrane of PSI-LHCI (B) Pigment organization in PSI-LHCI.*

## PHOTOSYSTEM II:

### Photosystem II core complex

PS II cores occur as dimers (Dekker and Boekema 2005, Hohmann-Marriott and Blankenship 2011, Rogner et al. 1996). Each monomeric PS II core unit contains 35 Chls and 12 Cars. The X-ray structures of the PS II complex has been reported at 1.9 Å resolution (Umena et al. 2011). The PS II core complex contains the pigment-protein complexes CP43 and CP47, which function as core antenna. Their pigments are organized in two layers located near the cytoplasmic and the luminal sides of the membrane. The PSII RC consists of the D<sub>1</sub> and D<sub>2</sub> polypeptides, four Chls *a*, two quinone molecules (Q<sub>A</sub> and Q<sub>B</sub>), cytochrome b-559 and photosystem b (Psb) genes, binds 6 Chls and 2 Pheo, and 2 β-carotene molecules (Ferreira et al. 2004, Satoh 1996, Takahashi et al. 1996). The D<sub>1</sub> branch is responsible for carrying out electron transfer to the quinone Q<sub>A</sub>, whereas the D<sub>2</sub> branch does not take part in

## **Introduction**

primary electron transfer but is involved in photo-protection of the RC (Martinez-Junza et al. 2008).

### **Photosystem II Light -harvesting complexes**

In plants, most of the Chls are not bound to the PSII core complex, but to light-harvesting complexes (LHCs). The light-harvesting antenna complex is composed of 6 polypeptides. The main component of the PSII light-harvesting system is LHCII, which consist of heterotrimers of *Lhcb1-3*. The high resolution structures of trimeric LHCII from spinach (Liu et al. 2004) and pea (Standfuss et al. 2005) show the presence of 8 Chl *a*, 6 Chl *b* and 4 xanthophyll (Xan) molecules per monomer.

The other 3 polypeptides *Lhcb4-6* also known as CP29, CP26 and CP24 respectively are monomers and are categorized as minor antennas. They bind 8-10 Chls and 2 Xans molecule per polypeptide (Bassi et al. 1993, Sandona et al. 1998, van Amerongen and Dekker 2003). These minor antenna complexes play important role in connecting LHCII to the core (Dall'Osto et al. 2014)

### **Photosystem II supercomplex**

In plants and cyanobacteria, the PSII core forms a supramolecular structure together with the antenna system. The PSII supercomplex consist of a dimeric PS II core complex, which is associated with two copies of each minor light-harvesting protein, two strongly bound LHCII trimers, and one or more less tightly bound trimer(s) (Boekema et al. 2000, Dekker and Boekema 2005, Yakushevskaya et al. 2001).

PSII-LHCII supercomplex is the functional form of PSII, and these supercomplexes are organized in arrays and are mainly located in appressed grana membranes. However, the assembly of newly synthesized PSII-LHCII subunits and the repair of photodamaged PSII core occur through the monomeric form of PSII. Dynamic and reversible oligomerization, monomerization, and reoligomerization of PSII are, indeed, required for the synthesis of PSII and for the maintenance of PSII activity. It is important to note that the monomerization process of the PSII-LHCII supercomplex requires lateral migration of different oligomerization states of PSII-LHCII along the thylakoid membrane system. PSII-LHCII complexes form highly organized arrays of supercomplexes in the grana core, and the structure is gradually monomerized via the dimeric state of PSII towards the stroma lamellae (Danielsson et al. 2006).



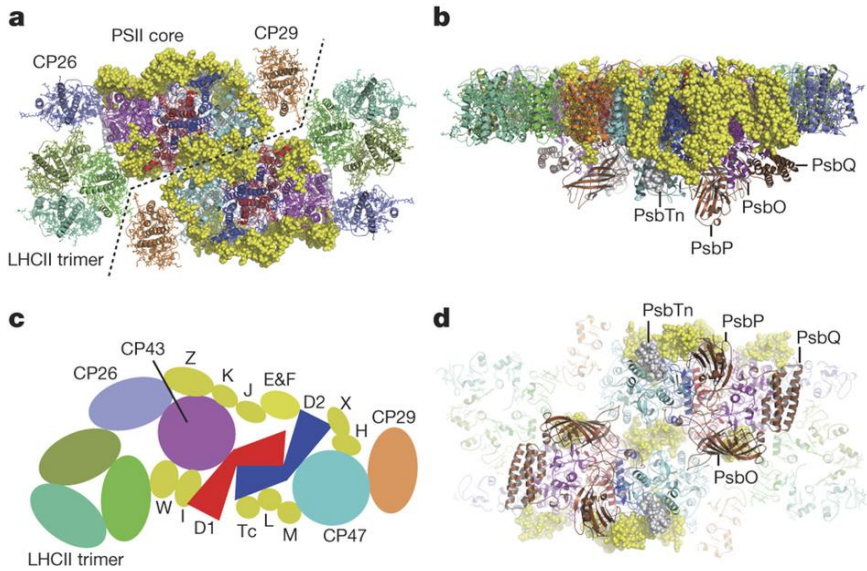


Figure 7: **a, b**, Structure of the spinach  $C_2S_2$ -type PSII-LHCII supercomplex (is taken from (Wei et al. 2016) with permission). **a**, View from the stromal side along membrane normal. **b**, Side view along membrane plane. Dashed lines indicate estimated interfacial regions between the two monomers. **c**, Cartoon diagram of the supercomplex. Only one monomer is shown and the colour codes are consistent with those in **a**. **d**, Lumen-exposed regions of the supercomplex.

During the past decade, great progress has been made towards solving the three-dimensional structure of the PSII-LHCII complex at high resolution. Several X-ray crystallographic structures have become available for cyanobacterial PSII (Ferreira et al. 2004, Guskov et al. 2009, Yan et al. 2007) and the detailed structure of LHCII has been resolved (Liu et al. 2004, Standfuss et al. 2005, Yan et al. 2007). Yet, the complete structure of PSII from higher plants is still missing.

Recently, the structures of the spinach PSII-LHCII supercomplex has been resolved at 3.2 Å resolution (Wei et al. 2016) through single-particle cryo-electron microscopy. The structure shows a homo-dimeric supramolecular system in which each monomer contains 25 protein subunits, 105 chlorophylls, 28 carotenoids and other cofactors. Whereas, one major trimeric and two minor monomeric LHCII associate with each core-complex monomer.

## Non-photochemical Quenching

The main topic of chapter 5 in this thesis is non-photochemical quenching (NPQ) in plants. Both algae and plants experience continuous natural fluctuations of light

## **Introduction**

intensity in nature. These organisms have developed several long- and short-term regulatory response mechanisms in order to avoid energy overloading of the photosynthetic apparatus, which can easily lead to photodamage (Björkman and Demmig-Adams 1995). The longer-term response which acts on the time scale of hours to days, is an adaptation of the organism via modification of the light-harvesting system such as the synthesis or degradation of pigments, protein or lipids in order to regulate the absorbed energy under the given environmental conditions. One interesting example is the modification of the antenna size in different light conditions (Anderson and Andersson 1988, Lindahl et al. 1995). On the contrary, during their short-term response plants are unable to regulate the amount of light absorbed. Instead, they enable the dissipation of excess absorbed energy in the form of harmless heat in order to avoid photooxidative damage in the photosystems (Demmig-Adams and Adams 1992, Eberhard et al. 2008, Szabo et al. 2005). The process is known as non-photochemical quenching and it leads to a decrease in fluorescence of PSII (Barber and Andersson 1992, Horton et al. 1996, Kulheim et al. 2002, Niyogi 1999).

Three main mechanisms contribute to NPQ, namely qE (fast energy dependent quenching), qT (state transition) and qI (a slow component related to photoinhibition) (Eberhard et al., 2008).

qE (fastest component): This is the so-called energy dependent quenching mechanism (Horton 1996) and it is activated very rapidly (sec to min) upon illumination (Müller et al. 2001). It can efficiently remove  $\frac{3}{4}$  of the absorbed photons from the system by thermally deactivating the Chl excited state energy (Demmig-Adams and Adams 1996). The molecular mechanism of this process is still unclear, but it is known that the activation of qE requires the pH gradient (Jahns and Heyde 1999, Müller et al. 2001). The pH gradient plays an important role in the protonation of PsbS, a PSII protein which is also an essential player in qE (Gilmore et al. 1998, Li et al. 2004, Müller et al. 2001, Takizawa et al. 2007). The exact location and functioning of PsbS in the thylakoid membrane are not known. There is also evidence that PsbS is involved in the macro-organization of PSII antenna (Kiss et al. 2008).

Secondly, the pH also plays an important role in the activation of the xanthophyll cycle, converting violaxanthin into zeaxanthin via antheraxanthin at high light. This cyclic reaction is catalysed by two enzymes called the violaxanthin-deepoxidase (VDE) which is located in thylakoid lumen and zeaxanthin-epoxidase (ZE) present in chloroplast stroma and is 5-10 times slower than VDE. The inter-conversion of these pigments is essential for qE and has been extensively studied in the literature

(Demmig-Adams and Adams 1996, Gilmore et al. 1995, Gilmore and Yamamoto 1992, Gilmore and Yamamoto 1993, Horton et al. 1996, Kalituho et al. 2007, Štroch et al. 2004).

The exact location of qE is not known so far, but there is a general agreement that qE is localized in some components of the PSII supercomplex, that consists of the PSII core, the major LHC II antenna and the three minor LHCs i.e. CP24, CP26 and CP29, as some reports suggest that it occurs in LHCII (including minor antenna) (Horton and Ruban 1992, Horton et al. 1996), where the xanthophyll cycle Cars are bound (Bassi et al. 1993, Peter and Thornber 1991, Ruban and Horton 1994), while others reported the occurrence of qE in PSII RC (Ivanov et al. 2008). Whereas, the two minor antenna CP26 and CP29 are reported to play a major role in qE (Bassi et al. 1993, Crofts and Yerkes 1994, Gilmore et al. 1996, Horton and Ruban 1992, Walters et al. 1994).

## **This Thesis**

In this thesis, I have focused on the application and development of fluorescence spectroscopy techniques to study two important biological processes: (1) DNA dynamics and (2) plant photosynthesis.

**Chapter 2** describes in detail the single molecule FRET technique, the setup and the application of this technique to study the structure and dynamics of complex biological systems.

**Chapter 3** We demonstrate by both simulations and experiments using doubly labelled DNA hairpins that resolving dynamic conformational states with a lifetime in the order of a few milliseconds is possible.

In **Chapter 4** picosecond fluorescence decay kinetics for stacked and unstacked BBY complexes were compared in order to evaluate the efficiency of excitation energy transfer between the layers of PSII enriched thylakoid membrane.

In **Chapter 5** to determine the kinetics of the early steps in photosynthesis and the photoprotective mechanisms, we have used picosecond fluorescence measurements on intact spinach leaves to study the excited-state kinetics of photosystems I (PSI) and II (PSII) both for open and closed RCs in the leaves *in vivo*, as a function of actinic light intensity.

## **Introduction**

## **References**

- ALBERTSSON P-Å. 2001. A quantitative model of the domain structure of the photosynthetic membrane. *Trends in plant science* 6: 349-354.
- AMUNTS A, DRORY O AND NELSON N. 2007. The structure of a plant photosystem I supercomplex at 3.4 Å resolution. *Nature* 447: 58-63.
- AMUNTS A, TOPORIK H, BOROVIKOVA A AND NELSON N. 2010. Structure determination and improved model of plant photosystem I. *The Journal of biological chemistry* 285: 3478-3486.
- ANDERSON JM AND ANDERSSON B. 1988. The dynamic photosynthetic membrane and regulation of solar energy conversion. *Trends in biochemical sciences* 13: 351-355.
- BARBER J AND ANDERSSON B. 1992. Too much of a good thing: light can be bad for photosynthesis. *Trends in biochemical sciences* 17: 61-66.
- BASSI R, PINEAU B, DAINESE P AND MARQUARDT J. 1993. Carotenoid-binding proteins of photosystem II. *European journal of biochemistry* 212: 297-303.
- BENSON AA AND CALVIN M. 1950. CARBON DIOXIDE FIXATION BY GREEN PLANTS. *Annual review of plant physiology and plant molecular biology* 1: 25-42.
- BIRCH DJS AND IMHOF RE 1999. Time-Domain Fluorescence Spectroscopy Using Time-Correlated Single-Photon Counting. In: LAKOWICZ, JR (Ed.) *Topics in Fluorescence Spectroscopy: Techniques*, Boston, MA: Springer US, p. 1-95.
- BJÖRKMAN O AND DEMMIG-ADAMS B 1995. Regulation of Photosynthetic Light Energy Capture, Conversion, and Dissipation in Leaves of Higher Plants. In: SCHULZE, E-D AND CALDWELL, MM (Eds.) *Ecophysiology of Photosynthesis*, Berlin, Heidelberg: Springer Berlin Heidelberg, p. 17-47.
- BLANKENSHIP RE 2002. *Molecular Mechanisms of Photosynthesis*. Oxford, United Kingdom: Blackwell Science.
- BLUMBERG S, GAJRAJ A, PENNINGTON MW AND MEINERS JC. 2005. Three-dimensional characterization of tethered microspheres by total internal reflection fluorescence microscopy. *Biophysical journal* 89: 1272-1281.
- BOEKEMA EJ, VAN BREEMEN JFL, VAN ROON H AND DEKKER JP. 2000. Arrangement of photosystem II supercomplexes in crystalline macrodomains within the thylakoid membrane of green plant chloroplasts<sup>1</sup>. *Journal of molecular biology* 301: 1123-1133.
- BOPP MA, JIA Y, LI L, COGDELL RJ AND HOCHSTRASSER RM. 1997. Fluorescence and photobleaching dynamics of single light-harvesting complexes. *Proceedings of the National Academy of Sciences of the United States of America* 94: 10630-10635.
- BORST JW, HINK MA, VAN HOEK A AND VISSER AJ. 2005. Effects of refractive index and viscosity on fluorescence and anisotropy decays of enhanced cyan and yellow fluorescent proteins. *Journal of fluorescence* 15: 153-160.
- CROCE R AND VAN AMERONGEN H. 2013. Light-harvesting in photosystem I. *Photosynthesis research* 116: 153-166.
- CROFTS AR AND YERKES CT. 1994. A molecular mechanism for qE-quenching. *FEBS Lett* 352: 265-270.

- DALL'OSTO L, UNLU C, CAZZANIGA S AND VAN AMERONGEN H. 2014. Disturbed excitation energy transfer in *Arabidopsis thaliana* mutants lacking minor antenna complexes of photosystem II. *Biochim Biophys Acta* 1837: 1981-1988.
- DANIELSSON R, SUORSA M, PAAKKARINEN V, ALBERTSSON P-Å, STYRING S, ARO E-M AND MAMEDOV F. 2006. Dimeric and Monomeric Organization of Photosystem II: DISTRIBUTION OF FIVE DISTINCT COMPLEXES IN THE DIFFERENT DOMAINS OF THE THYLAKOID MEMBRANE. *Journal of Biological Chemistry* 281: 14241-14249.
- DEKKER JP AND BOEKEMA EJ. 2005. Supramolecular organization of thylakoid membrane proteins in green plants. *Bba-Bioenergetics* 1706: 12-39.
- DEMMIG-ADAMS B AND ADAMS WW. 1992. PHOTOPROTECTION AND OTHER RESPONSES OF PLANTS TO HIGH LIGHT STRESS. *Annual review of plant physiology and plant molecular biology* 43: 599-626.
- DEMMIG-ADAMS B AND ADAMS WW. 1996. The role of xanthophyll cycle carotenoids in the protection of photosynthesis. *Trends in plant science* 1: 21-26.
- EBERHARD S, FINAZZI G AND WOLLMAN FA. 2008. The dynamics of photosynthesis. *Annual review of genetics* 42: 463-515.
- ELF J, LI GW AND XIE XS. 2007. Probing transcription factor dynamics at the single-molecule level in a living cell. *Science* 316: 1191-1194.
- FERREIRA KN, IVERSON TM, MAGHLAOU K, BARBER J AND IWATA S. 2004. Architecture of the Photosynthetic Oxygen-Evolving Center. *Science* 303: 1831-1838.
- FLORS C, HOTTA J, UJI-I H, DEDECKER P, ANDO R, MIZUNO H, MIYAWAKI A AND HOFKENS J. 2007. A stroboscopic approach for fast photoactivation-localization microscopy with *Dronpa* mutants. *Journal of the American Chemical Society* 129: 13970-13977.
- FÖRSTER T. 1948. Zwischenmolekulare Energiewanderung und Fluoreszenz. *Ann Phys* 437: 55-75.
- GILMORE AM, HAZLETT TL, DEBRUNNER PG AND GOVINDJEE. 1996. Photosystem II chlorophyll a fluorescence lifetimes and intensity are independent of the antenna size differences between barley wild-type and chlorina mutants: Photochemical quenching and xanthophyll cycle-dependent nonphotochemical quenching of fluorescence. *Photosynthesis research* 48: 171-187.
- GILMORE AM, HAZLETT TL AND GOVINDJEE. 1995. Xanthophyll cycle-dependent quenching of photosystem II chlorophyll a fluorescence: formation of a quenching complex with a short fluorescence lifetime. *Proceedings of the National Academy of Sciences of the United States of America* 92: 2273-2277.
- GILMORE AM, SHINKAREV VP, HAZLETT TL AND GOVINDJEE G. 1998. Quantitative analysis of the effects of intrathylakoid pH and xanthophyll cycle pigments on chlorophyll a fluorescence lifetime distributions and intensity in thylakoids. *Biochemistry* 37: 13582-13593.
- GILMORE AM AND YAMAMOTO HY. 1992. Dark induction of zeaxanthin-dependent nonphotochemical fluorescence quenching mediated by ATP. *Proceedings of the National Academy of Sciences of the United States of America* 89: 1899-1903.

## **Introduction**

- GILMORE AM AND YAMAMOTO HY. 1993. Linear models relating xanthophylls and lumen acidity to non-photochemical fluorescence quenching. Evidence that antheraxanthin explains zeaxanthin-independent quenching. *Photosynthesis research* 35: 67-78.
- GOVINDJEE. 2005. Discoveries in Photosynthesis. *Advances in Photosynthesis and Respiration*, Dordrecht: Springer Netherlands.
- GUSKOV A, KERN J, GABDULKHAKOV A, BROSER M, ZOUNI A AND SAENGER W. 2009. Cyanobacterial photosystem II at 2.9-Å resolution and the role of quinones, lipids, channels and chloride. *Nat Struct Mol Biol* 16: 334-342.
- HOHLBEIN J, CRAGGS TD AND CORDES T. 2014. Alternating-laser excitation: single-molecule FRET and beyond. *Chemical Society reviews* 43: 1156-1171.
- HOHMANN-MARRIOTT MF AND BLANKENSHIP RE. 2011. Evolution of photosynthesis. *Annual review of plant biology* 62: 515-548.
- HORTON P AND RUBAN AV. 1992. Regulation of Photosystem II. *Photosynthesis research* 34: 375-385.
- HORTON P, RUBAN AV AND WALTERS RG. 1996. Regulation of Light Harvesting in Green Plants. *Annual review of plant physiology and plant molecular biology* 47: 655-684.
- IVANOV AG, HURRY V, SANE PV, ÖQUIST G AND HUNER NPA. 2008. Reaction centre quenching of excess light energy and photoprotection of photosystem II. *Journal of Plant Biology* 51: 85.
- JABŁOŃSKI A. 1935. Über den Mechanismus der Photolumineszenz von Farbstoffphosphoren. *Zeitschrift für Physik* 94: 38-46.
- JAHS P AND HEYDE S. 1999. Dicyclohexylcarbodiimide alters the pH dependence of violaxanthin de-epoxidation. *Planta* 207: 393-400.
- JAMESON DM, CRONEY JC AND MOENS PD. 2003. Fluorescence: basic concepts, practical aspects, and some anecdotes. *Methods in enzymology* 360: 1-43.
- KALITUHO L, RECH J AND JAHS P. 2007. The roles of specific xanthophylls in light utilization. *Planta* 225: 423-439.
- KAPANIDIS AN, LEE NK, LAURENCE TA, DOOSE S, MARGEAT E AND WEISS S. 2004. Fluorescence-aided molecule sorting: analysis of structure and interactions by alternating-laser excitation of single molecules. *Proceedings of the National Academy of Sciences of the United States of America* 101: 8936-8941.
- KAROLCZAK J, KOMAR D, KUBICKI J, WRÓŻOWA T, DOBEK K, CIESIELSKA B AND MACIEJEWSKI A. 2001. The measurements of picosecond fluorescence lifetimes with high accuracy and subpicosecond precision. *Chemical Physics Letters* 344: 154-164.
- KASHA M. 1950. Characterization of electronic transitions in complex molecules. *Discussions of the Faraday Society* 9: 14-19.
- KISS AZ, RUBAN AV AND HORTON P. 2008. The PsbS protein controls the organization of the photosystem II antenna in higher plant thylakoid membranes. *The Journal of biological chemistry* 283: 3972-3978.
- KRÜGER TJAART P, ILIOAIA C, JOHNSON MATTHEW P, RUBAN ALEXANDER V, PAPAGIANNAKIS E, HORTON P AND VAN GRONDELLE R. 2012. Controlled Disorder in Plant Light-Harvesting Complex II Explains Its Photoprotective Role. *Biophysical journal* 102: 2669-2676.

- KRÜGER TPJ, ILIOAIA C, VALKUNAS L AND VAN GRONDELLE R. 2011. Fluorescence Intermittency from the Main Plant Light-Harvesting Complex: Sensitivity to the Local Environment. *The Journal of Physical Chemistry B* 115: 5083-5095.
- KRÜGER TPJ, NOVODEREZHNIKIN VI, ILIOAIA C AND VAN GRONDELLE R. 2010. Fluorescence Spectral Dynamics of Single LHCII Trimers. *Biophysical journal* 98: 3093-3101.
- KULHEIM C, AGREN J AND JANSSON S. 2002. Rapid regulation of light harvesting and plant fitness in the field. *Science* 297: 91-93.
- LAKOWICZ JR 1999. *Principles of Fluorescence Spectroscopy*. Kluwer Academic/Plenum.
- LAKOWICZ JR 2006. *Principles of fluorescence spectroscopy*. New York [etc.]: Springer.
- LAURENCE TA, KONG X, JAGER M AND WEISS S. 2005. Probing structural heterogeneities and fluctuations of nucleic acids and denatured proteins. *Proceedings of the National Academy of Sciences of the United States of America* 102: 17348-17353.
- LEE NK, KAPANIDIS AN, WANG Y, MICHALET X, MUKHOPADHYAY J, EBRIGHT RH AND WEISS S. 2005. Accurate FRET measurements within single diffusing biomolecules using alternating-laser excitation. *Biophysical journal* 88: 2939-2953.
- LI XP, GILMORE AM, CAFFARRI S, BASSI R, GOLAN T, KRAMER D AND NIYOGI KK. 2004. Regulation of photosynthetic light harvesting involves intrathylakoid lumen pH sensing by the PsbS protein. *The Journal of biological chemistry* 279: 22866-22874.
- LINDAHL M, YANG DH AND ANDERSSON B. 1995. Regulatory proteolysis of the major light-harvesting chlorophyll a/b protein of photosystem II by a light-induced membrane-associated enzymic system. *European journal of biochemistry* 231: 503-509.
- LIU Z, YAN H, WANG K, KUANG T, ZHANG J, GUI L, AN X AND CHANG W. 2004. Crystal structure of spinach major light-harvesting complex at 2.72 Å resolution. *Nature* 428: 287-292.
- MARTINEZ-JUNZA V, SZCZEPANIAK M, BRASLAVSKY SE, SANDER J, NOWACZYK M, ROGNER M AND HOLZWARTH AR. 2008. A photoprotection mechanism involving the D2 branch in photosystem II cores with closed reaction centers. *Photochemical & Photobiological Sciences* 7: 1337-1343.
- MAZOR Y, BOROVIKOVA A AND NELSON N. 2015. The structure of plant photosystem I super-complex at 2.8 Å resolution. *eLife* 4: e07433.
- MILOSLAVINA Y, GROUNOVA I, LAMBREV PH, LEPETIT B, GOSS R, WILHELM C AND HOLZWARTH AR. 2009. Ultrafast fluorescence study on the location and mechanism of non-photochemical quenching in diatoms. *Biochimica et Biophysica Acta (BBA) - Bioenergetics* 1787: 1189-1197.
- MIMURO M AND KATOH T 1991. Carotenoids in photosynthesis: absorption, transfer and dissipation of light energy. *Pure and Applied Chemistry*, p. 123.
- MOROSINOTTO T, BALLOTTARI M, KLIMMEK F, JANSSON S AND BASSI R. 2005. The association of the antenna system to photosystem I in higher plants. Cooperative interactions stabilize the supramolecular complex and enhance red-shifted spectral forms. *The Journal of biological chemistry* 280: 31050-31058.
- MULLER BK, ZAYCHIKOV E, BRAUCHLE C AND LAMB DC. 2005. Pulsed interleaved excitation. *Biophysical journal* 89: 3508-3522.

## **Introduction**

- MÜLLER P, LI X-P AND NIYOGI KK. 2001. Non-Photochemical Quenching. A Response to Excess Light Energy. *Plant physiology* 125: 1558-1566.
- MULLET JE, BURKE JJ AND ARNTZEN CJ. 1980. Chlorophyll proteins of photosystem I. *Plant physiology* 65: 814-822.
- NELSON N AND BEN-SHEM A. 2004. The complex architecture of oxygenic photosynthesis. 5: 971-982.
- NIYOGI KK. 1999. PHOTOPROTECTION REVISITED: Genetic and Molecular Approaches. *Annual review of plant physiology and plant molecular biology* 50: 333-359.
- O'CONNOR DV AND PHILLIPS D. 1984. Time-correlated single photon counting. Academic Press.
- PAULSEN H, FINKENZELLER B AND KUHLEIN N. 1993. Pigments induce folding of light-harvesting chlorophyll a/b-binding protein. *European journal of biochemistry* 215: 809-816.
- PETER GF AND THORNBURGH JP. 1991. Biochemical composition and organization of higher plant photosystem II light-harvesting pigment-proteins. *The Journal of biological chemistry* 266: 16745-16754.
- PETERMAN EJJ, GRADINARU CC, CALKOE F, BORST JC, VAN GRONDELLE R AND VAN AMERONGEN H. 1997. Xanthophylls in Light-Harvesting Complex II of Higher Plants: Light Harvesting and Triplet Quenching. *Biochemistry* 36: 12208-12215.
- PLUMLEY FG AND SCHMIDT GW. 1987. Reconstitution of chlorophyll a/b light-harvesting complexes: Xanthophyll-dependent assembly and energy transfer. *Proceedings of the National Academy of Sciences of the United States of America* 84: 146-150.
- RAVEN PH, EVERT RF AND EICHHORN SE. 2005. *Biology of Plants*. W. H. Freeman.
- RICHTER MF, BAIER J, COGDELL RJ, KÖHLER J AND OELLERICH S. 2007. Single-Molecule Spectroscopic Characterization of Light-Harvesting 2 Complexes Reconstituted into Model Membranes. *Biophysical journal* 93: 183-191.
- ROGNER M, BOEKEMA EJ AND BARBER J. 1996. How does photosystem 2 split water? The structural basis of efficient energy conversion. *Trends in biochemical sciences* 21: 44-49.
- RUBAN AV AND HORTON P. 1994. Spectroscopy of non-photochemical and photochemical quenching of chlorophyll fluorescence in leaves; evidence for a role of the light harvesting complex of Photosystem II in the regulation of energy dissipation. *Photosynthesis research* 40: 181-190.
- SANDONA D, CROCE R, PAGANO A, CRIMI M AND BASSI R. 1998. Higher plants light harvesting proteins. Structure and function as revealed by mutation analysis of either protein or chromophore moieties. *Biochim Biophys Acta* 1365: 207-214.
- SATOH K. 1996. Introduction to the Photosystem II Reaction Center- Isolation and Biochemical and Biophysical Characterization. In: ORT, DR, YOCUM, CF AND HEICHEL, IF (Eds.) *Oxygenic Photosynthesis: The Light Reactions*, Dordrecht: Springer Netherlands, p. 193-211.
- SCHILLER NH AND ALFANO RR. 1980. Picosecond characteristics of a spectrograph measured by a streak camera/video readout system. *Optics Communications* 35: 451-454.



- SLAVOV C, BALLOTTARI M, MOROSINOTTO T, BASSI R AND HOLZWARTH AR. 2008. Trap-Limited Charge Separation Kinetics in Higher Plant Photosystem I Complexes. *Biophysical journal* 94: 3601-3612.
- STAEHELIN LA. 2003. Chloroplast structure: from chlorophyll granules to supra-molecular architecture of thylakoid membranes. *Photosynthesis research* 76: 185-196.
- STANDFUSS J, TERWISSCHA VAN SCHELTINGA AC, LAMBORGHINI M AND KÜHLBRANDT W. 2005. Mechanisms of photoprotection and nonphotochemical quenching in pea light-harvesting complex at 2.5 Å resolution. *The EMBO journal* 24: 919-928.
- ŠTROCH M, ŠPUNDA V AND KURASOVÁ I. 2004. Non-Radiative Dissipation of Absorbed Excitation Energy Within Photosynthetic Apparatus of Higher Plants. *Photosynthetica* 42: 323-337.
- SZABO I, BERGANTINO E AND GIACOMETTI GM. 2005. Light and oxygenic photosynthesis: energy dissipation as a protection mechanism against photo-oxidation. *EMBO reports* 6: 629-634.
- TAKAHASHI Y, UTSUMI K, YAMAMOTO Y, HATANO A AND SATOH K. 1996. Genetic engineering of the processing site of D1 precursor protein of photosystem II reaction center in *Chlamydomonas reinhardtii*. *Plant & cell physiology* 37: 161-168.
- TAKIZAWA K, CRUZ JA, KANAZAWA A AND KRAMER DM. 2007. The thylakoid proton motive force in vivo. Quantitative, non-invasive probes, energetics, and regulatory consequences of light-induced pmf. *Biochim Biophys Acta* 1767: 1233-1244.
- TIETZ C, JELEZKO F, GERKEN U, SCHULER S, SCHUBERT A, ROGL H AND WRACHTRUP J. 2001. Single molecule spectroscopy on the light-harvesting complex II of higher plants. *Biophysical journal* 81: 556-562.
- TRISSEL HW AND WILHELM C. 1993. Why do thylakoid membranes from higher plants form grana stacks? *Trends in biochemical sciences* 18: 415-419.
- UMENA Y, KAWAKAMI K, SHEN JR AND KAMIYA N. 2011. Crystal structure of oxygen-evolving photosystem II at a resolution of 1.9 Å. *Nature* 473: 55-60.
- VALEUR B 2001. *Molecular Fluorescence: Principles and Applications*. 1 ed: Wiley-VCH.
- VAN AMERONGEN H AND CROCE R. 2013. Light harvesting in photosystem II. *Photosynthesis research* 116: 251-263.
- VAN AMERONGEN H AND DEKKER JP 2003. Light-Harvesting in Photosystem II. In: GREEN, BR AND PARSON, WW (Eds.) *Light-Harvesting Antennas in Photosynthesis*, Dordrecht: Springer Netherlands, p. 219-251.
- VAN HOEK A AND VISSER AJWG. 1985. Artefact and Distortion Sources in Time Correlated Single Photon Counting. *Instrumentation Science & Technology* 14: 359-378.
- VAN OORT B, MURALI S, WIENTJES E, KOEHORST RBM, SPRUIJT RB, VAN HOEK A, CROCE R AND VAN AMERONGEN H. 2009. Ultrafast resonance energy transfer from a site-specifically attached fluorescent chromophore reveals the folding of the N-terminal domain of CP29. *Chemical Physics* 357: 113-119.
- VAN STOKKUM IHM, VAN OORT B, VAN MOURIK F, GOBETS B AND VAN AMERONGEN H 2008. (Sub)-Picosecond Spectral Evolution of Fluorescence Studied with a Synchroscan Streak-Camera System and Target Analysis. In: AARTSMA, TJ AND MATYSIK, J (Eds.) *Biophysical Techniques in Photosynthesis*, Dordrecht: Springer Netherlands, p. 223-240.

## **Introduction**

- VISSER NV, BORST JW, HINK MA, VAN HOEK A AND VISSER AJ. 2005. Direct observation of resonance tryptophan-to-chromophore energy transfer in visible fluorescent proteins. *Biophysical chemistry* 116: 207-212.
- VOS K, VAN HOEK A AND VISSER AJ. 1987. Application of a reference convolution method to tryptophan fluorescence in proteins. A refined description of rotational dynamics. *European journal of biochemistry* 165: 55-63.
- WALTERS RG, RUBAN AV AND HORTON P. 1994. Higher plant light-harvesting complexes LHCIIa and LHCIIc are bound by dicyclohexylcarbodiimide during inhibition of energy dissipation. *European journal of biochemistry* 226: 1063-1069.
- WEI X, SU X, CAO P, LIU X, CHANG W, LI M, ZHANG X AND LIU Z. 2016. Structure of spinach photosystem II-LHCII supercomplex at 3.2 Å resolution. 534: 69-74.
- WIENTJES E, ROEST G AND CROCE R. 2012. From red to blue to far-red in Lhca4: how does the protein modulate the spectral properties of the pigments? *Biochim Biophys Acta* 1817: 711-717.
- WIENTJES E, VAN AMERONGEN H AND CROCE R. 2013. LHCII is an antenna of both photosystems after long-term acclimation. *Biochim Biophys Acta* 1827: 420-426.
- WISE RR AND HOOBER JK 2007. *The Structure and Function of Plastids*. Springer Netherlands.
- YAKUSHEVSKA AE, JENSEN PE, KEEGSTRA W, VAN ROON H, SCHELLER HV, BOEKEMA EJ AND DEKKER JP. 2001. Supermolecular organization of photosystem II and its associated light-harvesting antenna in *Arabidopsis thaliana*. *European journal of biochemistry* 268: 6020-6028.
- YAN H, ZHANG P, WANG C, LIU Z AND CHANG W. 2007. Two lutein molecules in LHCII have different conformations and functions: Insights into the molecular mechanism of thermal dissipation in plants. *Biochemical and biophysical research communications* 355: 457-463.

## CHAPTER 2

# **Studying DNA-protein interactions with single-molecule Förster resonance energy transfer**

based on:

Farooq, S., C. Fijen and J. Hohlbein (2014). "Studying DNA-protein interactions with single-molecule Förster resonance energy transfer." *Protoplasma* **251**(2): 317-332.

### **Abstract**

Single-molecule Förster resonance energy transfer (smFRET) has emerged as a powerful tool for elucidating biological structure and mechanisms on the molecular level. Here, we focus on applications of smFRET to study interactions between DNA and enzymes such as DNA and RNA polymerases. SmFRET, used as a nanoscopic ruler, allows for the detection and precise characterisation of dynamic and rarely occurring events, which are otherwise averaged out in ensemble-based experiments. In this review, we will highlight some recent developments that provide new means of studying complex biological systems either by combining smFRET with force-based techniques or by using data obtained from smFRET experiments as constraints for computer-aided modelling.

### **Introduction and theoretical background**

In order to understand the structure and function of biomolecular systems despite their often breath-taking complexity, scientists have been developing an ever-growing arsenal of sophisticated instrumentation and analytical methods. Nuclear magnetic resonance (NMR) spectroscopy (Foster et al. 2007, Wuthrich 2001) and X-ray crystallography (Ilari and Savino 2008), for example, provide structural information with atomic resolution, but both methods ultimately fall short of resolving dynamic interactions within and especially between biomolecular complexes under physiologically relevant conditions. A major limitation of conventional biochemical analysis originates from ensemble- and time-averaging effects. In other words, the analysis reports on averaged properties of a population rather than the properties of individual species forming this population. With the advent of single-molecule techniques, researchers gained new exciting possibilities to study time-dependent sample distributions, conformational dynamics (Fig. 1a), reaction pathways, intermediate states, and asynchronous reactions (Kapanidis and Strick 2009).

In this review, we will focus on an important member of the class of fluorescence based methods namely the single-molecule Förster resonance energy transfer (smFRET). This methodology allows detecting (relative) changes of distances between two fluorophores in the 2 to 10 nm range thus operating in a range comparable to the size of biomolecules such as proteins, lipids and nucleic acids. We will further limit our review to smFRET-based applications to study structure, dynamics and functions of DNA and DNA/protein interactions. We will also briefly discuss the development of techniques combining smFRET with force-based techniques such as optical and magnetic tweezers. For more general

reviews about single-molecule techniques and smFRET, the interested reader is referred to (Deniz et al. 2008, Hohlbein et al. 2010, Kim and Ha 2013, Moerner 2007b, Preus and Wilhelmsson 2012, Roy et al. 2008, Walter et al. 2008).

## Single-molecule Förster resonance energy transfer

FRET describes the distance-dependent and non-radiative energy transfer from a donor fluorophore to an acceptor chromophore via a dipole-dipole interaction and was first reported by Theodor Förster more than 60 years ago (Förster 1948). Three basic conditions need to be fulfilled for FRET to occur: (1) the spectra for donor emission and acceptor absorption must overlap, (2) donor and acceptor must be in close proximity (<10 nm) and (3) the relative orientation of the donor and the acceptor transition dipole moments must allow transfer of energy (Lakowicz 2006).

The FRET transfer efficiency  $E$  can be expressed using two rate constants, where  $k_D$  is the fluorescence emission rate constant of the donor in absence of the acceptor and  $k_T$  is the rate of energy transfer between the donor and the acceptor. These rates can be determined experimentally from the fluorescence lifetime of the donor in absence of the acceptor ( $\tau_D$ ) and in presence of the acceptor ( $\tau_T$ ). The transfer efficiency  $E$ , as shown by Förster, is inversely proportional to the sixth power of the distance  $R$  between the two transition dipoles according to

$$E = \frac{k_T}{k_D + k_T} = 1 - \frac{\tau_T}{\tau_D} = \frac{R_0^6}{R_0^6 + R^6}, \quad (1)$$

where  $R_0$  is known as the Förster radius and represents the distance between the transition dipoles corresponding to an energy transfer of 50 % between donor and acceptor (Fig. 1b).  $R_0$  is related to the properties of the fluorophores and the relative orientation of their dipole moments and is calculated using

$$R_0^6 = 8.8 \cdot 10^{-28} \frac{\Phi_D \kappa^2}{n^4} \int_0^\infty f_D(\lambda) A(\lambda) \lambda^4 d\lambda, \quad (2)$$

where  $\Phi_D$  is the donor quantum yield in absence of a nearby acceptor,  $n$  is the refractive index of the donor-acceptor intervening medium (for a discussion, see (Knox and van Amerongen 2002)), and  $\kappa^2$  is the orientation factor describing the mutual orientation of the two transition dipole moments. The orientation factor is often set to  $\kappa^2 = 2/3$ , which is justified as long as at least one of the fluorophores

## ***Studying DNA-protein interactions with smFRET***

has unrestricted rotational freedom (Dale et al. 1979). The spectral overlap integral is calculated using the molecular extinction coefficient of the acceptor ( $\epsilon_A$ ) and the wavelength-dependent emission spectrum of the donor ( $f_D$ ).

Ensemble-based FRET techniques have been used to study structural features and dynamics of biological systems (Clegg 1992, Jares-Erijman and Jovin 2003, Stryer and Haugland 1967). The outcome and interpretation of ensemble FRET data, however, is highly affected by the potential presence of dynamic or static heterogeneity in the sample (Haas et al. 1975). Observation of FRET at the single molecule level (Deniz et al. 1999, Ha et al. 1996) has overcome many of the shortcomings of ensemble FRET measurements and allows resolving this heterogeneity. smFRET is now widely applied to study (in vitro) molecular interactions and dynamics (Hohlbein et al. 2010, McKinney et al. 2006, Weiss 1999).

In order to detect fluorescence emitted from single fluorophores against any background noise, a number of experimental requirements needs to be fulfilled, as the detectable photon budget from a single fluorophore is limited. Thus, we require a small excitation and detection volume to reduce the background from a scattering or weakly fluorescent medium and to distinguish a molecule of interest from other members of the same species. Often, a low concentration of fluorophores can be achieved by simply diluting the sample. However, as soon as we want to detect dynamic interactions between different fluorescently labelled species, diluting the sample severely limits the number of biomolecular interactions which can be studied, as many interactions require high sample concentrations considering the dissociation constant of their interaction (Holzmeister et al. 2014, Levene et al. 2003). Single-molecule FRET measurements are mostly taken using either confocal microscopy or total internal reflection fluorescence (TIRF) microscopy, the latter being a special case of wide-field microscopy.

### **Diffusion-based confocal microscopy**

Diffusion-based confocal microscopy (Fig. 1c) requires dilute solutions containing typically a picomolar concentration of fluorescently labelled species (Deniz et al. 1999). The molecules diffuse through a femtolitre-sized excitation volume formed by a focused laser beam and a microscope objective with high numerical aperture. If the donor fluorophore is excited, it can transfer some of its energy to a nearby acceptor and causes the latter to fluoresce. In a confocal detection scheme, the objective used for excitation is also collecting the emitted fluorescence. After the emitted light is spectrally separated from the wavelength of the laser, the

fluorescence is spatially filtered by a pinhole eliminating intensity contributions from outside the focus.

For FRET detection, the fluorescence is split by a dichroic mirror into two channels, which cover the spectral range of the donor and acceptor emission, respectively. The FRET efficiency for every burst, representing the passage of one molecule through the focus (Fig. 1d), can be calculated in two ways: The first option uses the simultaneous recorded fluorescence lifetime of the donor as indicated in Eq. 1, but requires more sophisticated instrumentation using a pulsed laser and detectors with picosecond time-resolution. The second option is more common; it utilises the number of photons detected in the donor channel after donor excitation ( $f_{Dex}^{Dem}$ ) and the number of photons detected in the acceptor channel after donor excitation ( $f_{Dex}^{Aem}$ ). For each burst (Fig. 1e), the apparent FRET efficiency  $E^*$  is calculated as

$$E^* = \frac{f_{Dex}^{Aem}}{f_{Dex}^{Dem} + f_{Dex}^{Aem}} \quad (3)$$

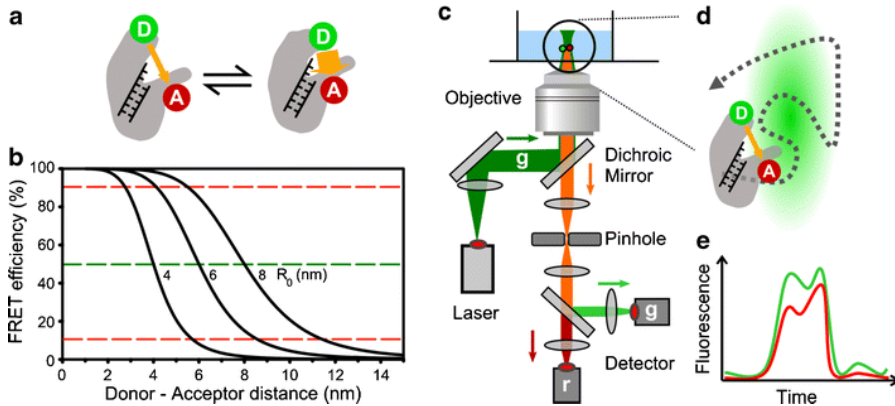


Figure 1: Implementation of single-molecule FRET in confocal microscopy. (a) One potential goal of smFRET-based experiments is the study of conformational changes occurring in enzymes. Here, a DNA polymerase bound to DNA is fluorescently labelled with a donor and an acceptor fluorophore. Depending on the conformational equilibrium, two different FRET states are expected (open and closed), whereas ensemble-based experiments would struggle resolving this dynamic heterogeneity. (b) The FRET efficiency  $E$  plotted as a function of Förster radius  $R_0$ . Most common pairs of fluorophores (e.g., Cy3 and Cy5) have a Förster radius around 6 nm allowing handlers to detect distances between 4 to 9 nm. (c) Schematic overview of a confocal setup suitable for detection of smFRET. The laser light is collimated, reflected by a dichroic mirror and focussed with an objective

## Studying DNA-protein interactions with smFRET

of high numerical aperture to a diffraction limited excitation spot in the sample volume. Fluorescence, originating from excited dyes attached to diffusing proteins or DNA, is collected by the same objective and spatially filtered with a pinhole. Further on, the emitted fluorescence is spectrally split into a green (donor) and a red (acceptor) detection channel. **(d)** During the transit of a donor-labelled molecule through the focus, some energy can be transferred to the acceptor via FRET. **(e)** Every burst is characterised by two photon numbers: The number of photons in the donor channel ( $f_{Dex}^{Dem}$ ) and the number of photons in the acceptor channel ( $f_{Dex}^{Aem}$ ).

It should be noted that  $E^*$  is not yet corrected for background, spectral crosstalk of the donor into the acceptor-emission channel and the instrument-dependent detection efficiencies of the dyes. For a step-by-step guide for obtaining an accurate FRET measure, the reader is referred to (Hohlbein et al. 2014a).

### Alternating-laser excitation (ALEX)

As described above, excitation with a single laser allows the calculation of an apparent FRET efficiency  $E^*$ . Using common fluorophores, however, the emission spectrum of the

donor is often broad and not fully spectrally covered by the donor detection channel. Instead, part of the donor fluorescence is detected in the acceptor detection channel, with the consequence that even a donor-only sample will show a FRET distribution with a mean  $E^*$  peak slightly above zero. The challenge researchers faced was how to discriminate low-FRET molecules with a fluorescently active acceptor from species in which the acceptor is not present or has been photo bleached before. To tackle this issue, Kapanidis and co-workers developed the ALEX scheme in which short periods of donor excitation alter with short periods of direct acceptor excitation (Hohlbein et al. 2014b, Kapanidis et al. 2004) to verify the presence and state of the acceptor fluorophore in a fluorescently active form. ALEX provides an additional number for each burst  $f_{Aex}^{Aem}$ , which represents the number of photons in the acceptor channel after direct excitation of the acceptor. Using that number, we can calculate the (raw) stoichiometry for each burst according to

$$S^{raw} = (f_{Dex}^{Dem} + f_{Dex}^{Aem}) / (f_{Dex}^{Dem} + f_{Dex}^{Aem} + f_{Aex}^{Aem}).$$

The stoichiometry represents the ratio of the total number of photons detected after donor excitation divided by the total number of photons detected in each



burst. We obtain  $S_{\text{raw}} \sim 1$  for donor-only species (as  $f_{A_{\text{ex}}}^{A_{\text{em}}} \sim 0$ ) and  $S_{\text{raw}} \sim 0$  for acceptor-only species (as  $f_{D_{\text{ex}}}^{D_{\text{em}}} + f_{D_{\text{ex}}}^{A_{\text{em}}} \sim 0$ ).

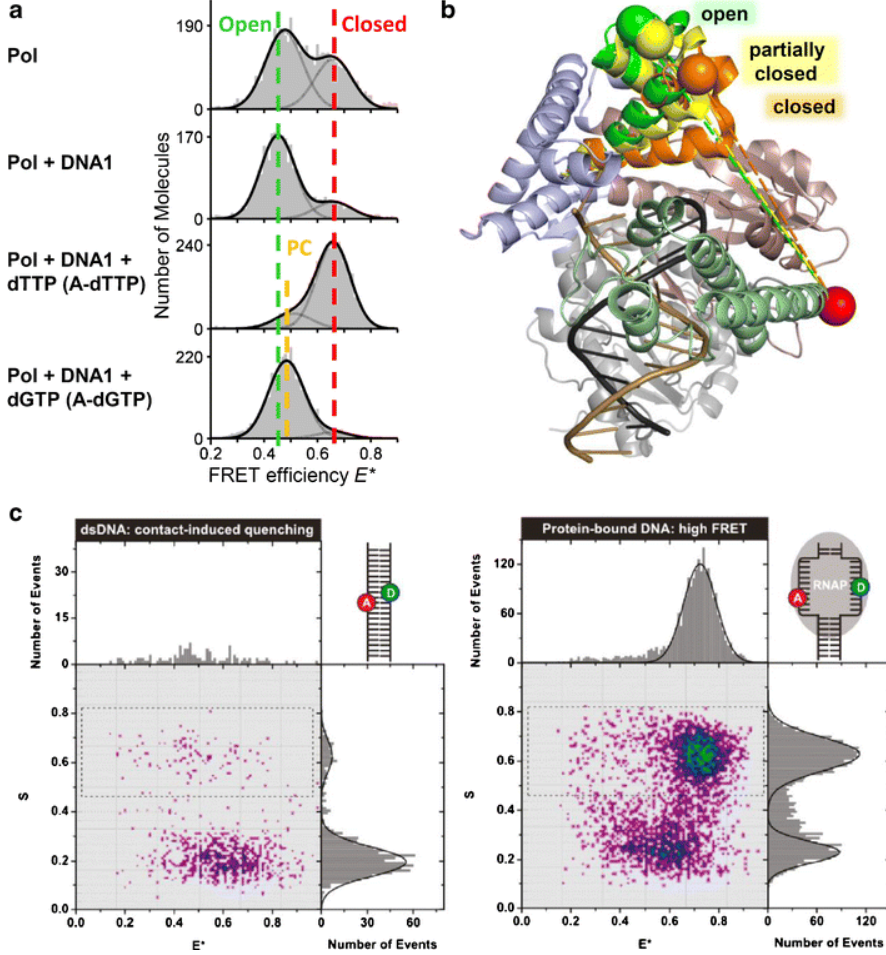


Figure 2: Applications of smFRET for studying DNA polymerases (a, b), adapted from reference (Hohlbein et al. 2013a) and RNA polymerases (c). (Reprinted with permission from Cordes et al. 2010. Copyright (2010) American Chemical Society). (a) Conformational landscapes of DNA polymerase 1 (Klenow fragment) (Hohlbein et al. 2013a). The unliganded enzymes show a dynamic equilibrium between at least two conformations of the fingers-subdomain. The binary complex of enzyme and DNA (with A as the templating base) shows an equilibrium shifted to the open conformation. Upon

## **Studying DNA-protein interactions with smFRET**

addition of correct nucleotide (1 mM dTTP), most molecules are the closed conformation, whereas the ternary complex formed with incorrect nucleotides (1mM dGTP) adopts a partially closed conformation. **(b)** Proposed crystal structures of the three conformations. The Pol–DNA binary complex (PDB accession code 1L3U, mobile section in green; Johnson et al. 2003) is superimposed on a ternary complex where the fingers adopt a partially closed conformation (PDB accession code 3HPO, mobile section in yellow; Wu and Beese 2011) and a ternary complex where the fingers adopt the closed conformation (PDB accession code 1LV5, mobile section in orange; Johnson et al. 2003). The distances between the C $\beta$  positions of residue 550 (red sphere) and 744 (sphere on the fingers) are 5.2 nm, 5.0 nm and 4.2 nm. The predicted distance change of 0.2 nm upon going from the open to the partially closed conformation is consistent with the observed shift of  $\Delta E^*=0.04$  seen in **(a)**. **(c)** Working principle of quFRET presented based on a two dimensional histogram of the transfer efficiency  $E^*$  versus the stoichiometry as introduced in the main text. Two fluorophores are attached in very close proximity on each strand of a dsDNA so that the fluorescence of both probes is suppressed and only the acceptor-only species is visible (left panel, low stoichiometry). Upon formation of the transcription bubble by a bacterial RNA polymerase, high FRET values are observed as the fluorophores do not quench each other anymore (right panel).

Depending on the relative count rates after donor and acceptor excitation, the (raw) stoichiometry for correctly labelled species bearing both donor and acceptor fluorophores can be tuned such that by plotting the corresponding  $E^*$  values versus the  $S^{\text{raw}}$  values for each burst in a two-dimensional ES histogram we can clearly separate this donor-acceptor species from species bearing only one active fluorophore (see also Fig. 2c, right panel). Moreover, we can resolve more complex binding mechanisms if, for example, two acceptor-labelled enzymes bind a donor-labelled DNA (Hohlbein et al. 2014b).

## **Imaging-based TIRF microscopy**

A major limitation of solution-based approaches is the short observation time dictated by the transit time of a molecule diffusing through the confocal volume (<3 ms). Therefore, a burst basically represents a snapshot of a molecule, but the history and fate of the particular molecule remains unknown. Immobilising molecules of interest on a surface can overcome the problem of the limited observation time and camera-based schemes such as TIRF microscopy allow for monitoring hundreds of single fluorescent molecules in parallel (Holden et al. 2010, Moerner and Fromm 2003). TIRF microscopy is based on the total internal reflection phenomena, in which an evanescent wave is generated, as light cannot enter from a medium with a high refractive index into a medium with a lower refractive index at an angle greater than a given critical angle. The intensity of the

evanescent wave decays exponentially within a few hundred nanometer above the glass surface, hence considerably reducing the background fluorescence from solution. Therefore, this methodology allows for monitoring higher concentrations of analytes in solution than diffusion-based confocal microscopy.

One main challenge for imaging-based single-molecule detection is the precise control of the photophysics of fluorophores. Premature photobleaching and photo-induced blinking of fluorophores limit the number of detectable photons, but these difficulties can be largely avoided by using additives for oxygen scavenging and triplet quenching or by using newly developed fluorophores (Cordes et al. 2009, Ha and Tinnefeld 2012, Rasnik et al. 2006a, Vogelsang et al. 2008, Zheng et al. 2014) making it nowadays possible to detect up to a million photons from a single Cy5 fluorophore (Zheng et al. 2014).

## **DNA processing enzymes**

A large number of the smFRET studies investigate the interactions between DNA and proteins. Modified DNA, for example labelled with a FRET pair of fluorophores, is commercially available and can be easily immobilised on a modified glass surface. After immobilisation, the DNA acts as a binding target for enzymes freely diffusing in solution. Whereas some interactions can be studied even without labelling the DNA processing enzyme, others use smFRET between two fluorophores attached to the enzyme and the DNA, respectively.

## **DNA polymerases**

In 1953, (Watson and Crick 1953) identified the double helix as the main structural element of salt DNA. The authors noted that pairing between both strands might be the basis for a copying mechanism. In fact, only several years later, the group of Arthur Kornberg identified a first enzyme in *Escherichia coli* that synthesized DNA based on a templating DNA strand (Lehman et al. 1958). The enzyme was simply termed "DNA polymerase" but later classified as DNA polymerase I, when it became evident that five different polymerases coexist in this organism (Hastings et al. 2010, Hübscher 2010a). The fidelity by which different polymerases incorporate nucleotides into a (growing) DNA strand is known to vary depending on the cellular role of the specific enzyme (Hübscher 2010b). *E. coli* DNA polymerases I and III, which are involved in DNA replication, have high fidelity with a frequency of correct incorporations in the order of 1,000,000:1. To achieve that accuracy, they are utilising their intrinsic 3'-5' exonuclease activity, which allows the removal of wrongly incorporated bases. *E. coli* DNA polymerases IV

and V, on the other hand, are involved in translesion DNA synthesis, in which the addition of any nucleotide to resolve the stalling of DNA replication is more important than adding the correct one and have therefore a lower fidelity. Knowledge about polymerase fidelity and its structural basis is important as it concerns the very basic level of information storage and genetic stability in a cell. X-ray crystal structures and NMR studies have been essential to shed light on nucleotide-polymerase interactions, but static structures are limited in their ability to provide insights in the dynamic processes that occur during nucleotide selection and incorporation.

One of the best studied DNA polymerases is *E. coli* DNA polymerase I (Klenow fragment), which is a cleavage product from bacterial DNA polymerase I (Klenow and Henningsen 1970). It possesses 5'-3' polymerase activity and 3'-5' exonuclease activity, but it lacks 5'-3' exonuclease activity from full-length Pol I. The structure of the Klenow fragment resembles a human right hand and consists of four subdomains: 3'-5' exonuclease, thumb, palm, and a so-called "fingers" subdomain, which is thought to have a particular important role in nucleotide selection and incorporation (Fig. 2a and b). It was shown that the "fingers" close during nucleotide selection, thereby transferring the nucleotide to the active site, where the next step involves incorporation of the nucleotide in the growing DNA strand (Johnson et al. 2003, Joyce et al. 2008, Wu and Beese 2011). As will be explained below, this "fingers closing" mechanism was found to contribute to the fidelity of the polymerase. A number of smFRET studies have improved our understanding of the conformational changes and dynamics that contribute to polymerase fidelity. Most studies described below used the exonuclease-deficient Klenow fragment (the exonuclease activity can be deactivated with a D424A substitution), as it is easier to handle and has only one internal cysteine, facilitating convenient labelling with organic fluorophores.

In a 2009 study, smFRET-based TIRF microscopy was used to visualise DNA synthesis (Christian et al. 2009a). A DNA template was labelled with a donor dye and Klenow fragment was labelled with an acceptor moiety at the back of the palm subdomain that is expected to be static towards the DNA during fingers opening and closing. An increase in distance between Klenow fragment and the donor attached to the DNA was observed as soon as the binary complex was provided with nucleotides (dNTPs) complementary to the bases forming the single-stranded DNA. This approach resulted in base pair resolution of the synthesis mechanism, and the observation of several distinct conformational changes related to nucleotide insertion. In a following publication, Markiewicz and co-workers studied the stability of the Klenow fragment-DNA complex in the presence of

different nucleotides using single-molecule protein-induced fluorescence enhancement (smPIFE; see (Hwang et al. 2011, Hwang and Myong 2014, Markiewicz et al. 2012). It was shown that correct (complementary) dNTPs stabilize the polymerase-DNA complex more than correct rNTPs, while all other incorrect nucleotides destabilize the complex. The authors suggested that a steric clash between the template and an incorrect nucleotide would lead to a higher dissociation constant of the complex as a whole. However, more incorrect nucleotides than correct nucleotides are present under physiological conditions. It was therefore hypothesized that an incorrect nucleotide may be rejected in a step preceding the steric clash to prevent disintegration of the polymerase-DNA complex.

In 2010, it was shown using confocal-based smFRET that the fingers closing mechanism of DNA Pol I does not only occur in a ternary complex of polymerase, (non-extendable) DNA and a correct nucleotide, but also in binary complexes composed of polymerase and DNA and even in the unliganded enzyme (Santoso et al. 2010a). The conformational landscape was probed by labelling the mobile part of the fingers subdomain with a donor and a static position on the thumb subdomain with an acceptor dye. Consequently, a change in FRET efficiency corresponds to a change in conformation: a higher FRET efficiency indicates a "fingers closed" conformation, while a lower efficiency marks an open conformation. Thus, Pol I is able to switch between different conformational states, though it depends on the complex which state is preferred. Binary complexes were mainly found in the open conformation, whereas ternary complexes with correct nucleotides were mostly found in the closed conformation. This study also introduced a new method for analysing smFRET data termed burst variance analysis (BVA). BVA is based on monitoring the standard deviation of FRET calculated from small photon numbers within each burst and allows handlers to distinguish between static and dynamic heterogeneity in a sample (Torella et al. 2011). In the experiments on Pol I, BVA revealed the presence of conformational dynamics in the unliganded polymerase in absence of both DNA and nucleotides (Santoso et al. 2010a). This result suggested that fingers closing are not necessarily an indication for successful incorporation of a nucleotide and those other mechanisms are in place to check nucleotides for their compatibility to the base of the templating DNA strand before they are incorporated.

More support for this model came from the fact that the fingers do not close completely in ternary complexes with mispaired dNTPs or when ribonucleotides are added (Hohlbein et al. 2013, Santoso et al. 2010a). Instead, molecules were observed showing a mean FRET efficiency only slightly higher than the one

indicating the open conformation (Fig. 2a and b). Seemingly, Pol I can detect a mispair before full fingers closing would occur. This suggests that one or more intermediate states exist, in which the incoming nucleotide is previewed and subsequently rejected or incorporated in the DNA. In 2011, a crystal structure of *Bst* Pol I (a close structural homologue to *E. coli* Pol I) bound to DNA was published (Wu and Beese 2011). This crystal structure revealed the presence of an intermediate (ajar) conformation of the fingers subdomain when bound to an incorrect nucleotide. Recent smFRET-based studies have identified an intermediate conformation as being present in ternary complexes with incorrect nucleotides (Berezhna et al. 2012) and two studies found direct evidence for the population of an intermediate state even in the presence of correct nucleotide substrates (Hohlbein et al. 2013, Rothwell et al. 2013).

The identification of three instead of two different conformations of the fingers domain raises the question how the polymerase interconverts between these states and how that depends on the type of complex formed. Both, Rothwell and co-workers and Hohlbein and co-workers analysed the equilibrium conditions and possible transitions and dynamics between the open, closed and intermediate conformation. Variants of probability distribution analysis (PDA) were used for predicting FRET efficiency distributions from a mixture of static or dynamically interconverting FRET species (Antonik et al. 2006, Kalinin et al. 2007, Kalinin et al. 2008, Nir et al. 2006, Santoso et al. 2010b). A comparison between experimental data and data generated by PDA allows for the identification and characterization of (dynamic) subspecies. In addition, (Hohlbein et al. 2013) used wild-type Klenow fragment and mutator derivatives with decreased fidelity to calculate a free energy landscape in which the partially closed state was identified as a major fidelity checkpoint for nucleotide insertion.

The Klenow fragment 3'-5' exonuclease (exo) domain, which catalyses the excision of mismatched nucleotides, has also been subject of single-molecule studies. Using an smFRET approach, it was shown that mismatched primer-template termini bind to the polymerase in a different orientation than matched termini (Markiewicz et al. 2012). In a similar study, the static thumb subdomain and the DNA primer strand were labelled with a FRET pair (Lamichhane et al. 2013). Using this approach, the binding of Klenow fragment to the template-primer duplex was shown, but also an unexpected switching of the DNA between the pol and exo domains was observed. This finding is in contradiction to the data presented by Markiewicz and co-workers, in which exclusive binding of mismatched DNA in the exo site rather than switching of DNA between two positions was suggested. In both studies, the DNA was labelled several base pairs away from the mismatch,

but the labelling position chosen by Lamichhane and co-workers may have been optimized to report on DNA switching. Lamichhane and co-workers found that internal mismatches in the DNA increased the rate of switching between the pol and exo site, which agrees with wrongly inserted nucleotides being excised at the exo domain. Addition of dNTPs also influences pol–exo switching: if the primer terminus is correctly base-paired, a dNTP stabilizes the DNA in the pol site. However, if the primer terminus is mispaired, the same dNTP accelerates switching of the template to the exo domain. Even dNTPs that do not form a correct new base pair (any of the three others) are able to accelerate binding of an already mispaired primer terminus to the exo domain. This means that even incorrect nucleotides have an active role in processes to increase polymerase fidelity. This counterintuitive result is in line with an earlier observation by the same group (Berezina et al. 2012) in which they showed that primer termini are moved to the exo domain when incorrect nucleotides are trapped in the "ajar" conformation.

Taken together, smFRET has been successfully used to study conformational changes and conformational dynamics within DNA polymerases and between DNA polymerases and DNA. For the studied derivatives of DNA polymerase I, the newly characterized partially closed ('ajar') conformation appears to play an important role as a fidelity checkpoint. Whether this intermediate state is present in other DNA polymerases and whether the conformational dynamics can be linked to fidelity and DNA catalysis will be the subject of upcoming research.

## **RNA polymerases**

RNA polymerases (RNAPs) facilitate the transcription of DNA into RNA, which stands at the basis of protein synthesis. As for DNA polymerases, much of our current knowledge of RNAPs is derived from X-ray crystal structures and ensemble studies. Single molecule studies on RNAPs have mainly focussed on two species: bacterial RNAP and eukaryotic RNA polymerase II (Pol II). Both RNAPs follow the same general sequence of events for transcription initiation (Zhang et al. 2012). First, the polymerase binds to promoter regions on the DNA to form a so-called "closed complex". Second, local melting of the DNA results in the formation of a so-called "transcription bubble", which forms an "open complex" together with the polymerase. As soon as the open complex starts transcription, it is called an "initial transcribing complex". RNA synthesis is often limited to short RNA products in the first stage of transcription. Once a polymerase produces a longer RNA product (~10 nucleotides for RNAP and ~3 nucleotides for Pol II), it enters a stage of processive RNA synthesis. This event triggers release of initiation factors

## ***Studying DNA-protein interactions with smFRET***

and the polymerase leaves the promoter region, leading to the formation of a polymerase-DNA "elongation complex" (as reviewed by (Hahn 2004, Saecker et al. 2011)).

In 2006, (Kapanidis et al. 2006) evaluated three proposed models for initial transcription by the RNAP initial transcribing complex. The models were based on observations showing the formation of RNA products, even when the polymerase did not appear to move along the DNA. The first model stated that RNAP moves along the DNA as a unit, but returns to its initial position after release of RNA (Carpousis and Gralla 1985). The second model involved stretching of a flexible element in RNAP, resulting in movement relative to the DNA of the leading, but not the trailing edge of the polymerase (Krummel and Chamberlin 1989, Straney and Crothers 1987). A third model stated that the polymerase itself does not move. In contrast, this model predicted expansion and contraction of the DNA strand, called "scrunching" (Carpousis and Gralla 1985, Hsu 2002, Pal et al. 2005). In order to determine which model is correct, Kapanidis and co-workers monitored FRET changes between different elements of the complex labelled with donor and acceptor dyes by means of smFRET. rNTPs were added to RNAP-DNA complexes to start transcription. A FRET change in agreement with one of the models was only found for a donor-acceptor pair located on the DNA: upon addition of rNTPs an increase in FRET efficiency was observed, indicating a decrease in distance, which ultimately proved that the third "DNA scrunching" model is correct.

A new technique called quenchable FRET (quFRET; Fig. 2c) was developed by Cordes et al. to study DNA melting after formation of the open complex (Cordes et al. 2010). Quenchable FRET relies on contact-induced quenching of two dyes as long as they are in close proximity ( $<2$  nm). The authors placed a FRET donor (Cy3B) on the first DNA strand and an acceptor (ATTO647N) on the complementary strand. As soon as both strands were annealed, fluorescence detectable from both dyes was greatly diminished. Upon formation of the transcription bubble in the RNAP open complex, dequenching accompanied by a high FRET efficiency was observed. The authors used this principle to derive rate constants for the formation of the open complex and showed that quFRET can be used as a quantitative tool.

RNAP contains a clamp structure that is known to open and close. The dynamics of this opening and closing are thought to be important during RNAP complex formation: the open state allows for accommodation of dsDNA, while the closed state can only accommodate ssDNA (Cramer et al. 2001, Gnatt et al. 2001, Murakami et al. 2002, Zhang et al. 1999). A third "collapsed" state does not leave



room for any DNA. (Chakraborty et al. 2012) labelled the clamp with a FRET donor and an immobile part on the enzyme with a FRET acceptor, in order to study the conformational dynamics of the clamp. Free RNAP holo-enzyme showed a FRET efficiency distribution that can be fitted with three Gaussian functions, each of which can be attributed to a different state of the clamp: open, closed and collapsed. The open state appeared to be the predominant state. It remained predominant during formation of the closed complex. Upon formation of the open complex, however, the clamp adopts only the closed state. This is also the case for the initial transcribing complex and the elongation complex. These results suggest that the clamp is triggered to close only after interaction with ssDNA in the open complex.

Eukaryotic Pol II requires the concerted action of several different transcription factors (TFs) to regulate transcription initiation. Studies on Pol II have therefore focussed on the path of the growing RNA strand and the positions of various TFs in the initiation and elongation complexes. TFIIB is such a TF and is associated with the polymerase. It aids in the attachment of promoter DNA and TATA box binding protein (TBP) to the enzyme (the term "TATA box" refers to the name of a recognition element for TFs in the promoter sequence). (Andrecka et al. 2008) found evidence for eventual complete TFIIB displacement from Pol II, as it showed that the growing RNA chain in the elongation complex interacts with the same dock domain as TFIIB. In their later work, (Muschielok et al. 2008b) used their Nano Positioning System (NPS) to study this interaction again. They found that the TF remains associated to the dock domain longer than they initially expected. This could mean that TFIIB might have a role in guiding the new RNA strand to the Rpb4/7 substructure of the polymerase, which is of physiological importance as this substructure has a role in recruitment of 3' end processing factors (Runner et al. 2008).

In 2012, (Treutlein et al. 2012) published an extensive study in which they constructed a model for a minimal Pol II open promoter complex. This model included a TATA box, a mismatched DNA region, TBP, Pol II and transcription factors TFIIB and TFIIF. The model was constructed using known X-ray crystal structures and smFRET. The NPS combined data from these two techniques to make accurate predictions about the location of several subunits in the complex. Using this setup, it was found that the B core of TFIIB is displaced in the open complex, but it is likely that it still interacts with DNA and the TATA box binding protein. Furthermore, the authors found that the open complex has TBP and TATA DNA located above the cleft. Downstream DNA was found to switch between a position inside the cleft of the enzyme and a position on top of the cleft. This

switch occurs on a timescale of seconds and is therefore considered to be an important kinetic trap. Detection of this kind of flexible behaviour is an excellent example of the strength of smFRET studies: indeed, this switching of DNA is exactly the reason why the Pol II open complex could not be trapped crystallographically before.

### **DNA helicases**

Helicases are motor proteins that separate double stranded nucleic acids such as DNA, RNA or DNA-RNA hybrids by using energy derived from ATP hydrolysis (Lohman 1992). In DNA replication, for example, DNA helicases unzip dsDNA starting from a position known as replication origin. DNA helicases unwind DNA by breaking the hydrogen bonds that keep the two strands of DNA together, thereby forming the replication fork in which the separated strands serve as template strands for leading and lagging strand DNA synthesis.

Various single-molecule techniques have contributed to a better mechanistic understanding of helicase activity (Kim and Ha 2013, Yodh et al. 2010). Here we will focus on assays utilising smFRET as a high precision technique to monitor the structural change in DNA upon interaction with DNA helicases.

In 2002, Ha and co-workers studied the mechanism by which *E. coli* Rep helicase initiates DNA unwinding (Ha et al. 2002). They immobilised DNA molecules consisting of a short DNA duplex and a single-stranded overhang on a glass surface. TIRF microscopy was applied to detect the fluorophores that were attached on opposite strands at the junction between single- and double-stranded DNA. Rep helicase was found to bind to the single-stranded DNA and then to shuttle towards the junction fuelled by ATP hydrolysis. Upon binding to the junction, fluctuations in the FRET efficiency indicated conformational fluctuations of the DNA, but processive unwinding only occurred after binding of an additional protein. Their analysis suggested that the limited unwinding observed in vitro for Rep is due to the relative instability of the functional complex, caused by DNA rewinding upon complex dissociation and rounds of reinitiation upon reformation of the functional helicase complex.

In 2004, Resnik and co-workers developed an assay for site-specifically labelling of REP helicase (Rasnik et al. 2006b) that was later used to monitor repetitive shuttling of REP along single-stranded DNA (Myong et al. 2005). Interestingly, after moving in the 3' to 5' direction of the single stranded DNA using ATP hydrolysis, Rep snaps back close to the 3' end, a mechanism likely to be caused by a conformational change of the protein after approaching the DNA junction. It was

hypothesised that the shuttling of the DNA helicase along ssDNA might be an effective way of clearing the DNA from unwanted, bound molecules.

The hepatitis C virus NS3 protein is a bifunctional helicase that can unwind both DNA and RNA substrates. It was shown in 2007 that that NS3 unwinds DNA in discrete steps of about 3 bp (Myong et al. 2007). The fluorescence assay consisted of a double-stranded DNA, labelled with fluorophores on each strand at the DNA junction where one strand continued with single stranded DNA. Unwinding led to a stepwise decrease in FRET efficiency, and six steps were found for the 18-bp-long double-stranded DNA. As the dwell time histogram showed non-exponential behaviour, the authors fitted a Gamma distribution suggesting that every 3-bp step is composed of three hidden steps of one base pair each. Using additional experiments, the authors suggested a model in which, based on the three domains of NS3, domains 1 and 2 move along the tracking strand (3' to 5') one nucleotide at a time, consuming one ATP for each base pair. The third domain stays behind by attaching itself to the DNA until three of such steps have taken place. After the third step, the domain 3 moves forward in a burst motion, unzipping 3 bp as a consequence. NS3 continues unwinding in 3-bp steps until 18 bp. On longer duplexes, the helicases showed repetitive unwinding.

## **DNA topoisomerases, DNA recombinases and transcription factors**

In this part, we will briefly discuss two important classes of DNA processing enzymes that allow the cutting and re-joining of DNA, DNA topoisomerases and DNA recombinases, before continuing with a short discussion about DNA transcription factors (TF).

DNA topoisomerases regulate DNA supercoiling, which is a consequence of the varying DNA topology ranging from densely packed DNA to accessible DNA required for DNA replication and transcription. DNA gyrase, for example, is a type II topoisomerase found mainly in prokaryotes. The enzyme is capable of introducing negative supercoiling using ATP hydrolysis. Tension that builds up after the unwinding of DNA is revealed by cutting the strands and re-annealing them after the enzyme passed a different DNA segment through. One recent study of this DNA-gate conformation using single molecule FRET claimed that high and low FRET states, corresponding to open and closed conformations of the DNA gate, are equally populated in topoisomerase II (Smiley et al. 2007). By directly monitoring the conformational state of the DNA gate in DNA gyrase, it was found that the gate is mainly closed and gate opening is a rare event that

## ***Studying DNA-protein interactions with smFRET***

occurs only briefly to allow the transfer DNA to pass (Gubaev et al. 2009). Further studies on GyrA, which is a subunit of the heterotetrameric DNA gyrase, elucidated how binding of DNA to the DNA binding region affects the conformational cycle for supercoiling DNA by DNA gyrase (Lanz and Klostermeier 2011, Lanz and Klostermeier 2012). A recent report by (Lee et al. 2012) on human topoisomerase II $\alpha$  revealed that cleavage and opening of DNA is tightly regulated by magnesium ions controlling the bending of gate-DNA. By visualizing the individual steps of the DNA cleaving reaction, the authors shed light on the mechanism, by which the probability of accidental double-strand breaks is minimised (Fig. 3a and b).

The second class of enzymes, DNA recombinases, plays an important role in the cellular rearrangement of DNA required, for example, in chromosome segregation. Two recent publications investigated the mechanics of site-specific recombination using Cre-*loxP* (Pinkney et al. 2012) and XerCD-*dif* complexes (Zawadzki et al. 2013). SmFRET was utilised to monitor the formation of the synaptic complex. A donor and acceptor fluorophore were placed close to both target sites, which were initially well separated (Fig. 3c and d). Upon complex formation, both target sites are brought together and FRET can occur between the fluorophores. Interestingly, both publications used up to three independent observables from single fluorescent molecules: (1) FRET, (2) size of the fitted point spread function (PSF), and (3) protein-induced fluorescence enhancement (PIFE; (Hwang et al. 2011)) to monitor short- and long-ranged conformational changes of the DNA induced via recombination complexes.

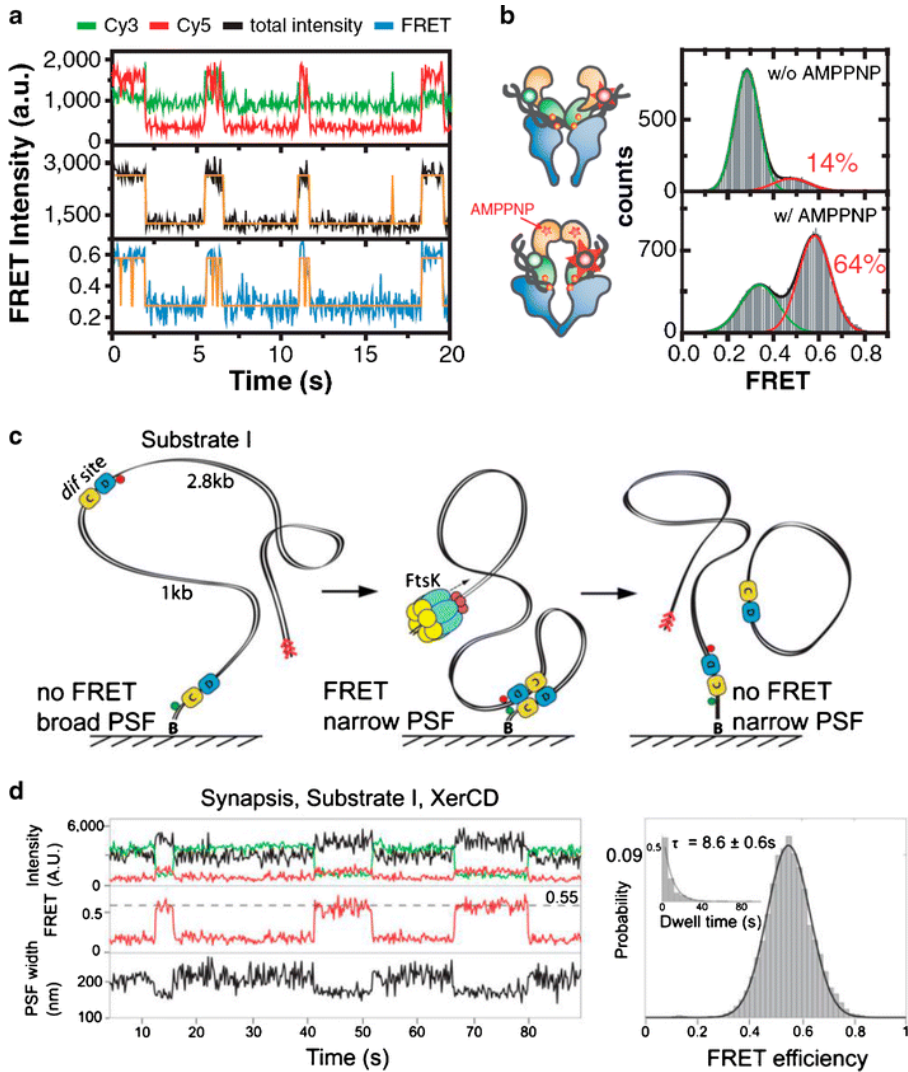


Figure 3: Applications of smFRET for studying topoisomerases (**a** and **b** reprinted with permission from Lee et al. 2012) and DNA recombination complexes (**c** and **d**, reprinted with permission from Zawadzki et al. 2013). (**a**) Representative fluorescence intensity and FRET time traces of fluorescently labelled cleavable DNA containing the binding site of human topoisomerase IIa. Upon binding of the enzyme and in the presence of AMPPNP (a non hydrolysable analogue of ATP), the intensity of the donor increases due to protein induced fluorescence enhancement and an increase in FRET indicates a conformational change of the complex of DNA and enzyme. (**b**) The FRET histograms with AMPPNP (bottom) and without AMPPNP (top) show that the gate clamping induces a substantial deformation of the DNA gate. (**c**) Schematic representation of the recombination reaction. The long DNA has the fluorophores (indicated with red and green circles) attached adjacent

## **Studying DNA-protein interactions with smFRET**

to each dif site. Recombination can be monitored using FRET between donor and acceptor and the width of the point spread function (PSF) after direct excitation of the acceptor. Successful recombination between the dif sites leads to formation of two DNA molecules. The red arrow heads indicate the preferential binding site for FtsK. **(d)** Formation of nonproductive synaptic complexes is indicated by two observables: (1) an increase in FRET calculated using the intensities of donor (green) and acceptor (red) under donor excitation and (2) an increase in fluorescence intensity detected after direct excitation of the acceptor (black) and an decrease in the fitted PSF width as the acceptor is brought closer to the surface. The histogram (right) show the distributions of FRET efficiencies ( $E^*$ ) and the dwell times (inset) of XerCD–dif synaptic complexes.

The precise control of gene expression is essential for every living cell and therefore tightly controlled by DNA binding proteins known as transcription factors (TF). TFs act as natural biosensors and switches modulating gene expression of target genes by either promoting or blocking the recruitment of RNAPs. Several human diseases such as diabetes, autoimmune diseases, and cancer have been linked to mutations in TFs such as p53 (Vogelstein et al. 2000). Therefore, assays for efficient detection of transcriptions factors are highly desirable as they might provide a platform for diagnostics. In 2010, TF-dependent DNA coincidence was detected using ALEX spectroscopy (Lymperopoulos et al. 2010). In the presented assay, two DNA half sites labelled with donor and acceptor, respectively, contain a complementary region of ssDNA that forms the binding site of the catabolite activator protein (CAP) TF. Without the presence of a TF, the binding of the complementary half sites is too weak to form a stable complex as indicated by a single peak in the stoichiometry histogram which reports on the number of different species in the solution bearing an acceptor fluorophore. Upon addition of CAP, the binding of both DNA half sites is stabilised and a second peak can be seen in the histogram. Depending on the concentration of half sites, TF concentrations in the low nanomolar range are detectable. Based on this TF assay, the encapsulation and entrapment of CAP inside a DNA cage was successfully demonstrated (Crawford et al. 2013). Within the cage, which is based on a DNA tetrahedron, the TF is inactive and cannot bind to cellular DNA. Using acceptor labelled

CAP and a donor labelled cage, it was confirmed that CAP is positioned within the cage. Moreover, DNase I was shown to degrade the cage leading to a release of CAP. A different assay was used to detect the binding of CAP via binding-induced bending of a doubly labelled DNA construct containing the CAP binding site (Crawford et al. 2012).

## Increasing the information content of smFRET experiments

In this section, we will highlight some recent developments utilising dual-colour FRET between one donor and one acceptor. For publications introducing three- or four-colour FRET, we refer the reader to reviews elsewhere (Hohlbein et al. 2010, Hohng et al. 2014, Kim and Ha 2013).

## Combining smFRET with force-based techniques

In the following, we will briefly discuss some recent developments aiming to combine fluorescence-based techniques with force-based techniques such as atomic force microscopy (AFM), optical tweezers and magnetic tweezers. Many designs, often based on DNA spanned between a glass surface and a moveable bead, have been envisioned as early as 1999 (Weiss 1999). The experimental realisation, however, has proven to be very challenging and widespread use has not yet been achieved, despite their promise of providing new means of studying the sub-molecular structure, conformational dynamics and transition states of biological systems. We refer the interested reader to recent reviews, which discuss potential merits in greater detail (Hohlbein et al. 2010, Hohng et al. 2014, Kapanidis and Strick 2009, Kim and Ha 2013).

AFM has initially been developed for topographical imaging of molecules (Binnig et al. 1986). This technique uses a tip that is scanned along the sample surface and the deflection of the tip is measured using a laser and a photo detector. The combination of AFM with single-molecule-based TIRF microscopy was demonstrated by (Hugel et al. 2002), who investigated extension of a polymer made of bistable photosensitive azobenzenes, and by (Sarkar et al. 2004), who measured the forced unfolding of ubiquitin after calibrating the distance-dependent intensity decay of an evanescent wave using AFM. The promising combination of AFM and TIRF was reviewed in (Shaw et al. 2006). A combination of (ensemble-based) FRET and AFM was shown by Vickery (Vickery and Dunn 2001) and by (Nakamura et al. 2007), but only very recently was the combination of smFRET and AFM demonstrated (He et al. 2012, Lu 2014).

Rapid progress has been achieved for the combination of smFRET with optical tweezers, which utilize an infrared laser to trap and control the position of a bead. By spanning a single DNA molecule between the surface of the bead and the surface of the cover slide (or a pipette tip), strain can be applied simply by moving the bead in respect to the cover slide and the relative position of the bead can be imaged using a camera. The combination of an optical trap and single-molecule

## ***Studying DNA-protein interactions with smFRET***

fluorescence detection in the visible spectrum was shown in 2003 (Lang et al. 2003). Brau et al. (2006) improved the longevity of the fluorophore, which normally severely suffers from photo damage caused by the infrared laser, by alternating between bead trapping and direct excitation of the fluorophore. Combinations of optical tweezers with smFRET detection were successfully demonstrated in 2007 (Tarsa et al. 2007; Hohng et al. 2007) by Tarsa and co-workers using smFRET to monitor the opening and closing of a DNA hairpin whilst being under tension applied via the optical trap. Likewise, Hohng et al. (2007) mapped the reaction landscape of DNA Holliday junctions, which is a four-stranded DNA structure that switches between open and closed stacking conformations. In a series of beautiful force-fluorescence experiments, Zhou et al. (2011) studied the behaviour of the single-stranded DNA binding protein (SSB) interacting with DNA (Fig. 4). The authors showed that ssDNA bound to SSB unravels at low forces ( $<6$  pN) and that larger forces lead to the dissociation of SSB. More intriguingly, the authors also found that ssDNA migrates on SSB via reptation rather than that SSB rolls around the DNA.



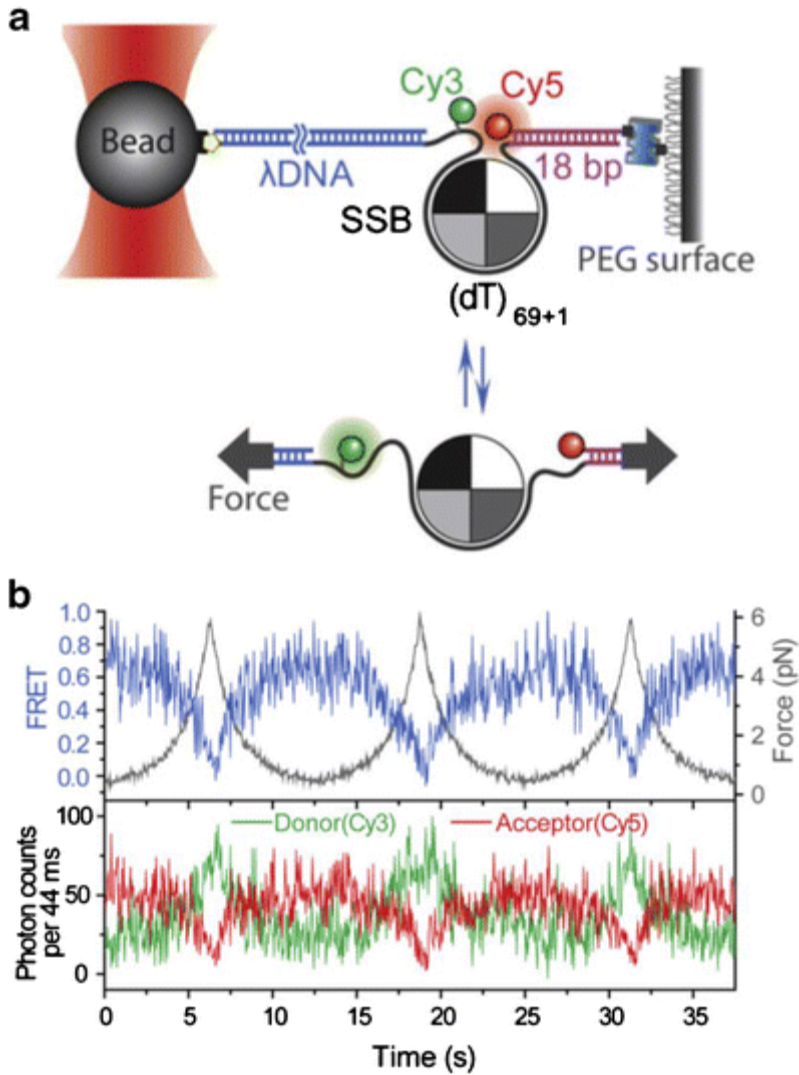


Figure 4: Combining smFRET with force-based techniques reprinted from Zhou et al. (2011), with permission from Elsevier. **(a)** The experimental scheme shows a DNA molecule attached between a PEGylated glass surface (right) and a bead (left). The bead is optically trapped and can therefore be used to pull the DNA containing a region of single-stranded DNA to which the single stranded binding protein (SSB) is bound. Unraveling of ssDNA is expected to increase the distance between donor and acceptor. **(b)** The experimental realisation shows that increasing the pulling force at low levels leads to an unraveling of ssDNA indicated by a decrease in FRET and a clear anticorrelation of the donor and acceptor intensity. The process of unravelling is reversible and larger forces (not shown here) leads to dissociation of SSB.

Another candidate for applying forces are magnetic tweezers, in which a small magnetic bead allows the application of strain and even torque to a surface-immobilised DNA molecule. In addition, magnetic tweezers do not cause photo bleaching of fluorophores which is advantageous to maximise observation time. In 2005, Shroff et al. (2005) showed that changing the distance between a FRET pair can be used to calibrate the force response of a DNA sensor. Lee et al. (2010) showed that negative superhelicity of DNA and low tension induced by magnetic tweezers is sufficient to trigger the formation of Z-DNA formation deviating from the canonical B-DNA. By labelling the DNA on both strands of a CG core strand, the appearance of Z-DNA was indicated by an increase in distance between the fluorophores and therefore a decrease of the FRET efficiency. Very recently, Long et al. (2013) probed the force-depended unfolding of G-quadruplex DNA. Again, smFRET was used to probe the conformational change in the nanometer range showing that the transition-state barrier for unfolding is closer to the unfolded state than the folded state of the complex.

### **Quantitative smFRET and computer-aided modelling**

Even though smFRET has been coined as a molecular ruler, converting FRET efficiencies to actual distances requires careful corrections to account for background fluorescence and the spectral properties of the fluorophores (Lee et al. 2005; Hohlbein et al. 2013b). An important factor that needs to be considered is that any calculated FRET distance refers to the distance between the emission dipole of the donor and the excitation dipole of the acceptor fluorophore and not to the distance between the points of attachment on the DNA or the enzyme of interest. This notion is particularly important as most fluorophores are attached by means of flexible linkers, thus the position of the fluorophore in respect to the DNA or the enzyme is rarely static. Instead, the fluorophore resembles a certain accessible volume. This will result in a distribution of possible values of the orientation factor  $\kappa^2$  and distances between dipole and residue, causing a potential discrepancy between the distance of interest and the actual distance derived from smFRET.

Several methods have been developed to improve the quality of distance information that can be extracted from smFRET data (Craggs and Kapanidis 2012). In 2008, Muschielok and co-workers introduced a method called NPS (thereby aptly referring to GPS) (Muschielok et al. 2008). It uses a system comprising a so-called antenna dye molecule and several satellite dye molecules to calculate a three-dimensional probability distribution of dye positions. Additionally, information such as the accessible volume derived from X-ray crystallography

structures can be taken into account. The calculated dye positions reflect experimental uncertainties, as opposed to previous methods that were only able to show the most likely dye position. In 2011, NPS was extended by taking FRET anisotropy into account. The inclusion of average transition dipole moments of the dyes significantly improved localization accuracy (Muschielok and Michaelis 2011).

Another comprehensive framework for combining quantitative smFRET measurements and molecular modelling named FPS (FRET-restrained positioning and screening) was introduced in 2012 (Kalinin et al. 2012). FPS consists of overall six steps as shown in Fig. 5. In step one, a starting model is created, which includes all known information about a system such as

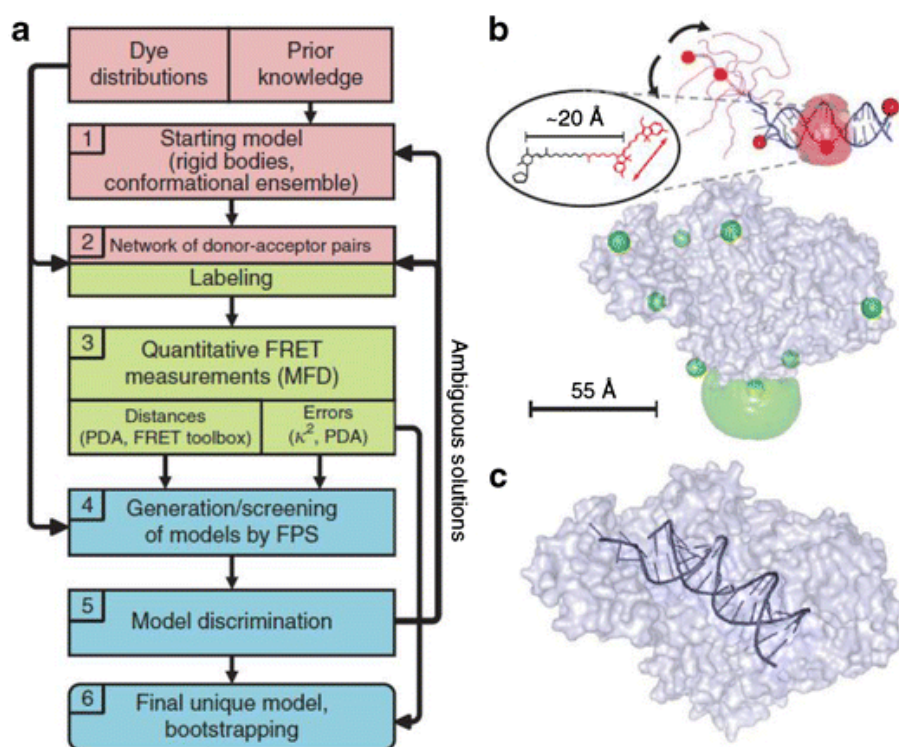


Figure 5: The FRET-restrained positioning and screening (FPS) framework (reprinted with permission from Kalinin et al. 2012, Macmillan Publishers Ltd, copyright 2012). **a** FPS consists of three main parts: (1) experimental design, (2) measurement and analysis, and (3) structural modelling and validation. **b** The structure of HIV-1 reverse transcriptase (PDB accession code 1R0A; Peletskaya et al. 2004) was separated into protein (grey) and dsDNA (blue). The different labelling positions for the acceptor on the DNA (red) and for the donor on the protein (green) are indicated. Clouds around the labelling positions

## **Studying DNA-protein interactions with smFRET**

*indicate the accessible volume of the fluorophores. Potential solutions of the unresolved ssDNA are shown in magenta. c Structural model of the joined complex obtained after rigid-body docking.*

crystal structures or known conformational changes. In step two, a network of donor-acceptor pairs (similar to antennas and satellites as described above) is designed. After sample preparation, single-molecule multiparameter fluorescence detection (MFD) measurements are performed to obtain the required distances (step three). The (diffusion-based) MFD scheme includes measurements of the fluorescence lifetime and the anisotropy in addition to the fluorescence intensity information (Rothwell et al. 2003; Widengren et al. 2006). The smFRET data is used to generate new models (step four), which are then checked against the initial model in step five. At this point, it might be necessary to revert to step one or two and develop a model that is expected to fit FRET data better. In the final step, a procedure in which noise is added to the calculated set of distances is performed to determine the precision of the model. Using their approach, the authors generated a detailed model for DNA bound to HIV-1 reverse transcriptase, adding a part of the structure that has not been resolved by X-ray crystallography before. More importantly, FRET-based structural modelling allows utilising position data derived from transient conformational states, which are often difficult to trap in X-ray crystallography.

## **Conclusion**

In the past 20 years, smFRET has emerged as an undisputable powerful tool to elucidate biological processes on the molecular level. Using smFRET-based techniques, researchers are able to study samples under close to physiologically relevant conditions whilst having access to sub-nanometre accuracy to study (dynamic) interactions of and between single-molecules. Especially the study of DNA-protein interactions has greatly benefited, as many interactions can be studied using commercially available, fluorescently labelled DNA. Many previous issues such as premature photo bleaching and the lack of algorithms and software to analyse data have been largely addressed (for an overview of available software packages, see Preus and Wilhelmsson 2012), and we hope that the threshold for applying smFRET can be further reduced especially by developing easier labelling strategies for proteins and providing access and support to software and instrumentation. In the coming years, we expect smFRET to gain further popularity as a tool for structural and molecular biology.

## Acknowledgments

We thank Herbert van Amerongen and Arjen Bader for critically reading the manuscript and providing helpful suggestions. S.F. acknowledges funding from the Foundation for Fundamental Research on Matter (FOM), which is part of the Netherlands Organisation for Scientific Research (NWO).

## References

- ANDRECKA J, LEWIS R, BRÜCKNER F, LEHMANN E, CRAMER P AND MICHAELIS J. 2008. Single-molecule tracking of mRNA exiting from RNA polymerase II. *Proceedings of the National Academy of Sciences* 105: 135-140.
- ANTONIK M, FELEKYAN S, GAIDUK A AND SEIDEL CA. 2006. Separating structural heterogeneities from stochastic variations in fluorescence resonance energy transfer distributions via photon distribution analysis. *The journal of physical chemistry B* 110: 6970-6978.
- BEREZHNA SY, GILL JP, LAMICHHANE R AND MILLAR DP. 2012. Single-Molecule Förster Resonance Energy Transfer Reveals an Innate Fidelity Checkpoint in DNA Polymerase I. *Journal of the American Chemical Society* 134: 11261-11268.
- BINNIG G, QUATE CF AND GERBER C. 1986. Atomic Force Microscope. *Physical review letters* 56: 930-933.
- CARPOUSIS AJ AND GRALLA JD. 1985. Interaction of RNA polymerase with lacUV5 promoter DNA during mRNA initiation and elongation. Footprinting, methylation, and rifampicin-sensitivity changes accompanying transcription initiation. *Journal of molecular biology* 183: 165-177.
- CHAKRABORTY A ET AL. 2012. Opening and Closing of the Bacterial RNA Polymerase Clamp. *Science* 337: 591-595.
- CHRISTIAN TD, ROMANO LJ AND RUEDA D. 2009. Single-molecule measurements of synthesis by DNA polymerase with base-pair resolution. *Proceedings of the National Academy of Sciences* 106: 21109-21114.
- CLEGG RM. 1992. Fluorescence resonance energy transfer and nucleic acids. *Methods in enzymology* 211: 353-388.
- CORDES T, SANTOSO Y, TOMESCU AI, GRYTE K, HWANG LC, CAMARÁ B, WIGNESHWERARAJ S AND KAPANIDIS AN. 2010. Sensing DNA Opening in Transcription Using Quenchable Förster Resonance Energy Transfer. *Biochemistry* 49: 9171-9180.
- CORDES T, VOGELSANG J AND TINNEFELD P. 2009. On the mechanism of Trolox as antiblinking and antibleaching reagent. *Journal of the American Chemical Society* 131: 5018-5019.
- CRAMER P, BUSHNELL DA AND KORNBERG RD. 2001. Structural Basis of Transcription: RNA Polymerase II at 2.8 Ångstrom Resolution. *Science* 292: 1863-1876.
- CRAWFORD R, ERBEN CM, PERIZ J, HALL LM, BROWN T, TURBERFIELD AJ AND KAPANIDIS AN. 2013. Non-covalent Single Transcription Factor Encapsulation Inside a DNA Cage. *Angewandte Chemie International Edition* 52: 2284-2288.

## ***Studying DNA-protein interactions with smFRET***

- CRAWFORD R, KELLY DJ AND KAPANIDIS AN. 2012. A Protein Biosensor That Relies on Bending of Single DNA Molecules. *Chemphyschem : a European journal of chemical physics and physical chemistry* 13: 918-922.
- DALE RE, EISINGER J AND BLUMBERG WE. 1979. The orientational freedom of molecular probes. The orientation factor in intramolecular energy transfer. *Biophysical journal* 26: 161-193.
- DENIZ AA, DAHAN M, GRUNWELL JR, HA T, FAULHABER AE, CHEMLA DS, WEISS S AND SCHULTZ PG. 1999. Single-pair fluorescence resonance energy transfer on freely diffusing molecules: Observation of Förster distance dependence and subpopulations. *Proceedings of the National Academy of Sciences* 96: 3670-3675.
- DENIZ AA, MUKHOPADHYAY S AND LEMKE EA. 2008. Single-molecule biophysics: at the interface of biology, physics and chemistry. *Journal of The Royal Society Interface* 5: 15-45.
- FÖRSTER T. 1948. Zwischenmolekulare Energiewanderung und Fluoreszenz. *Ann Phys* 437: 55-75.
- FOSTER MP, MCELROY CA AND AMERO CD. 2007. Solution NMR of Large Molecules and Assemblies. *Biochemistry* 46: 331-340.
- GNATT AL, CRAMER P, FU J, BUSHNELL DA AND KORNBERG RD. 2001. Structural Basis of Transcription: An RNA Polymerase II Elongation Complex at 3.3 Å Resolution. *Science* 292: 1876-1882.
- GUBAEV A, HILBERT M AND KLOSTERMEIER D. 2009. The DNA-gate of *Bacillus subtilis* gyrase is predominantly in the closed conformation during the DNA supercoiling reaction. *Proceedings of the National Academy of Sciences* 106: 13278-13283.
- HA T, ENDERLE T, OGLETREE DF, CHEMLA DS, SELVIN PR AND WEISS S. 1996. Probing the interaction between two single molecules: fluorescence resonance energy transfer between a single donor and a single acceptor. *Proceedings of the National Academy of Sciences of the United States of America* 93: 6264-6268.
- HA T, RASNIK I, CHENG W, BABCOCK HP, GAUSS GH, LOHMAN TM AND CHU S. 2002. Initiation and re-initiation of DNA unwinding by the *Escherichia coli* Rep helicase. 419: 638-641.
- HA T AND TINNEFELD P. 2012. Photophysics of fluorescent probes for single-molecule biophysics and super-resolution imaging. *Annual review of physical chemistry* 63: 595-617.
- HAAS E, WILCHEK M, KATCHALSKI-KATZIR E AND STEINBERG IZ. 1975. Distribution of end-to-end distances of oligopeptides in solution as estimated by energy transfer. *Proceedings of the National Academy of Sciences of the United States of America* 72: 1807-1811.
- HAHN S. 2004. Structure and mechanism of the RNA polymerase II transcription machinery. *Nat Struct Mol Biol* 11: 394-403.
- HASTINGS PJ, HERSH MN, THORNTON PC, FONVILLE NC, SLACK A, FRISCH RL, RAY MP, HARRIS RS, LEAL SM AND ROSENBERG SM. 2010. Competition of *Escherichia coli* DNA Polymerases I, II and III with DNA Pol IV in Stressed Cells. *PLoS ONE* 5: e10862.
- HE Y, LU M, CAO J AND LU HP. 2012. Manipulating Protein Conformations by Single-Molecule AFM-FRET Nanoscopy. *ACS Nano* 6: 1221-1229.

- HOHLBEIN J, AIGRAIN L, CRAGGS TD, BERMEK O, POTAPOVA O, SHOOLIZADEH P, GRINDLEY ND, JOYCE CM AND KAPANIDIS AN. 2013. Conformational landscapes of DNA polymerase I and mutator derivatives establish fidelity checkpoints for nucleotide insertion. *Nature communications* 4: 2131.
- HOHLBEIN J, CRAGGS TD AND CORDES T. 2014a. Alternating-laser excitation: single-molecule FRET and beyond. *Chemical Society reviews* 43: 1156-1171.
- HOHLBEIN J, CRAGGS TD AND CORDES T. 2014b. Alternating-laser excitation: single-molecule FRET and beyond. *Chemical Society reviews* 43: 1156-1171.
- HOHLBEIN J, GRYTE K, HEILEMANN M AND KAPANIDIS AN. 2010. Surfing on a new wave of single-molecule fluorescence methods. *Physical biology* 7: 031001.
- HOHNG S, LEE S, LEE J AND JO MH. 2014. Maximizing information content of single-molecule FRET experiments: multi-color FRET and FRET combined with force or torque. *Chemical Society reviews* 43: 1007-1013.
- HOLDEN SJ, UPHOFF S, HOHLBEIN J, YADIN D, LE RESTE L, BRITTON OJ AND KAPANIDIS AN. 2010. Defining the limits of single-molecule FRET resolution in TIRF microscopy. *Biophysical journal* 99: 3102-3111.
- HOLZMEISTER P, ACUNA GP, GROHMANN D AND TINNEFELD P. 2014. Breaking the concentration limit of optical single-molecule detection. *Chemical Society reviews* 43: 1014-1028.
- HSU LM. 2002. Promoter clearance and escape in prokaryotes. *Biochimica et Biophysica Acta (BBA) - Gene Structure and Expression* 1577: 191-207.
- HÜBSCHER U 2010a. History and Discovery of DNA Polymerases. *DNA Polymerases: WORLD SCIENTIFIC*, p. 1-58.
- HÜBSCHER U 2010b. DNA Polymerases in the Three Kingdoms of Life: Bacteria, Archaea and Eukaryotes. *DNA Polymerases: WORLD SCIENTIFIC*, p. 59-83.
- HUGEL T, HOLLAND NB, CATTANI A, MORODER L, SEITZ M AND GAUB HE. 2002. Single-Molecule Optomechanical Cycle. *Science* 296: 1103-1106.
- HWANG H, KIM H AND MYONG S. 2011. Protein induced fluorescence enhancement as a single molecule assay with short distance sensitivity. *Proceedings of the National Academy of Sciences of the United States of America* 108: 7414-7418.
- HWANG H AND MYONG S. 2014. Protein induced fluorescence enhancement (PIFE) for probing protein-nucleic acid interactions. *Chemical Society reviews* 43: 1221-1229.
- ILARI A AND SAVINO C 2008. Protein Structure Determination by X-Ray Crystallography. In: KEITH, JM (Ed.) *Bioinformatics: Data, Sequence Analysis and Evolution*, Totowa, NJ: Humana Press, p. 63-87.
- JARES-ERIJMAN EA AND JOVIN TM. 2003. FRET imaging. *Nature biotechnology* 21: 1387-1395.
- JOHNSON SJ, TAYLOR JS AND BEESE LS. 2003. Processive DNA synthesis observed in a polymerase crystal suggests a mechanism for the prevention of frameshift mutations. *Proceedings of the National Academy of Sciences* 100: 3895-3900.
- JOYCE CM, POTAPOVA O, DELUCIA AM, HUANG X, BASU VP AND GRINDLEY NDF. 2008. Fingers-Closing and Other Rapid Conformational Changes in DNA Polymerase I (Klenow Fragment) and Their Role in Nucleotide Selectivity. *Biochemistry* 47: 6103-6116.

- KALININ S, FELEKYAN S, ANTONIK M AND SEIDEL CA. 2007. Probability distribution analysis of single-molecule fluorescence anisotropy and resonance energy transfer. *The journal of physical chemistry B* 111: 10253-10262.
- KALININ S, FELEKYAN S, VALERI A AND SEIDEL CAM. 2008. Characterizing Multiple Molecular States in Single-Molecule Multiparameter Fluorescence Detection by Probability Distribution Analysis. *The Journal of Physical Chemistry B* 112: 8361-8374.
- KAPANIDIS AN, LEE NK, LAURENCE TA, DOOSE S, MARGEAT E AND WEISS S. 2004. Fluorescence-aided molecule sorting: analysis of structure and interactions by alternating-laser excitation of single molecules. *Proceedings of the National Academy of Sciences of the United States of America* 101: 8936-8941.
- KAPANIDIS AN, MARGEAT E, HO SO, KORTKHONJIA E, WEISS S AND EBRIGHT RH. 2006. Initial transcription by RNA polymerase proceeds through a DNA-scrunching mechanism. *Science* 314: 1144-1147.
- KAPANIDIS AN AND STRICK T. 2009. Biology, one molecule at a time. *Trends in biochemical sciences* 34: 234-243.
- KIM H AND HA T. 2013. Single-molecule nanometry for biological physics. *Reports on progress in physics Physical Society (Great Britain)* 76: 016601.
- KLENOW H AND HENNINGSEN I. 1970. Selective elimination of the exonuclease activity of the deoxyribonucleic acid polymerase from *Escherichia coli* B by limited proteolysis. *Proceedings of the National Academy of Sciences of the United States of America* 65: 168-175.
- KNOX RS AND VAN AMERONGEN H. 2002. Refractive Index Dependence of the Förster Resonance Excitation Transfer Rate. *The Journal of Physical Chemistry B* 106: 5289-5293.
- KRUMMEL B AND CHAMBERLIN MJ. 1989. RNA chain initiation by *Escherichia coli* RNA polymerase. Structural transitions of the enzyme in early ternary complexes. *Biochemistry* 28: 7829-7842.
- LAKOWICZ JR 2006. *Principles of fluorescence spectroscopy*. New York [etc.]: Springer.
- LAMICHHANE R, BEREZHNA SY, GILL JP, VAN DER SCHANS E AND MILLAR DP. 2013. Dynamics of Site Switching in DNA Polymerase. *Journal of the American Chemical Society* 135: 4735-4742.
- LANZ MA AND KLOSTERMEIER D. 2011. Guiding strand passage: DNA-induced movement of the gyrase C-terminal domains defines an early step in the supercoiling cycle. *Nucleic Acids Research* 39: 9681-9694.
- LANZ MA AND KLOSTERMEIER D. 2012. The GyrA-box determines the geometry of DNA bound to gyrase and couples DNA binding to the nucleotide cycle. *Nucleic Acids Research* 40: 10893-10903.
- LEE S, JUNG S-R, HEO K, BYL JAW, DEWEESE JE, OSHEROFF N AND HOHNG S. 2012. DNA cleavage and opening reactions of human topoisomerase II $\alpha$  are regulated via Mg<sup>2+</sup>-mediated dynamic bending of gate-DNA. *Proceedings of the National Academy of Sciences* 109: 2925-2930.
- LEHMAN IR, BESSMAN MJ, SIMMS ES AND KORNBERG A. 1958. Enzymatic synthesis of deoxyribonucleic acid. I. Preparation of substrates and partial purification of an enzyme from *Escherichia coli*. *The Journal of biological chemistry* 233: 163-170.



- LEVENE MJ, KORLACH J, TURNER SW, FOQUET M, CRAIGHEAD HG AND WEBB WW. 2003. Zero-mode waveguides for single-molecule analysis at high concentrations. *Science* 299: 682-686.
- LOHMAN TM. 1992. Escherichia coli DNA helicases: mechanisms of DNA unwinding. *Molecular Microbiology* 6: 5-14.
- LU HP. 2014. Sizing up single-molecule enzymatic conformational dynamics. *Chemical Society reviews* 43: 1118-1143.
- LYMPEROPOULOS K, CRAWFORD R, TORELLA JP, HEILEMANN M, HWANG LC, HOLDEN SJ AND KAPANIDIS AN. 2010. Single-Molecule DNA Biosensors for Protein and Ligand Detection. *Angewandte Chemie International Edition* 49: 1316-1320.
- MARKIEWICZ RP, VRTIS KB, RUEDA D AND ROMANO LJ. 2012. Single-molecule microscopy reveals new insights into nucleotide selection by DNA polymerase I. *Nucleic Acids Research* 40: 7975-7984.
- MCKINNEY SA, JOO C AND HA T. 2006. Analysis of single-molecule FRET trajectories using hidden Markov modeling. *Biophysical journal* 91: 1941-1951.
- MOERNER WE. 2007. New directions in single-molecule imaging and analysis. *Proceedings of the National Academy of Sciences* 104: 12596-12602.
- MOERNER WE AND FROMM DP. 2003. Methods of single-molecule fluorescence spectroscopy and microscopy. *Review of Scientific Instruments* 74: 3597-3619.
- MURAKAMI KS, MASUDA S AND DARST SA. 2002. Structural Basis of Transcription Initiation: RNA Polymerase Holoenzyme at 4 Å Resolution. *Science* 296: 1280-1284.
- MUSCHIELOK A, ANDRECKA J, JAWHARI A, BRUCKNER F, CRAMER P AND MICHAELIS J. 2008. A nano-positioning system for macromolecular structural analysis. 5: 965-971.
- MYONG S, BRUNO MM, PYLE AM AND HA T. 2007. Spring-Loaded Mechanism of DNA Unwinding by Hepatitis C Virus NS3 Helicase. *Science* 317: 513-516.
- MYONG S, RASNIK I, JOO C, LOHMAN TM AND HA T. 2005. Repetitive shuttling of a motor protein on DNA. 437: 1321-1325.
- NAKAMURA C, MIYAMOTO C, OBATAYA I, TAKEDA S, YABUTA M AND MIYAKE J. 2007. Enzymatic nanolithography of FRET peptide layer using V8 protease-immobilized AFM probe. *Biosensors and Bioelectronics* 22: 2308-2314.
- NIR E, MICHALET X, HAMADANI KM, LAURENCE TA, NEUHAUSER D, KOVCHEGOV Y AND WEISS S. 2006. Shot-noise limited single-molecule FRET histograms: comparison between theory and experiments. *The journal of physical chemistry B* 110: 22103-22124.
- PAL M, PONTICELLI AS AND LUSE DS. 2005. The Role of the Transcription Bubble and TFIIB in Promoter Clearance by RNA Polymerase II. *Molecular Cell* 19: 101-110.
- PINKNEY JNM, ZAWADZKI P, MAZURYK J, ARCISZEWSKA LK, SHERRATT DJ AND KAPANIDIS AN. 2012. Capturing reaction paths and intermediates in Cre-loxP recombination using single-molecule fluorescence. *Proceedings of the National Academy of Sciences* 109: 20871-20876.
- PREUS S AND WILHELMSSON LM. 2012. Advances in Quantitative FRET-Based Methods for Studying Nucleic Acids. *Chembiochem : a European journal of chemical biology* 13: 1990-2001.
- RASNIK I, MCKINNEY SA AND HA T. 2006a. Nonblinking and long-lasting single-molecule fluorescence imaging. 3: 891-893.

## ***Studying DNA-protein interactions with smFRET***

- RASNIK I, MCKINNEY SA AND HA T. 2006b. Nonblinking and long-lasting single-molecule fluorescence imaging. *Nature methods* 3: 891-893.
- ROTHWELL PJ, ALLEN WJ, SISAMAKIS E, KALININ S, FELEKYAN S, WIDENGREN J, WAKSMAN G AND SEIDEL CAM. 2013. dNTP-dependent Conformational Transitions in the Fingers Subdomain of KlenTaq1 DNA Polymerase: INSIGHTS INTO THE ROLE OF THE "NUCLEOTIDE-BINDING" STATE. *Journal of Biological Chemistry* 288: 13575-13591.
- ROY R, HOHNG S AND HA T. 2008. A practical guide to single-molecule FRET. *Nature methods* 5: 507-516.
- RUNNER VM, PODOLNY V AND BURATOWSKI S. 2008. The Rpb4 subunit of RNA polymerase II contributes to cotranscriptional recruitment of 3' processing factors. *Molecular and cellular biology* 28: 1883-1891.
- SAECKER RM, RECORD MT, JR. AND DEHASETH PL. 2011. Mechanism of bacterial transcription initiation: RNA polymerase - promoter binding, isomerization to initiation-competent open complexes, and initiation of RNA synthesis. *Journal of molecular biology* 412: 754-771.
- SANTOSO Y, JOYCE CM, POTAPOVA O, LE RESTE L, HOHLBEIN J, TORELLA JP, GRINDLEY ND AND KAPANIDIS AN. 2010a. Conformational transitions in DNA polymerase I revealed by single-molecule FRET. *Proceedings of the National Academy of Sciences of the United States of America* 107: 715-720.
- SANTOSO Y, TORELLA JP AND KAPANIDIS AN. 2010b. Characterizing single-molecule FRET dynamics with probability distribution analysis. *Chemphyschem : a European journal of chemical physics and physical chemistry* 11: 2209-2219.
- SARKAR A, ROBERTSON RB AND FERNANDEZ JM. 2004. Simultaneous atomic force microscope and fluorescence measurements of protein unfolding using a calibrated evanescent wave. *Proceedings of the National Academy of Sciences of the United States of America* 101: 12882-12886.
- SHAW JE, OREOPOULOS J, WONG D, HSU JCY AND YIP CM. 2006. Coupling evanescent-wave fluorescence imaging and spectroscopy with scanning probe microscopy: challenges and insights from TIRF-AFM. *Surf Interface Anal* 38: 1459-1471.
- SMILEY RD, COLLINS TRL, HAMMES GG AND HSIEH T-S. 2007. Single-molecule measurements of the opening and closing of the DNA gate by eukaryotic topoisomerase II. *Proceedings of the National Academy of Sciences* 104: 4840-4845.
- STRANEY DC AND CROTHERS DM. 1987. A stressed intermediate in the formation of stably initiated RNA chains at the Escherichia coli lac UV5 promoter. *Journal of molecular biology* 193: 267-278.
- STRYER L AND HAUGLAND RP. 1967. Energy transfer: a spectroscopic ruler. *Proceedings of the National Academy of Sciences of the United States of America* 58: 719-726.
- TORELLA JP, HOLDEN SJ, SANTOSO Y, HOHLBEIN J AND KAPANIDIS AN. 2011. Identifying molecular dynamics in single-molecule FRET experiments with burst variance analysis. *Biophysical journal* 100: 1568-1577.
- TREUTLEIN B, MUSCHIELOK A, ANDRECKA J, JAWHARI A, BUCHEN C, KOSTREWA D, HÖG F, CRAMER P AND MICHAELIS J. 2012. Dynamic Architecture of a Minimal RNA Polymerase II Open Promoter Complex. *Molecular Cell* 46: 136-146.

- VICKERY SA AND DUNN RC. 2001. Combining AFM and FRET for high resolution fluorescence microscopy. *Journal of Microscopy* 202: 408-412.
- VOGELSANG J, KASPER R, STEINHAEUER C, PERSON B, HEILEMANN M, SAUER M AND TINNEFELD P. 2008. A Reducing and Oxidizing System Minimizes Photobleaching and Blinking of Fluorescent Dyes. *Angewandte Chemie International Edition* 47: 5465-5469.
- VOGELSTEIN B, LANE D AND LEVINE AJ. 2000. Surfing the p53 network. 408: 307-310.
- WALTER NG, HUANG CY, MANZO AJ AND SOBHAY MA. 2008. Do-it-yourself guide: how to use the modern single-molecule toolkit. *Nature methods* 5: 475-489.
- WATSON JD AND CRICK FHC. 1953. Molecular Structure of Nucleic Acids: A Structure for Deoxyribose Nucleic Acid. 171: 737-738.
- WEISS S. 1999. Fluorescence spectroscopy of single biomolecules. *Science* 283: 1676-1683.
- WU EY AND BEESE LS. 2011. The Structure of a High Fidelity DNA Polymerase Bound to a Mismatched Nucleotide Reveals an "Ajar" Intermediate Conformation in the Nucleotide Selection Mechanism. *Journal of Biological Chemistry* 286: 19758-19767.
- WUTHRICH K. 2001. The way to NMR structures of proteins. 8: 923-925.
- YODH JG, SCHLIERF M AND HA T. 2010. Insight into helicase mechanism and function revealed through single-molecule approaches. *Quarterly Reviews of Biophysics* 43: 185-217.
- ZAWADZKI P, MAY PFJ, BAKER RA, PINKNEY JNM, KAPANIDIS AN, SHERRATT DJ AND ARCISZEWSKA LK. 2013. Conformational transitions during FtsK translocase activation of individual XerCD-dif recombination complexes. *Proceedings of the National Academy of Sciences* 110: 17302-17307.
- ZHANG G, CAMPBELL EA, MINAKHIN L, RICHTER C, SEVERINOV K AND DARST SA. 1999. Crystal Structure of *Thermus aquaticus* Core RNA Polymerase at 3.3 Å Resolution. *Cell* 98: 811-824.
- ZHANG Y, FENG Y, CHATTERJEE S, TUSKE S, HO MX, ARNOLD E AND EBRIGHT RH. 2012. Structural Basis of Transcription Initiation. *Science* 338: 1076-1080.
- ZHENG Q, JUETTE MF, JOCKUSCH S, WASSERMAN MR, ZHOU Z, ALTMAN RB AND BLANCHARD SC. 2014. Ultra-stable organic fluorophores for single-molecule research. *Chemical Society reviews* 43: 1044-1056.



## CHAPTER 3

# **Improving the time resolution in single-molecule FRET TIRF microscopy by combining stroboscopic alternating-laser excitation with dynamic probability distribution analysis**

based on:

Farooq, S. and J. Hohlbein (2015). "Camera-based single-molecule FRET detection with improved time resolution." *Phys Chem Chem Phys* **17**(41): 27862-27872.

### **Abstract**

The achievable time resolution of camera-based single-molecule detection is often limited by the frame rate of the camera. Especially in experiments utilizing single-molecule Förster resonance energy transfer (smFRET) to probe conformational dynamics of biomolecules, increasing the frame rate by either pixel-binning or cropping the field of view decreases the number of molecules that can be monitored simultaneously. Here, we present a generalised excitation scheme termed stroboscopic alternating-laser excitation (sALEX) that significantly improves the time resolution without sacrificing highly parallelised detection in total internal reflection fluorescence (TIRF) microscopy. In addition, we adapt a technique known from diffusion-based confocal microscopy to analyse the complex shape of FRET efficiency histograms. We apply both sALEX and dynamic probability distribution analysis (dPDA) to resolve conformational dynamics of interconverting DNA hairpins in the millisecond time range.

### **Introduction**

Powerful methods based on the detection of fluorescence emitted from single molecules have significantly expanded our capabilities to study biological and chemical processes at the molecular level (Farooq et al. 2014, Hohlbein et al. 2010, Joo et al. 2008, Moerner 2007a). One prominent technique is single-molecule Förster resonance energy transfer (smFRET), which is used to monitor distances and molecular interactions in the nanometre range (Hohlbein et al. 2013, Preus and Wilhelmsson 2012, Weiss 1999). In addition to providing static structural information (Kalinin et al. 2012, Muschielok et al. 2008a), there is a growing interest in applying smFRET to probe conformational dynamics within single enzymes (Henzler-Wildman et al. 2007, Santos et al. 2010b) and, ideally, even to probe those dynamics during reactions such as monitoring conformational changes of DNA polymerases during DNA synthesis. However, the two standard schemes for smFRET detection (Walter et al. 2008), diffusion-based confocal microscopy and camera-based total internal reflection fluorescence (TIRF) or widefield microscopy (Axelrod et al. 1984, Holden et al. 2010), are ultimately limited in their ability to combine parallel detection of many molecules with obtaining data at sufficiently high time resolution. Recent attempts of achieving higher time resolution in FRET microscopy involve camera-based detection in combination with micro- and nanofluidic devices (Tyagi et al. 2014), tethering of fluorescently labelled species to slowly diffusing liposomes in confocal microscopy (Kim et al. 2015) or utilising correlation and transition-point analysis together with short binning of

fluorescence lifetime-resolved confocal data (Chung et al. 2012, Henzler-Wildman et al. 2007, Olofsson et al. 2014).

We have previously reported on the conformational landscape of the unliganded DNA polymerase I, which exhibits fast conformational changes between an open and a closed conformation of the fingers-subdomain in the low millisecond time range (Hohlbein et al. 2013, Santoso et al. 2010a, Santoso et al. 2010b, Torella et al. 2011). However, the DNA pol I dynamics are too slow to directly resolve them using diffusion-based confocal microscopy and too fast to monitor them with a camera. As of 2015, the latest generation of emCCD cameras is achieving frame rates of around 60 Hz for full frame detection (512 by 512 pixel) and sCMOS cameras, which have not yet been widely adapted for single-molecule fluorescence detection, run at frame rates of up to 100 Hz.

Here, we report on a generalised outline for camera-based smFRET detection, which combines the concepts of alternating-laser excitation (ALEX) (Hohlbein et al. 2014b, Kapanidis et al. 2004, Laurence et al. 2005, Lee et al. 2005, Muller et al. 2005) and stroboscopic illumination (Blumberg et al. 2005, Elf et al. 2007, Flors et al. 2007) to achieve a significant improvement in time resolution. In order to analyse dynamics faster than the corresponding frame rates of the camera, we adapt dynamic probability distribution analysis (dPDA), a technique widely used in diffusion-based confocal microscopy (Antonik et al. 2006, Kalinin et al. 2007, Kalinin et al. 2010b, Nir et al. 2006, Santoso et al. 2010b), for data obtained using TIRF microscopy allowing us to close the currently existing gap in obtainable time resolution between confocal and camera-based single-molecule detection. In contrast to diffusion-based microscopy, our technique allows monitoring the fate of single, surface-immobilised molecule for extended periods of time with up to hundreds of molecules in parallel. We demonstrate by both simulations and experiments using doubly labelled DNA hairpins (Hartmann et al. 2014, Tsukanov et al. 2013a) that resolving dynamic conformational states with a lifetime in the order of a few milliseconds is possible.

## **Experiments and theoretical analysis**

### **Stroboscopic alternating-laser excitation (sALEX)**

In our implementation of ALEX, we use stroboscopic illumination to excite donor fluorophores in our FRET system (DNA hairpin, Fig. 1a) only for a short time during each frame acquired by the camera (Fig. 1b). As a result, FRET values calculated from the fluorescence intensities of the molecules in the donor and acceptor detection channel represent short snapshots of the underlying FRET

dynamics. Let us consider for simplicity a molecular system that switches between a low and a high FRET state. If the dynamics are faster than the corresponding acquisition rate of the camera, FRET time traces and FRET efficiency histograms measured using the conventional excitation scheme show temporal averaging, whereas the stroboscopic excitation allows a distinction of the two states depending on the duration of each excitation interval (Fig. 1c). After donor excitation, the direct excitation of acceptor molecules allows monitoring their presence and photophysical state (Hohlbein et al. 2014b).

### **Single-molecule FRET microscopy**

The general design of the single-molecule FRET TIRF setup was described previously (Hohlbein et al. 2014b, Holden et al. 2010). Instead of a conventional microscope body, we used a RAMM system (rapid-automated-modular-microscope) as a stage holder (ASI, USA) together with a motorised  $x, y$  scanning stage with a  $z$ -piezo for controlling precise sample placement along the optical axis of the microscope. For excitation, we used a fibre-coupled laser engine (Omicron, Germany) equipped with four lasers of different wavelengths (405 nm, 473 nm, 561 nm, and 642 nm). A home-written LabVIEW program independently controlled the laser intensities and triggered the camera. The single mode fibre generated a Gaussian shaped beam profile and a point source output at the other end of the fibre. The divergent light is collimated ( $f = 100$  mm, Thorlabs, Germany) and a second lens focuses ( $f = 200$  mm, Thorlabs, Germany) the light back into the back focal plane of a  $100\times$  NA 1.49 TIRF objective (Nikon, Japan). A custom-made multicolour polychroic mirror (zt405/473/561/640rpc, Chroma, USA) and a multibandpass filter (zet405/473/561/640m, Chroma, USA) are used to block any laser light in the emission path. After spatial filtering of the fluorescence with a two-lens system consisting of two tube lenses ( $f = 200$  mm, Thorlabs, Germany) and an adjustable slit (Thorlabs, Germany), the light was spectrally split using two dichroic mirrors (zt561rdc and zt640rdc, Chroma) and a mirror into three beams corresponding to a blue, green, and red fluorescence detection channel. The three beams were then focused ( $f = 300$  mm) on an Ixon Ultra 897 emCCD camera with  $512 \times 512$  pixel (Andor, Northern-Ireland) that was operated in a photon-counting mode giving direct access to photon numbers.



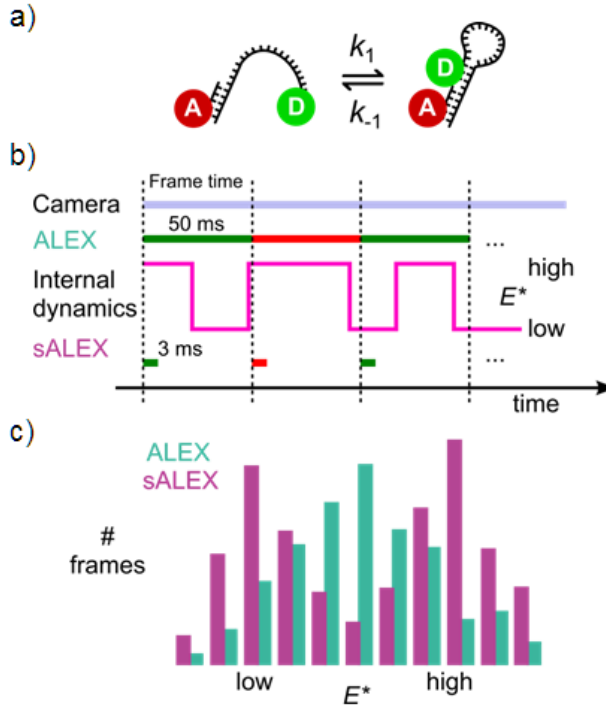


Figure 1. Conceptual framework of stroboscopic alternating-laser excitation (sALEX). **(a)** Scheme of a fluorescently labelled DNA hairpin undergoing conformational changes between a low FRET (left) and a high FRET state (right). **(b)** The maximum frame rate of the camera used for fluorescence detection imposes an upper limit of the achievable time resolution in smFRET TIRF microscopy. Whereas in conventional ALEX the direct excitation of either donor or acceptor dye takes place for the entire duration of each frame, the excitation of the donor is limited to a short interval within each frame using sALEX. **(c)** The histogram of FRET efficiencies of a system undergoing conformational changes shows an averaged peak for FRET dynamics that are significantly faster than the corresponding frame time (ALEX). Both conformational states can be resolved if the duration of excitation approaches the lifetime of the states (sALEX).

The acquisition rate of the camera was set to 20 Hz. We used laser powers of 1.5 mW (561 nm laser) and 0.75 mW (642 nm) for experiments in which the laser was exciting fluorophores for the full duration of each camera frame (50 ms). In case of stroboscopic excitation (3 ms), we increased the laser powers to 30 mW (561 nm laser) and 15 mW (642 nm) in order to obtain a similar count rate of our fluorophores. Movies were recorded for 1000 frames. Sets of experiments comparing 50 ms excitation with short stroboscopic excitation (3 ms) were performed in the same sample well. Further information on labelling, purification,

## ***Improving the time resolution in smFRET TIRF microscopy***

immobilisation and imaging of DNA can be found in the Supplementary Information (SI).

### **Image analysis**

For image analysis we used a modified version of TwoTone, a freely available, MATLAB-based software package, which identifies molecules and measures the photon counts by fitting the molecular point spread functions to two dimensional Gaussians (Holden et al. 2010). Molecules with an elongated shape indicating two overlapping molecules or molecules with an inter-molecular distance of less than around 500 nm were withdrawn from further analysis. For all remaining molecule containing both donor and acceptor, we obtained three photon streams  $DD$  (donor detection channel after direct excitation of the donor),  $DA$  (acceptor detection channel after direct excitation of the donor, FRET channel) and  $AA$  (acceptor detection channel after direct excitation of the acceptor) allowing us to calculate the apparent FRET efficiency  $E^* = DA/(DD + DA)$  and the stoichiometry  $S_{PR} = (DD + DA)/(DD + DA + AA)$ . The data shown in the FRET efficiency histograms was filtered by applying two threshold criteria to each time frame:  $DD + DA > 60$  photons and  $AA > 30$  photons for simulated data. For the experimental data, we increased the intensity thresholds to  $DD + DA > 200$  photons and  $AA > 50$  photons and used an additional stoichiometry-based threshold of  $0.4 \leq S_{PR} \leq 0.9$  to account for the higher sample complexity featuring donor- and acceptor-only molecules. No other frames or molecules were excluded from analysis unless explicitly stated.

### **Signal to noise considerations in smFRET TIRF microscopy**

An analytic expression for the standard deviation  $\sigma(E)$  of observed FRET distributions in TIRF microscopy has been previously derived (Holden et al. 2010). The expression accounts for heterogeneity in static homogeneous samples caused by shot noise, background photons, noise due to the electron-multiplying gain register of emCCD cameras, read-out noise and dark noise and is given by

$$\sigma(E) = 1.33 \sqrt{\frac{f_G^2 E_0 (1 - E_0)}{D + A} + \frac{4\pi}{a^2 (D + A)^4} (A^2 s_D^2 b_D^2 + D^2 s_A^2 b_A^2)}, \quad (1)$$

where  $E_0$  is the mean apparent FRET value;  $s_D$  and  $s_A$  are the widths of the point spread function (PSF) in the donor and acceptor channel;  $b_D$  and  $b_A$  are the observed standard deviations (photons per pixel) of the background noise in each channel;  $D$  (same as  $DD$  signal mentioned above) and  $A$  ( $AA$ ) are the photon counts for the entire PSF, in the donor and acceptor channels respectively;  $a$  is the

pixel size; and  $f_G = \sqrt{2}$  is the excess noise factor accounting for noise introduced by the emCCD. The additional factor of 1.33 accounts for the excess heterogeneity introduced by the fitting algorithm of the PSF, which does, in our implementation, not account for shot noise in the recorded images (Holden et al. 2010, Tyagi et al. 2014). Using values introduced in the section describing the simulations yields standard deviations in the order of  $\sigma(E) \sim 0.06$  which we used as starting values of the excess widths for data fitting using dynamic probability distribution analysis described below. Under experimental conditions, however, we expect additional heterogeneity introduced by, for example, focal drift and intermolecular heterogeneity (Holden et al. 2010).

### Dynamic probability distribution analysis (dPDA) in TIRF microscopy

The acquisition of brief snapshots using sALEX imposes limitations to the way the data of smFRET time traces can be analysed as the conformational changes occurring during periods of no excitation are hidden and cannot be monitored. Thereby, the stroboscopic excitation prevents the analysis of single time traces with hidden Markov modelling (HMM) which has been applied to determine FRET dynamics as long as the dynamics are slower than the rate of data acquisition (McKinney et al. 2006, Uphoff et al. 2011). In fact, the brief snapshots are comparable to data from diffusion-based confocal microscopy in which fluorescently labelled entities give rise to short (1–3 ms) (Santoso et al. 2010a) bursts of fluorescence as the molecules diffuse through the confocal spot. Therefore, we decided to adapt a concept known from diffusion-based confocal microscopy, (dynamic) probability distribution analysis (dPDA), which uses the experimentally obtained distribution of photon counts to recapitulate complex FRET distributions (Antonik et al. 2006, Kalinin et al. 2007, Kalinin et al. 2010b, Nir et al. 2006, Santoso et al. 2010b). The shape and width of these distributions is influenced by the potential presence of static FRET species as well as by species dynamically interconverting between two or more conformations.

The dynamic model of a two-state system, here represented by a low FRET (open) and high-FRET (closed) DNA hairpin (Fig. 1a), is fully described by two peak positions ( $E_o^*$  and  $E_c^*$ ), two excess widths ( $\sigma_o$  and  $\sigma_c$ ) and two rate constants  $k_{oc}$  and  $k_{co}$ . The excess width describes to which extent the width of the histogram of a single static species deviates from the width predicted by shot-noise limited fluorescence emission and detection and has been discussed extensively for confocal microscopy (Kalinin et al. 2010a, McKinney et al. 2006, Tsukanov et al. 2013a, Uphoff et al. 2011) suggesting that acceptor photophysics is the main source of the observed broadening. In TIRF microscopy, however, additional sources of

noise such as camera read-out, stage drift and fitting algorithms have to be considered (Holden et al. 2010).

The dPDA algorithm calculates a semi-empirical histogram of FRET efficiencies based on various parameters and has been described in greater detail for confocal microscopy (Santoso et al. 2010b). In our implementation, the algorithm consisted of the following steps: (1) we choose an oversampling factor (normally set to 10) to reduce the statistical noise of the random number generators used and a model of six parameters ( $E_o^*$ ,  $E_c^*$ ,  $\sigma_o$ ,  $\sigma_c$ ,  $k_{oc}$  and  $k_{co}$ ). Before fitting, initial guesses of all six parameters were provided. (2) For each molecule and each frame, which fulfilled the three thresholds discussed above ( $DD + DA$ ,  $AA$ ,  $S_{PR}$ ) and a  $E^*$  standard deviation based threshold criteria discussed below, we calculated the probabilities of finding the molecule in one of the two states based on the initial guesses of the interconversion rates. Using these probabilities and the measured number of photons detected after donor excitation in the particular frame given by  $DD + DA$ , we draw two new binominal-distributed random numbers describing the expected number of photons from each conformational state  $f_{o,i}$  or  $f_{c,i}$ . If necessary, this is repeated, as several interconversions can happen within one frame leading to two final photon numbers of  $f_o$  and  $f_c$  for each frame. (3) To account for the excess width of FRET distributions in smFRET TIRF microscopy, we decided to take a different approach to the one previously used for confocal microscopy in which the excess width was introduced by adding normal distributed noise to the distances calculated from the initial guesses of  $E_o^*$  and  $E_c^*$  (Santoso et al. 2010b, Torella et al. 2011). Here, we added normal distributed random numbers with a standard deviation given by the excess width  $\sigma_i$  directly to the initial  $E_i^*$  value for each valid frame. Even though the original approach would account better for distance fluctuations between the fluorophores, it introduces asymmetry in the later back-calculated FRET histograms due to the non-linear relation between  $E^*$  and the distances which prevented good fits for our simulated and experimental data. Instead of using both approaches of artificially broadening the predicted FRET efficiency distributions, we decided to use only the addition of noising to the initially set  $E_o^*$  and  $E_c^*$  to keep the model as simple as possible. In any case, the contribution of distance variations at the time scale of a single frame can be considered negligible compared to various dynamic and static sources of heterogeneity discussed previously (Holden et al. 2010). In fact, the authors found that focal drift and intermolecular heterogeneity caused by either slowly-interconverting photophysically distinct states of the acceptor or slow fluctuations in donor-acceptor separation account for most of the detectable excess width (Holden et al. 2010) (4) Using  $E_o^*$ ,  $E_c^*$ ,  $f_o$  and  $f_c$  (again for each frame and each molecule) we draw two new binominal-distributed random numbers describing

how many photons can be expected in the donor channel for each of the underlying two conformational states during each frame and the duration of excitation therein. These two numbers are then summed up and normalized by the number of photons measured experimentally or taken from the analysed simulated data to yield an expected FRET efficiency. (5) Steps 2–4 are repeated according to the oversampling factor and normalised accordingly. (6) The histograms of the predicted FRET efficiencies are then compared to the experimentally determined FRET efficiencies. The initially set values are varied to achieve a better agreement of the histograms using a least-mean-squares algorithm implemented in MATLAB and C++ (Lourakis 2004).

To evaluate the goodness of the fit between the simulated or experimental data and the predicted dPDA fit, we calculated the reduced chi-squared statistic as similarly suggested previously (Kalinin et al. 2007):

$$\chi^2 = \frac{1}{z - y} \sum_{i=1}^z \frac{[Freq(X_i) - Freq_M(X_i)]^2}{Freq(X_i)f}, \quad (2)$$

where  $y$  is the number of fitted parameters (here 6),  $z$  the total number of bins (here 100) and  $Freq$  and  $Freq_M$  represent the frequency of data falling into bin  $i$  in either the data ( $Freq$ ) or the prediction ( $Freq_M$ ), respectively. The calculation of chi-squared considered only data bins in which at least one data point is present. The software for dPDA is available free of charge upon request.

## Monte-Carlo simulations of camera-based, single-molecule FRET experiments

The Monte-Carlo simulations were performed using custom written C/C++ software developed to resemble single-molecule experiments as closely as possible. The software was described previously (Holden et al. 2010, Torella et al. 2011), but updated to allow the simulation of conformational dynamics faster than the acquisition time of the camera. Discrete time steps of 100  $\mu$ s were used in which 150 randomly distributed particles would fluoresce and undergo conformational changes resulting in time dependent changes in their FRET efficiencies. We used forward and backward rates set to  $k_{oc} = k_{co} = 200 \text{ s}^{-1}$  leading to a lifetime of 5 ms for each conformational states. Each simulated movie consisted of 1000 frames. The simulated frame time of the camera was set to 50 ms and the excitation time was chosen to be between 1 ms and 50 ms. We simulated an area of 512 by 340 pixel with a virtual pixel size of 130 nm, representing the dimensions of the field of view under experimental conditions. The intensity profile around each molecule

position is assumed to be Gaussian in  $x$  and  $y$  direction and the characteristic width of the point spread function was set to 130 nm for donor and to 150 nm for acceptor fluorophores. We set the brightness to 250 photons per molecule per excitation period for donor and emission after donor excitation and 100 photons per molecule per excitation period for acceptor emission after acceptor emission, values which are achievable under experimental conditions. For the simulated data, we set the Förster radius  $R_0$  to 6 nm and the corresponding distances between donor and acceptor fluorophore to 7 nm for the open and to 5 nm for the closed conformation. The leakage describing the probability of detecting photons emitted from the donor in the acceptor detection channel due to the spectral characteristics of the fluorophores and the experimental setup was set to 0.1. The quantum yield of each fluorophore was set to unity. Gaussian distributed background noise was added as follows with a mean value of 4 photons for the donor excitation, donor detection channel (DD channel), 5 photons for the donor excitation, acceptor emission channel (DA channel), 2 photons for the acceptor excitation donor emission channel (AD, which does not contain any further signal and is therefore excluded from further considerations), and 6 photons for the acceptor excitation acceptor emission channel (AA channel). The standard deviation of all background noise was set to 2 photons per pixel. Albeit possible in the simulation, we did not simulate other fluorophore properties such as blinking, bleaching and potential direct excitation of the acceptor by the laser used for donor excitation.

### **Simulation results**

#### **sALEX: identification of conformational dynamics in the millisecond time range**

We started exploring the potential of sALEX to resolve conformational dynamics by running a set of Monte Carlo simulations using parameters closely resembling experimental conditions and constraints. The main advantage of simulating single-molecule FRET microscopy is that the rates of the conformational changes can be directly set and later be compared to the results obtained from fitting the FRET efficiency histograms by dPDA. For the set of five simulations presented (Fig. 2), we varied the duration of the excitation per frame from 50 ms to 1 ms but kept all remaining parameters constant. Two consecutive frames of the simulated raw data (3 ms excitation time) show the two detection channels after donor excitation (Fig. 2a; DD and DA) and after acceptor excitation (Fig. 2b; AA). Individual particles are visible and those are then analysed to obtain individual time traces and FRET efficiencies. For conformational rates of  $200\text{ s}^{-1}$ , an excitation duration of 50 ms during a 50 ms acquisition frame time led to severe averaging of the FRET

efficiencies yielding a single, albeit broadened, FRET distribution centred around  $E^* \sim 0.55$  (Fig. 2c, top). Only using an illumination shorter than the lifetime of the respective conformational states ( $1/200 \text{ s}^{-1} = 5 \text{ ms}$ ) led to the appearance of two global maxima that can be attributed to the open and the closed conformation of the simulated molecules. In fact, exciting the molecules for 1 ms shows two clearly distinguishable species with only limited temporal averaging between them (Fig. 2c, bottom). We plotted single-molecule time trajectories for 50 ms (Fig. 2d) and 3 ms excitation time (Fig. 2e), respectively. As expected, the trajectories of DD, DA and  $E^*$  in the case of a 3 ms excitation time show fluctuations with larger amplitudes than for 50 ms excitation time.

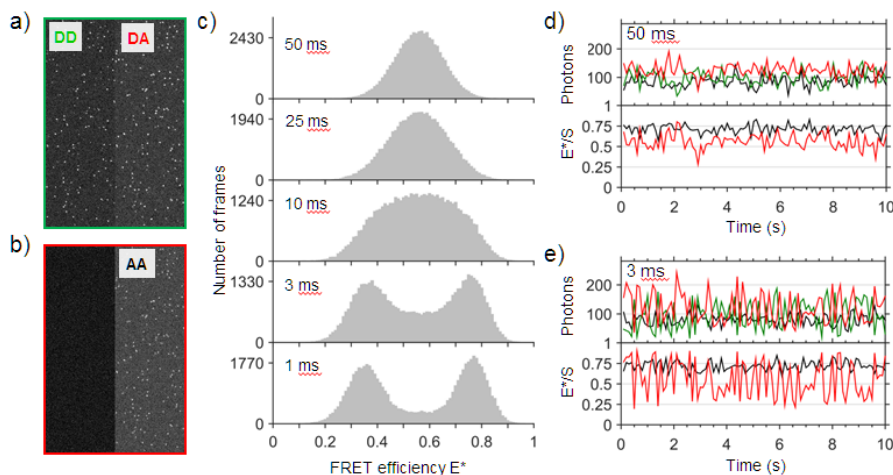


**Figure 2. Simulations. Stroboscopic alternating-laser excitation (sALEX) in smFRET TIRF microscopy.** Complete movies were simulated using parameters closely resembling experimental conditions. The conformational dynamics of the FRET species were simulated using a forward and backward rate of  $k_{oc} = k_{co} = 200 \text{ s}^{-1}$ , respectively. The frame rate of the camera was set to 20 Hz. **(a+b)** Simulated individual frames after **(a)** green and **(b)** red excitation shown for a 3 ms excitation time (Materials and Methods). FRET is shown via simultaneous detection of molecules in the green (DD) and red (DA) detection channel after green excitation. **(c)** Histograms (100 bins) of transfer efficiencies ( $E^* = DA / (DA + DD)$ ) from individual time traces after fitting all molecules. The respective excitation time is indicated. For excitation times corresponding to the frame time of the camera (50 Hz), the underlying fast conformational changes are averaged out. Decreasing the excitation time leads to a separation of both FRET species. **(d+e)** Individual time traces for 50 ms **(d)** and 3 ms **(e)** excitation time. Upper panel: donor signal after donor excitation (green trace, DD), acceptor signal after donor excitation (red trace, DA), acceptor signal after acceptor excitation (black trace, AA). Lower panel: transfer efficiencies (red trace,  $E^*$ ) and stoichiometry (black trace,  $S = DD + DA / (DD + DA + AA)$ ).

In the simulations we have not included any intermolecular heterogeneity; all molecules undergo conformational changes with dynamics defined by the rate constants. In our experience, this is rarely the case for experimental data in which intermolecular heterogeneity is often present and has to be carefully addressed to avoid “cherry picking” which might lead to biased data interpretation. Here we suggest to use a threshold criterion that is based on calculating the standard deviation of all FRET frames measured for each molecule similar to burst variance analysis in confocal microscopy (Torella et al. 2011). For the simulated data (Fig. 2b, 3 ms excitation), we plotted the pseudo-colour coded, one dimensional FRET histogram for each molecule showing the expected homogeneity for the simulations (Fig. 3a top panel). For each single time trace, we calculated the standard deviation of all FRET values. Whereas the exact value depends on the FRET peak positions in the FRET histogram and the overall photon count rate per frame, all standard deviation values are here equally centred around 0.2 confirming the homogeneity in the simulated sample. As we will show for the experimental data, non-interconverting molecules can be identified and excluded from further analysis as their standard deviation of FRET values is considerably lower. Taken together, Monte Carlo simulations reveal that the enhanced time resolution of sALEX improves our capabilities of identify heterogeneity in FRET samples.

### **dPDA: quantifying conformational dynamics in the millisecond time range**

For the simulations, we set the rates of the interconversions to  $200\text{ s}^{-1}$ , which we now aim to recover by analysing the FRET efficiency histograms using dynamic probability distribution analysis (dPDA). We took the simulated data using the 3 ms excitation and chose the following initial guesses  $^iE_o^* = 0.2$ ,  $^iE_c^* = 0.8$ ,  $^ik_{oc} = 150\text{ s}^{-1}$ ,  $^ik_{co} = 250\text{ s}^{-1}$  and  $^i\sigma_o = ^i\sigma_c = 0.06$  for further optimization. The initial peak positions and rates were chosen such that they deviate significantly from the final fit. After fitting, we obtained  $E_o^* = 0.352 \pm 0.001$ ,  $E_c^* = 0.773 \pm 0.002$ ,  $k_{oc} = (205 \pm 6)\text{ s}^{-1}$ ,  $k_{co} = (205 \pm 6)\text{ s}^{-1}$  and  $\sigma_o = 0.055 \pm 0.003$  and  $\sigma_c = 0.049 \pm 0.003$  with  $\chi^2 = 1.4$  representing an excellent fit with small residuals (Fig. 3b). Whereas the peak position can be visually verified and the excess width can be estimated for the simulations as discussed above, the influence of both rates on the shape of the predicted

FRET efficiency histogram is more difficult to assess. Therefore, we fixed the peak positions and the excess widths to the values obtained from the fit and asked how the  $\chi^2$  values change for systematically altered rate constants without running the



optimization algorithm (Fig. 3c). If we consider a  $\chi^2 < 5$  as a reasonable approximation of the data using a dPDA prediction, we find that the minimization surface yields rates of  $k_{oc} = k_{co} = (200 \pm 30) \text{ s}^{-1}$  in excellent agreement with the simulated rates. Fits of the FRET efficiency histograms for the cases of 10 ms and 1 ms excitation also show excellent agreement with the simulated data and can be found in Fig. S1.

Finally, we used the six parameters obtained from the original fit of the simulated 3 ms data (Fig. 2b and 3b) to predict the FRET histogram (black stairs) in the case of a 50 ms excitation period (Fig. 3d). As shown before, the simulated data shows a single peak due to the averaging effect of quickly interconverting FRET species. The predicted histogram resembles the data reasonably well ( $\chi^2 = 3.8$ ) matching both the mean peak position and the general shape and width of the histogram. The residuals and the PDA prediction show a larger jump at  $E^* = 0.5$ , which is likely to be an artefact of histogramming  $E^*$  values calculated from low integer values representing the two detection channels after excitation of the donor. Fitting the single peak with a model of interconverting FRET species is possible albeit not recommended.

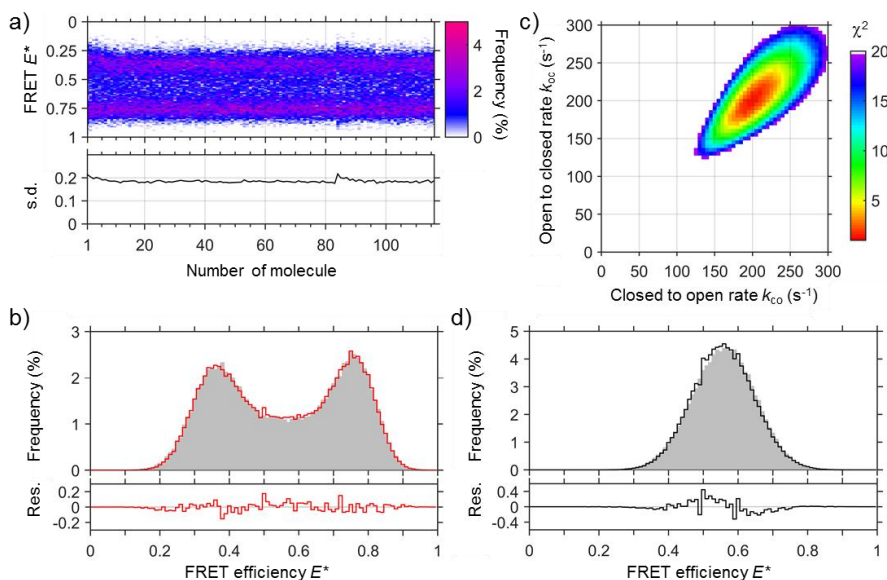


Figure 3. Simulations. Analysing conformational dynamics using dynamic probability distribution analysis (dPDA). (a) top: Colour coded one-dimensional histograms of FRET efficiencies ( $E^*$ ) plotted for each single simulated molecules (for the cumulated histogram of all molecules see **Figure 2b**: 3 ms excitation time and simulated using  $k_{oc} = k_{co} = 200 \text{ s}^{-1}$ ) showing the expected homogeneity among all simulated molecules. bottom: Standard

deviation of the FRET efficiencies for each molecule. **(b)** The cumulated  $E^*$  histogram (grey bars; **Figure 2b** (3 ms excitation time) and fitted using a dynamic two-species model. After optimization based on a Levenberg-Marquardt algorithm, the final fit (red line) shows small residuals and yielded  $k_{oc} = 197 \text{ s}^{-1}$  and  $k_{co} = 199 \text{ s}^{-1}$  ( $\chi^2 = 1.2$ ). **(c)** Plotted  $\chi^2$  values comparing the PDA model and the simulated data as a function of different forward and backward rates using the fitted peak positions and excess widths obtained in (c) as fixed parameters. **(d)** Visualization of the predicted histogram (black stairs) based on parameters obtained in (b) for a 3 ms excitation period plotted on top of the histogram of transfer efficiencies obtained from simulated data with a 50 ms excitation period (grey bars) ( $\chi^2 = 3.2$ ). No further fitting was performed.

as the six parameters used for building the PDA model would still require constraints derived from fitting the sALEX data to stay within a reasonable value space. Nevertheless, the non-fitted PDA prediction allows to visually confirm the accuracy of values obtained from fitting sALEX data.

### dPDA and sALEX for strongly biased equilibria

In order to test the ability of recovering rates in systems which are strongly biased towards one conformation, we set up a simulation using a forward rate of  $k_{oc} = 5 \text{ s}^{-1}$  (lifetime of 200 ms) and a backward rate of  $k_{co} = 200 \text{ s}^{-1}$  (lifetime of 5 ms). All other parameters were kept as described previously. The resulting FRET histogram assuming an excitation of 3 ms is shown in Supplementary Information, Fig. S2. In our simulated case, the equilibrium ratio is  $k_{co}/k_{oc} = 40$  and we therefore expect that the molecules are populating primarily the closed conformation. Even though dPDA is in principle capable of retrieving the rates with  $k_{co} = (216 \pm 15) \text{ s}^{-1}$  and  $k_{oc} = (7 \pm 2) \text{ s}^{-1}$  ( $\chi^2 = 9.1$ ), any experimental validation of systems featuring equilibrium ratios of larger than around 20, in which, on average, 95% of molecules would be in one conformational state and 5% in another state, is challenging and often simply limited by the uniformity and purity of the sample.

### Experimental results using DNA hairpins

For the experimental realization of sALEX and application of dPDA, we decided to use simple DNA hairpin molecules labelled with both donor and acceptor fluorophores. By changing the concentration of salt (here NaCl) in the buffer medium, the conformational equilibrium of DNA hairpins can be tuned (Hartmann et al. 2014, Tsukanov et al. 2013a, Tsukanov et al. 2013b). We chose a DNA hairpin in which the template DNA showed a self-complementarity of 6 neighboured bases designed to open and close rapidly compared to the frame time

of our camera (50 ms). At zero salt concentration, the DNA construct fully populated a low FRET species ( $E^* \sim 0.16$ ) indicating the open form of the DNA hairpin (Fig. 4a, top panel). The sALEX data showed a very similar distribution characterised by the same peak position ( $E^* \sim 0.16$ ) and the same shape of the distribution (Fig. 4b, top panel). Upon addition of salt, the peak position of the main distribution in the 50 ms data shifted gradually from the FRET efficiency indicating the open conformation ( $E^* \sim 0.20$ ) to a FRET efficiency ( $E^* \sim 0.76$ ) indicating the closed conformation (Fig. 4a). Whilst shifting, the width of the distribution changed reaching its maximum at a salt concentration of around 300 mM NaCl. Only at 400 mM NaCl and above, two underlying species with varying peak positions can be identified.

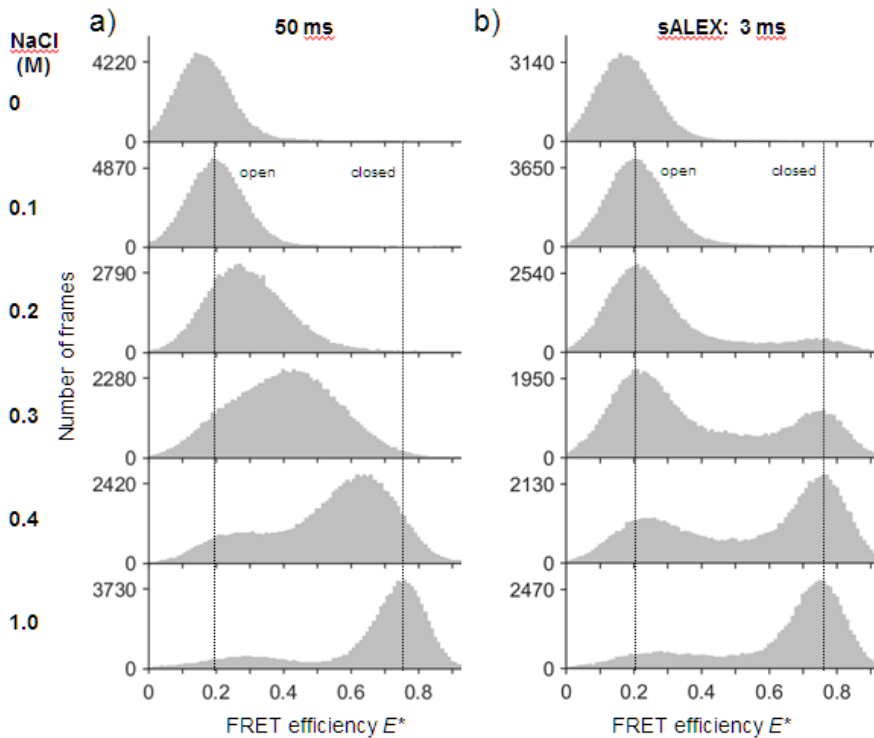


Figure 4. Experiments. Analysing conformational dynamics with dynamic probability distribution analysis (dPDA). (a+b) Surface-immobilized DNA hairpins were measured as a function of different salt concentrations at different excitation times: 50ms (a) and 3 ms (b). The histograms (grey bars, 100 bins) of FRET efficiencies  $E^*$  were calculated from individual time traces after fitting all molecules. The two dotted vertical lines mark the mean  $E^*$  values of the primarily open (0.1 M NaCl) and primarily closed (1 M NaCl) FRET species. Whereas for increasing salt concentrations the mean peak position shifts

towards higher  $E^*$  for a 50 ms excitation time (a), only sALEX allows the identification of a dynamic equilibrium between a open and a closed conformation (b).

For salt concentrations above 100 mM NaCl, the FRET efficiency histograms of the sALEX data started to differ from the conventional ALEX data as the two main populations representing the open and the closed conformation of the hairpin can now be clearly identified and distinguished in every histogram (Fig. 4b). With increasing salt concentrations the conformational equilibrium shifted towards the closed conformation. Whereas the main peak position of the closed conformation is constant for all concentrations above 100 mM NaCl ( $E_c^* \sim 0.76$ ), we note a peak shift of the open conformation from  $E_o^* \sim 0.20$  to a FRET efficiency ( $E_o^* \sim 0.29$ ) consistent with reports describing a compaction of single stranded DNA due to electrostatic screening (Murphy et al. 2004).

To prove the high signal to noise ratio obtainable at short excitation times, we plotted individual frames without any additional averaging after green and red excitation, respectively (Fig. 5a and b). Both images allow the identification and subsequent determination of photon counts for single molecules. Before continuing with the determination of rates using dPDA, we note that the histograms in Fig. 4a at NaCl concentrations of 300 mM showed a small shoulder at around  $E^* \sim 0.20$  which cannot be entirely explained by averaging effects due to fast dynamics. Here, we observed the influence of non-converting DNA hairpins which are stuck in the open conformation.

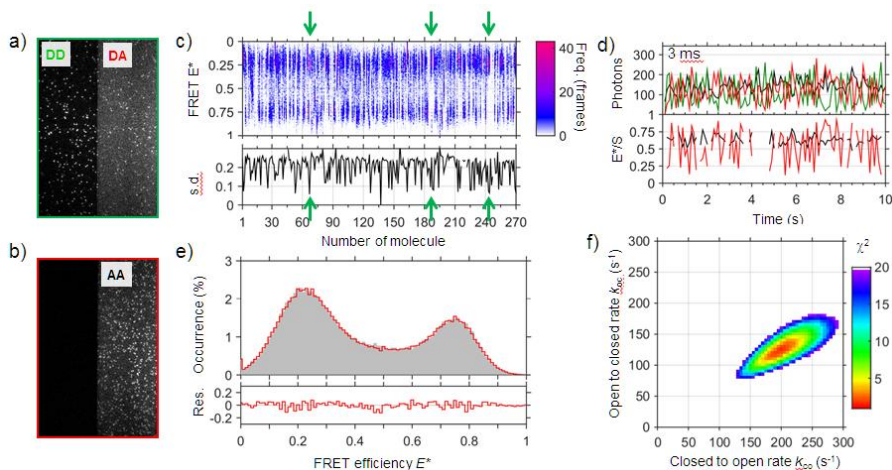


Figure 5. Experimental data using a 3 ms excitation time for a DNA hairpin in presence of 300 mM NaCl. **(a+b)** Individual frames (343 by 512 pixel with a pixel size of 130 nm) after **(a)** green and **(b)** red excitation. **(c)** top: Colour coded one-dimensional histograms of FRET

efficiencies ( $E^*$ ) from three movies plotted for each analysed molecules (for the cumulated histogram of all molecules see **Figure 4b**) showing heterogeneity between the molecules. (bottom) Standard deviations calculated from individual  $E^*$  time traces. Three representative molecules with a low standard deviation are indicated (arrows). **(d)** Individual time traces. Upper panel: donor signal after donor excitation (green trace, DD), acceptor signal after donor excitation (red trace, DA), acceptor signal after acceptor excitation (black trace, AA). Lower panel: transfer efficiencies (red trace,  $E^*$ ) and stoichiometry (black trace, S). The gaps in the lower time traces are due to photon counts below the threshold of  $DD + DA < 200$  and  $AA < 50$  photons per frame. **(e)** The  $E^*$  histogram after additional filtering for (standard deviation above 0.1) was fitted using a dynamic two-species model. After optimization, the final fit (red line) shows small residuals and yielded  $k_{oc} = 120 \text{ s}^{-1}$  and  $k_{co} = 193 \text{ s}^{-1}$  ( $\chi^2 = 1.9$ ). **(f)** Plotted  $\chi^2$  values comparing the PDA model and the experimental data as a function of different forward and backward rates using the fitted peak positions and excess widths obtained in (e) as fixed parameters.

For better visualisation and characterisation, we plotted the one dimensional, colour-coded FRET efficiency histograms of every analysed molecule and calculated the corresponding standard deviation from the time traces of the FRET efficiencies (Fig. 5c). Whereas most molecules show low and high FRET values, some (see arrows) show mainly a single conformation leading to lower standard deviations of the analysed individual time traces. Additionally, we plotted individual time traces of a single molecule (Fig. 5d) confirming the experimental realisation of the parameters such as the photon counts chosen for the simulations in Fig. 2 and 3. Due to the low standard deviation calculated from the FRET efficiency time traces of some molecules seen in Fig. 5c we decided to apply an additional threshold of  $\text{std}(E_{\text{trace}}^*) > 0.1$  to identify traces of non-interconverting DNA hairpins and exclude them from further analysis. The filtered histogram (3 ms, 300 mM NaCl, Fig. 5e) shows only a marginal difference in the relative peak heights of the closed and the open conformation to the corresponding histogram in Fig. 4b. For the PDA fitting, we chose the following starting values  $^iE_o^* = 0.25$ ,  $^iE_c^* = 0.75$ ,  $^ik_{oc} = 100 \text{ s}^{-1}$ ,  $^ik_{co} = 200 \text{ s}^{-1}$  and  $^i\sigma_o = ^i\sigma_c = 0.06$  and obtained  $E_o^* = 0.217 \pm 0.002$ ,  $E_c^* = 0.764 \pm 0.003$ ,  $k_{oc} = (117 \pm 4) \text{ s}^{-1}$ ,  $k_{co} = (188 \pm 6) \text{ s}^{-1}$  and  $\sigma_o = 0.087 \pm 0.002$  and  $\sigma_c = 0.069 \pm 0.004$  with  $\chi^2 = 2.0$  representing again an excellent fit with small residuals (Fig. 5e).

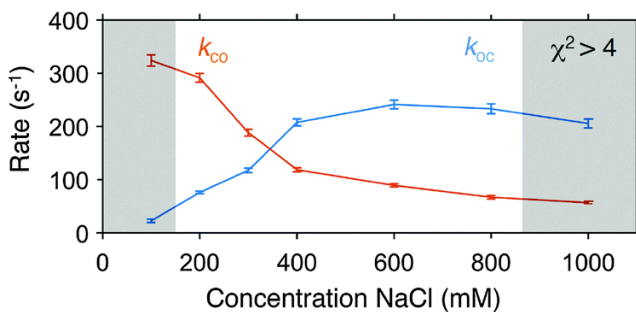


Figure. 6: Conformational dynamics of a DNA hairpin under different concentrations of NaCl. Rates were obtained by fitting histograms of FRET efficiencies with dPDA as discussed in the text. For the individual FRET histograms and the corresponding fits see Fig. 5 and ESI,† Fig. S3. The error bars represent 95% confidence intervals of the fit. The greyed area indicates fits with  $\chi^2 > 4$ .

Similar to the procedure discussed for the simulations, we fixed the positions and the excess widths and calculated the  $\chi^2$  characterising the goodness of the PDA prediction as a function of various forward and backward rates giving  $k_{oc} = (120 \pm 20) \text{ s}^{-1}$  and  $k_{co} = (195 \pm 30) \text{ s}^{-1}$  (Fig. 5f). The results from analysing the conformational rates show for increasing concentrations of NaCl that the rates of the open to close transition increase whereas the rates of the closed to open transition decrease (Fig. 6 and Fig. S1, for the individual dPDA fits) thereby qualitatively and quantitatively agreeing with observations of a similar DNA hairpin structure (Tsukanov et al. 2013a).

## Discussion

We characterised the ability of sALEX and dPDA to identify and quantify conformational dynamics of biomolecules by means of simulations and experimental data. With the simulations we established a comprehensive framework in which a variety of parameters such as conformational rates and distances between the fluorophores can easily be modified allowing to visualise the effect of those parameters on the shape of FRET efficiency histograms. Even without using sALEX for improving the time resolution, the simulations allow realistic predictions of experimentally obtainable data as the simulations explicitly consider sources of noise leading to a significant broadening of FRET distributions in TIRF microscopy (Holden et al. 2010). We demonstrated that the stroboscopic alternating-laser excitation has a dramatic effect on the shape of the FRET histograms of simulated interconverting species (Fig. 2c). By reducing the duration of the excitation (1 ms or 3 ms) below the simulated lifetime of each conformational

state (here 5 ms), we identified the two species whose FRET distributions are otherwise averaged out. As mentioned previously, we should emphasize that by reducing the excitation time below the frame time of the camera required to read and write the data, we lose information about the species between the periods of excitation. This information is largely irrelevant for the case of species in a conformational equilibrium, but has to be considered in cases where reactions such as DNA synthesis are studied (Christian et al. 2009b).

By recording snapshots of conformational states from individual molecules over extended periods of time, we introduced the analysis of the standard deviation of FRET efficiencies as a convenient way to identify inter molecular heterogeneity (Fig. 3a and 5c). In our case, we simply used a threshold criterion to exclude molecules from further analysis which did not undergo conformational changes. We suggest to use a value in the order of twice the theoretically calculated standard deviation introduced in eqn (1). A more detailed analysis of the FRET standard deviation using, for example, sliding windows of a few frames could be used to analyse other sources of dynamic heterogeneity in single entities such as pausing mechanisms in proteins and enzymes.

For analysing the underlying conformational dynamics in FRET efficiency histograms we implemented dynamic probability distribution analysis in TIRF microscopy. Our simulated data showed, that dPDA can accurately recover simulated conformational rates and that dPDA is therefore a promising tool to extract rates from experimental data. It should be noted that dPDA requires some temporal averaging to determine the rates of interconversions; if two species would be entirely separated in the FRET histogram, we could still provide an upper limit for the underlying rates as we can predict at which rates averaging effects would start to occur.

Along the same lines, the accuracy of the conformational analysis using dPDA benefits from well separated FRET peaks representing the two conformations which can, for dynamic species, be ensured by a sufficiently short excitation and a careful design of the FRET construct leading to relative changes in the donor to acceptor distances above 1 nm. Furthermore, the equilibrium ratio between the two species here defined as  $k_{co}/k_{oc}$  should be ideally kept around one to avoid cases in which dynamic heterogeneity of a small subset of molecules might severely bias dPDA analysis.

We note that dPDA can be expanded allowing analysis of species interconverting between more than two conformational states as well as combining dynamic and static species in a single sample.

## ***Improving the time resolution in smFRET TIRF microscopy***

We experimentally demonstrated an effective time resolution of 3 ms for a dynamic system of an interconverting DNA hairpin. The same stem sequence of six complementary bases (5' TGG ATT) which we used for our experiments has recently been used by Tsukanov *et al.* (Tsukanov *et al.* 2013a) who obtained opening and closing rates of  $\sim 200 \text{ s}^{-1}$  at a salt concentration of 300 mM NaCl comparable to our results of  $k_{oc} = (117 \pm 4) \text{ s}^{-1}$  and  $k_{co} = (188 \pm 6) \text{ s}^{-1}$ . Differences in the determined rates can be explained by our choice of a different donor fluorophore (Cy3B instead of ATTO 550) and different labelling positions as it has been shown that both can have a substantial influence on the conformational rates of DNA hairpins (Hartmann *et al.* 2014, Kugel *et al.* 2012). Similar to the experiments by Tsukanov *et al.*, we observed a decrease of the opening and an increase of the closing rate with increasing concentrations of NaCl. The main advantage of our imaging-based implementation is that it takes only tens of seconds to record the same amount of data that would take tens of minutes (or longer) in confocal microscopy.

Our dPDA fits showed (Fig. S1, and also Fig. 6) larger  $\chi^2$  values for conditions in which the DNA hairpin is primarily either in the open or the closed conformation, indicating that dPDA works most reliable if two global peak positions can be seen in the FRET efficiency histogram and both rates are close to each other. In our current experimental implementation, we concentrated on characterizing conformational dynamics that lead to changes in FRET efficiency under equilibrium conditions.

To obtain a broader overview about potential applications of sALEX, two points should be discussed. Firstly, as long as one is mainly interested in detecting FRET efficiencies, (stroboscopic) excitation of the acceptor fluorophore is not required as the stoichiometry parameter is only used to identify molecules bearing both donor and acceptor fluorophore. As recently suggested (Hohlbein *et al.* 2014b), however, combining protein induced fluorescence enhancement (Hwang *et al.* 2011, Hwang and Myong 2014) with single-molecule FRET could generate applications in which the time dependent change in stoichiometry would benefit from increasing the time resolution using stroboscopic excitation. Secondly, our current implementation requires that the molecules of interest are stationary. Whereas the immobilisation of DNA is mostly uses biotin-neutravidin linkage to biotinylated PEG crafted on the glass surface (Lamichhane *et al.* 2010), immobilising proteins requires either vesicle encapsulation (Boukobza *et al.* 2001, Okumus *et al.* 2004) or the use of biotinylated, anti-His5/His6-tag antibodies (Zhou *et al.* 2011).



Finally, if we consider the experimentally shown time-resolution of 3 ms as feasible, where is the current technological limit? Our main experimental limitation was the laser power of the green laser (<50 mW before entering the TIRF objective), which prevented us from increasing the time resolution whilst keeping the number of detected photons per excitation period constant. More powerful lasers could help to improve the time resolution further, but ultimately the achievable time resolution is limited by the photostability and the photon count rate of the organic fluorophores. Recent developments in recipes for photo protection such as oxygen scavengers in combination with triplet state quencher reviewed in (Ha and Tinnefeld 2012, Zheng et al. 2014) or “self-healing” dyes (van der Velde et al. 2013, Zheng et al. 2014) will help to push the number of photons detectable from single emitters further. Another promising technique in single-molecule detection is the use of nano-antennas which has been shown to increase the achievable count rate of organic fluorophores by up to two orders of magnitude (Acuna et al. 2012).

We expect sub-millisecond dynamics to become resolvable in TIRF microscopy especially considering that dPDA allows to analyse distributions of FRET efficiencies in which considerable temporal averaging took place pushing the effective time resolution even below the duration of excitation.

## **Conclusion**

The ability to resolve and characterize conformational dynamics of individual molecules under equilibrium conditions defines single molecule FRET as a powerful technique to study biologically relevant molecules and proteins. Here, we presented two techniques, stroboscopic alternating-laser excitation and dynamic probability distribution analysis for TIRF microscopy, which in combination allow the characterization of conformational dynamics in the 1–20 ms time range. Our sALEX excitation configuration can be easily implemented in existing setups by using, for example, acousto-optical modulators (AOTFs) that allow modulating the intensity of laser sources. Since we used a camera-based implementation that uses the full field of view of the camera instead of relying on cropping or pixel-binning to achieve higher time resolution, hundreds of molecules can be detected in parallel over extended periods. We believe that further developments improving the longevity of fluorophores as well as new technical advances in image acquisition combined with sALEX and dPDA will help to broaden the range of possible applications in single-molecule detection.

### **Acknowledgements**

The authors thank Joseph Torella for providing early versions of the PDA software and Jan-Willem Borst, Arjen Bader and Carel Fijen for critically reading the manuscript and providing helpful comments. S. F. is supported by the Netherlands Organization for Scientific Research (NWO) *via* a FOM (Foundation for Fundamental Research on Matter) grant awarded to Herbert van Amerongen, Wageningen University. J. H. acknowledges support from a Marie Curie Career Integration Grant (#630992).

### **REFERENCES**

- ACUNA GP, MOLLER FM, HOLZMEISTER P, BEATER S, LALKENS B AND TINNEFELD P. 2012. Fluorescence enhancement at docking sites of DNA-directed self-assembled nanoantennas. *Science* 338: 506-510.
- ANTONIK M, FELEKYAN S, GAIDUK A AND SEIDEL CA. 2006. Separating structural heterogeneities from stochastic variations in fluorescence resonance energy transfer distributions via photon distribution analysis. *The journal of physical chemistry B* 110: 6970-6978.
- AXELROD D, BURGHARDT TP AND THOMPSON NL. 1984. Total internal reflection fluorescence. *Annual review of biophysics and bioengineering* 13: 247-268.
- BLUMBERG S, GAJRAJ A, PENNINGTON MW AND MEINERS JC. 2005. Three-dimensional characterization of tethered microspheres by total internal reflection fluorescence microscopy. *Biophysical journal* 89: 1272-1281.
- BOUKOBZA E, SONNENFELD A AND HARAN G. 2001. Immobilization in Surface-Tethered Lipid Vesicles as a New Tool for Single Biomolecule Spectroscopy. *The Journal of Physical Chemistry B* 105: 12165-12170.
- CHRISTIAN TD, ROMANO LJ AND RUEDA D. 2009. Single-molecule measurements of synthesis by DNA polymerase with base-pair resolution. *Proceedings of the National Academy of Sciences of the United States of America* 106: 21109-21114.
- CHUNG HS, MCHALE K, LOUIS JM AND EATON WA. 2012. Single-molecule fluorescence experiments determine protein folding transition path times. *Science* 335: 981-984.
- CORDES T, VOGELSANG J AND TINNEFELD P. 2009. On the mechanism of Trolox as antiblinking and antibleaching reagent. *Journal of the American Chemical Society* 131: 5018-5019.
- ELF J, LI GW AND XIE XS. 2007. Probing transcription factor dynamics at the single-molecule level in a living cell. *Science* 316: 1191-1194.
- FAROOQ S, FIJEN C AND HOHLBEIN J. 2014. Studying DNA-protein interactions with single-molecule Forster resonance energy transfer. *Protoplasma* 251: 317-332.
- FLORS C, HOTTA J, UJI-I H, DEDECKER P, ANDO R, MIZUNO H, MIYAWAKI A AND HOFKENS J. 2007. A stroboscopic approach for fast photoactivation-localization microscopy with Dronpa mutants. *Journal of the American Chemical Society* 129: 13970-13977.
- HA T AND TINNEFELD P. 2012. Photophysics of fluorescent probes for single-molecule biophysics and super-resolution imaging. *Annual review of physical chemistry* 63: 595-617.
- HARTMANN A, KRAINER G AND SCHLIERF M. 2014. Different fluorophore labeling strategies and designs affect millisecond kinetics of DNA hairpins. *Molecules (Basel, Switzerland)* 19: 13735-13754.

- HENZLER-WILDMAN KA ET AL. 2007. Intrinsic motions along an enzymatic reaction trajectory. *Nature* 450: 838-844.
- HOHLBEIN J, AIGRAIN L, CRAGGS TD, BERMEK O, POTAPOVA O, SHOOLIZADEH P, GRINDLEY ND, JOYCE CM AND KAPANIDIS AN. 2013. Conformational landscapes of DNA polymerase I and mutator derivatives establish fidelity checkpoints for nucleotide insertion. *Nature communications* 4: 2131.
- HOHLBEIN J, CRAGGS TD AND CORDES T. 2014. Alternating-laser excitation: single-molecule FRET and beyond. *Chemical Society reviews* 43: 1156-1171.
- HOHLBEIN J, GRYTE K, HEILEMANN M AND KAPANIDIS AN. 2010. Surfing on a new wave of single-molecule fluorescence methods. *Physical biology* 7: 031001.
- HOLDEN SJ, UPHOFF S, HOHLBEIN J, YADIN D, LE RESTE L, BRITTON OJ AND KAPANIDIS AN. 2010. Defining the limits of single-molecule FRET resolution in TIRF microscopy. *Biophysical journal* 99: 3102-3111.
- HWANG H, KIM H AND MYONG S. 2011. Protein induced fluorescence enhancement as a single molecule assay with short distance sensitivity. *Proceedings of the National Academy of Sciences of the United States of America* 108: 7414-7418.
- HWANG H AND MYONG S. 2014. Protein induced fluorescence enhancement (PIFE) for probing protein-nucleic acid interactions. *Chemical Society reviews* 43: 1221-1229.
- JOO C, BALCI H, ISHITSUKA Y, BURANACHAI C AND HA T. 2008. Advances in single-molecule fluorescence methods for molecular biology. *Annual review of biochemistry* 77: 51-76.
- KALININ S, FELEKYAN S, ANTONIK M AND SEIDEL CA. 2007. Probability distribution analysis of single-molecule fluorescence anisotropy and resonance energy transfer. *The journal of physical chemistry B* 111: 10253-10262.
- KALININ S, PEULEN T, SINDBERT S, ROTHWELL PJ, BERGER S, RESTLE T, GOODY RS, GOHLKE H AND SEIDEL CA. 2012. A toolkit and benchmark study for FRET-restrained high-precision structural modeling. *Nature methods* 9: 1218-1225.
- KALININ S, SISAMAKIS E, MAGENNIS SW, FELEKYAN S AND SEIDEL CA. 2010a. On the origin of broadening of single-molecule FRET efficiency distributions beyond shot noise limits. *The journal of physical chemistry B* 114: 6197-6206.
- KALININ S, VALERI A, ANTONIK M, FELEKYAN S AND SEIDEL CA. 2010b. Detection of structural dynamics by FRET: a photon distribution and fluorescence lifetime analysis of systems with multiple states. *The journal of physical chemistry B* 114: 7983-7995.
- KAPANIDIS AN, LEE NK, LAURENCE TA, DOOSE S, MARGEAT E AND WEISS S. 2004. Fluorescence-aided molecule sorting: analysis of structure and interactions by alternating-laser excitation of single molecules. *Proceedings of the National Academy of Sciences of the United States of America* 101: 8936-8941.
- KIM JY, KIM C AND LEE NK. 2015. Real-time submillisecond single-molecule FRET dynamics of freely diffusing molecules with liposome tethering. *Nature communications* 6: 6992.
- KUGEL W, MUSCHIELOK A AND MICHAELIS J. 2012. Bayesian-inference-based fluorescence correlation spectroscopy and single-molecule burst analysis reveal the influence of dye selection on DNA hairpin dynamics. *Chemphyschem : a European journal of chemical physics and physical chemistry* 13: 1013-1022.
- LAMICHHANE R, SOLEM A, BLACK W AND RUEDA D. 2010. Single-molecule FRET of protein-nucleic acid and protein-protein complexes: surface passivation and immobilization. *Methods (San Diego, Calif)* 52: 192-200.

## ***Improving the time resolution in smFRET TIRF microscopy***

- LAURENCE TA, KONG X, JAGER M AND WEISS S. 2005. Probing structural heterogeneities and fluctuations of nucleic acids and denatured proteins. *Proceedings of the National Academy of Sciences of the United States of America* 102: 17348-17353.
- LEE NK, KAPANIDIS AN, WANG Y, MICHALET X, MUKHOPADHYAY J, EBRIGHT RH AND WEISS S. 2005. Accurate FRET measurements within single diffusing biomolecules using alternating-laser excitation. *Biophysical journal* 88: 2939-2953.
- LOURAKIS MIA. 2004. levmar: Levenberg-Marquardt nonlinear least squares algorithms in C/C++.
- MCKINNEY SA, JOO C AND HA T. 2006. Analysis of single-molecule FRET trajectories using hidden Markov modeling. *Biophysical journal* 91: 1941-1951.
- MOERNER WE. 2007. New directions in single-molecule imaging and analysis. *Proceedings of the National Academy of Sciences of the United States of America* 104: 12596-12602.
- MULLER BK, ZAYCHIKOV E, BRAUCHLE C AND LAMB DC. 2005. Pulsed interleaved excitation. *Biophysical journal* 89: 3508-3522.
- MURPHY MC, RASNIK I, CHENG W, LOHMAN TM AND HA T. 2004. Probing single-stranded DNA conformational flexibility using fluorescence spectroscopy. *Biophysical journal* 86: 2530-2537.
- MUSCHIELOK A, ANDRECKA J, JAWHARI A, BRUCKNER F, CRAMER P AND MICHAELIS J. 2008. A nano-positioning system for macromolecular structural analysis. *Nature methods* 5: 965-971.
- NIR E, MICHALET X, HAMADANI KM, LAURENCE TA, NEUHAUSER D, KOVCHEGOV Y AND WEISS S. 2006. Shot-noise limited single-molecule FRET histograms: comparison between theory and experiments. *The journal of physical chemistry B* 110: 22103-22124.
- OKUMUS B, WILSON TJ, LILLEY DM AND HA T. 2004. Vesicle encapsulation studies reveal that single molecule ribozyme heterogeneities are intrinsic. *Biophysical journal* 87: 2798-2806.
- OLOFSSON L, FELEKYAN S, DOUMAZANE E, SCHOLLER P, FABRE L, ZWIER JM, RONDARD P, SEIDEL CA, PIN JP AND MARGEAT E. 2014. Fine tuning of sub-millisecond conformational dynamics controls metabotropic glutamate receptors agonist efficacy. *Nature communications* 5: 5206.
- PREUS S AND WILHELMSSON LM. 2012. Advances in quantitative FRET-based methods for studying nucleic acids. *Chembiochem : a European journal of chemical biology* 13: 1990-2001.
- RASNIK I, MCKINNEY SA AND HA T. 2006. Nonblinking and long-lasting single-molecule fluorescence imaging. *Nature methods* 3: 891-893.
- SANTOSO Y, JOYCE CM, POTAPOVA O, LE RESTE L, HOHLBEIN J, TORELLA JP, GRINDLEY ND AND KAPANIDIS AN. 2010a. Conformational transitions in DNA polymerase I revealed by single-molecule FRET. *Proceedings of the National Academy of Sciences of the United States of America* 107: 715-720.
- SANTOSO Y, TORELLA JP AND KAPANIDIS AN. 2010b. Characterizing single-molecule FRET dynamics with probability distribution analysis. *Chemphyschem : a European journal of chemical physics and physical chemistry* 11: 2209-2219.
- TORELLA JP, HOLDEN SJ, SANTOSO Y, HOHLBEIN J AND KAPANIDIS AN. 2011. Identifying molecular dynamics in single-molecule FRET experiments with burst variance analysis. *Biophysical journal* 100: 1568-1577.
- TSUKANOV R, TOMOV TE, BERGER Y, LIBER M AND NIR E. 2013a. Conformational dynamics of DNA hairpins at millisecond resolution obtained from analysis of single-molecule FRET histograms. *The journal of physical chemistry B* 117: 16105-16109.

- TSUKANOV R, TOMOV TE, MASOUD R, DRORY H, PLAVNER N, LIBER M AND NIR E. 2013b. Detailed study of DNA hairpin dynamics using single-molecule fluorescence assisted by DNA origami. *The journal of physical chemistry B* 117: 11932-11942.
- TYAGIS, VANDELINDER V, BANTERLE N, FUERTES G, MILLES S, AGEZ M AND LEMKE EA. 2014. Continuous throughput and long-term observation of single-molecule FRET without immobilization. *Nature methods* 11: 297-300.
- UPHOFF S, GRYTE K, EVANS G AND KAPANIDIS AN. 2011. Improved temporal resolution and linked hidden Markov modeling for switchable single-molecule FRET. *Chemphyschem : a European journal of chemical physics and physical chemistry* 12: 571-579.
- VAN DER VELDE JH, PLOETZ E, HIERMAIER M, OELERICH J, DE VRIES JW, ROELFES G AND CORDES T. 2013. Mechanism of intramolecular photostabilization in self-healing cyanine fluorophores. *Chemphyschem : a European journal of chemical physics and physical chemistry* 14: 4084-4093.
- WALTER NG, HUANG CY, MANZO AJ AND SOBHY MA. 2008. Do-it-yourself guide: how to use the modern single-molecule toolkit. *Nature methods* 5: 475-489.
- WEISS S. 1999. Fluorescence spectroscopy of single biomolecules. *Science* 283: 1676-1683.
- ZHENG Q, JUETTE MF, JOCKUSCH S, WASSERMAN MR, ZHOU Z, ALTMAN RB AND BLANCHARD SC. 2014. Ultra-stable organic fluorophores for single-molecule research. *Chemical Society reviews* 43: 1044-1056.
- ZHOU R, KUNZELMANN S, WEBB MR AND HA T. 2011. Detecting intramolecular conformational dynamics of single molecules in short distance range with subnanometer sensitivity. *Nano letters* 11: 5482-5488.

## **SUPPLEMENTARY INFORMATION**

### **Labelling, purification and immobilization of DNA**

The DNA construct consisted of two DNA molecules: A primer strand (30 bases long, 5' CCT CAT TCT TCG TCC CAT TAC CAT ACA TCC) and a template DNA (75 bases long, 5' TGG ATT AAA AAA AAA AAA AAA AAA AAA AAA AAA AAA TCC ATT GGA TGT ATG GTA ATG GGA CGA AGA ATG AGG) that forms a hairpin structure owing to sequence complementarity of six consecutive bases in one region of the strand to another. The single stranded DNAs were prepared by automated synthesis (IBA, Germany). We labelled the 5' biotinylated primer strand with ATTO647N (ATTO-TEC, Germany) as the acceptor dye using the internally amino modified-dT base at position -12. The template DNA hairpin was labelled with Cy3B (GE Healthcare, UK) as the donor fluorophore on the 5' end. Both strands were first purified using denaturing polyacrylamide gel electrophoresis and then annealed by mixing equimolar amounts of top and bottom strand in annealing buffer (Tris-HCl pH 8, 500 mM NaCl, 1 mM EDTA) and heating to 95°C, followed by slow cooling to room temperature.

To ensure a controlled surface immobilisation of the DNA, the cover slips needed to be carefully modified. First, we placed the cover slips in a furnace for 1h at 500°C to remove any surface contaminations. We then silanized the glass surface with a mixture of 98% acetone and 2% Vectabond (Vectorlabs, USA). After rinsing the sample with deionised water and drying the cover slips under nitrogen, we mounted the cover slips to sticky, precast flow channels (sticky-slide VI, Ibidi, Germany). After forming the chambers, we dissolved 4 mg of NHS-PEG (mPEG-SPA MW 5000, Lyasan, USA) and 0.1 mg biotin-PEG-NHS (mPEG-SC MW 5000, Lyasan, USA) in 400 ml of 50 mM MOPS buffer (pH 7.5) and incubated the chambers for a few hours before rinsing with PBS buffer. To immobilise the biotinylated DNA, we incubated the chambers in 0.25 mg/ml Neutravidin that binds to the biotinylated PEG, and rinsed with PBS buffer after 10 minutes before adding the solution containing 10-50 pM of the DNA molecules containing a biotin for specific immobilisation. The surface density of the molecules was monitored with the camera. After reaching a desirable density, the remaining, non-bound molecules were washed off with PBS buffer. The imaging buffer consisted of 50mM Tris HCL pH 7.5, 1 mg/l BSA, 1 mM EDTA, 5% (v/v) glycerol, 1mM DTT, 1mM Trolox as a triplet-state quenching agent, 1% (v/v) of an oxygen scavenger system (0.1 mg/ml glucose oxidase and 7 mg/ml catalase) and 1% (w/v) D+ glucose (Cordes et al. 2009, Rasnik et al. 2006a).

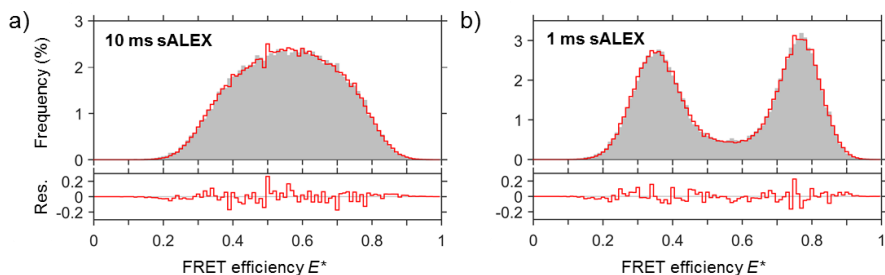


**Figure S1.** Simulations. The cumulated  $E^*$  histogram (grey bars; Figure 2b: 10 ms and 1 ms excitation time) and fitted using a dynamic two-species model. After optimization based on a Levenberg-Marquardt algorithm, the final fit (red line) shows small residuals and yielded **a)**  $E_o^* = 0.345 \pm 0.008$ ,  $E_c^* = 0.769 \pm 0.007$ ,  $k_{oc} = (201 \pm 10) \text{ s}^{-1}$ ,  $k_{co} = (190 \pm 10) \text{ s}^{-1}$  and  $\sigma_o = 0.053 \pm 0.007$  and  $\sigma_c = 0.053 \pm 0.012$  with  $\chi^2 = 2.0$  and **b)**  $E_o^* = 0.352 \pm 0.001$ ,  $E_c^* = 0.773 \pm 0.001$ ,  $k_{oc} = (189 \pm 7) \text{ s}^{-1}$ ,  $k_{co} = (188 \pm 7) \text{ s}^{-1}$  and  $\sigma_o = 0.057 \pm 0.002$  and  $\sigma_c = 0.051 \pm 0.002$  with  $\chi^2 = 2.0$

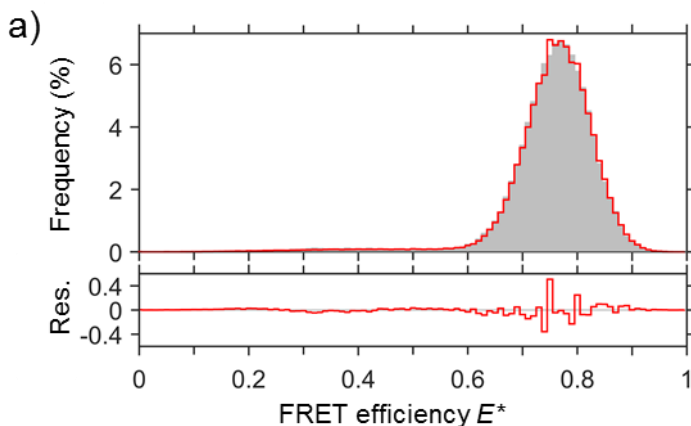


**Figure S2.** Simulations. Simulation using a forward rate of  $k_{oc} = 5 \text{ s}^{-1}$  and a backward rate of  $k_{co} = 200 \text{ s}^{-1}$ . All other parameters were kept as described previously. The final fit (red line) shows small residuals and yielded  $E_o^* = 0.350 \pm 0.058$ ,  $E_c^* = 0.771 \pm 0.001$ ,  $k_{oc} = (216 \pm 15) \text{ s}^{-1}$ ,  $k_{co} = (6 \pm 2) \text{ s}^{-1}$  and  $\sigma_o = 0.115 \pm 0.038$  and  $\sigma_c = 0.050 \pm 0.002$  with  $\chi^2 = 9.1$

## Improving the time resolution in smFRET TIRF microscopy

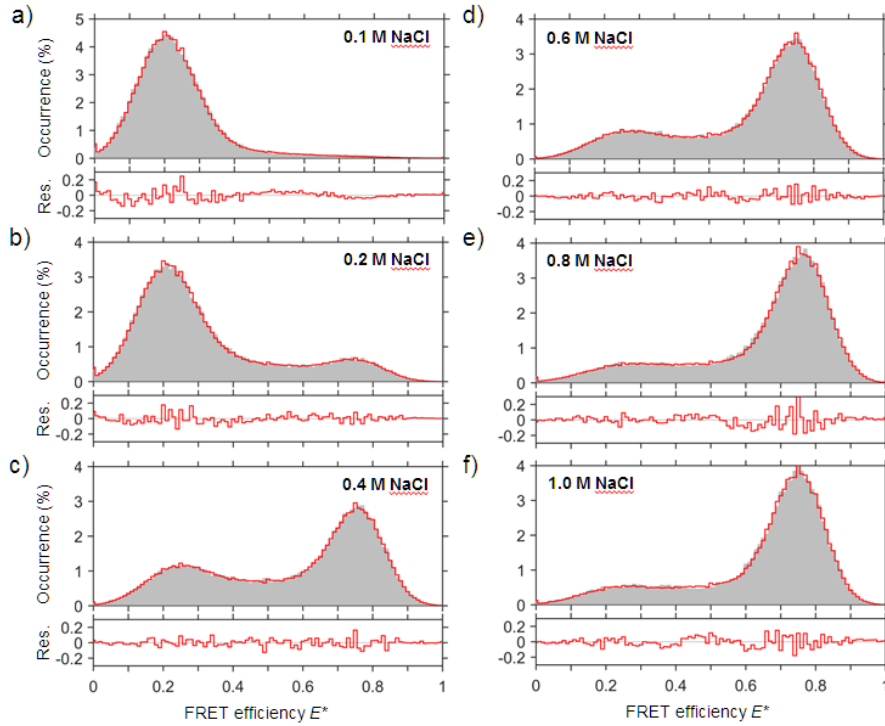


**Figure S3.** Experimental data. Additional FRET histograms for analysing conformational dynamics with dynamic probability distribution analysis. **(a) 100 mM NaCl**,  $E^*_o = 0.210 \pm 0.001$ ,  $E^*_c = 0.700 \pm 0.044$ ,  $k_{oc} = (23 \pm 3) \text{ s}^{-1}$  and  $k_{co} = (324 \pm 10) \text{ s}^{-1}$ , ( $\chi^2 = 12$ ). **(b) 200 mM NaCl**,  $E^*_o = 0.210 \pm 0.001$ ,  $E^*_c = 0.768 \pm 0.006$ ,  $k_{oc} = (76 \pm 2) \text{ s}^{-1}$  and  $k_{co} = (291 \pm 8) \text{ s}^{-1}$  ( $\chi^2 = 2.0$ ). **(c) 400 mM NaCl**  $E^*_o = 0.235 \pm 0.004$ ,  $E^*_c = 0.767 \pm 0.001$ ,  $k_{oc} = (207 \pm 7) \text{ s}^{-1}$  and  $k_{co} = (118 \pm 4) \text{ s}^{-1}$  ( $\chi^2 = 1.9$ ). **(d) 600 mM NaCl**  $E^*_o = 0.240 \pm 0.005$ ,  $E^*_c = 0.751 \pm 0.001$ ,  $k_{oc} = (241 \pm 8) \text{ s}^{-1}$  and  $k_{co} = (89 \pm 3) \text{ s}^{-1}$  ( $\chi^2 = 1.6$ ). **(e) 800 mM NaCl**  $E^*_o = 0.258 \pm 0.013$ ,  $E^*_c = 0.768 \pm 0.001$ ,  $k_{oc} = (233 \pm 9) \text{ s}^{-1}$  and  $k_{co} = (67 \pm 3) \text{ s}^{-1}$  ( $\chi^2 = 2.6$ ). **(f) 1 M NaCl**  $E^*_o = 0.261 \pm 0.011$ ,  $E^*_c = 0.755 \pm 0.001$ ,  $k_{oc} = (205 \pm 8) \text{ s}^{-1}$  and  $k_{co} = (56 \pm 3) \text{ s}^{-1}$  ( $\chi^2 = 4.4$ ).



## **REFERENCES**

- CORDES T, VOGELSANG J AND TINNEFELD P. 2009. On the mechanism of Trolox as antiblinking and antibleaching reagent. *Journal of the American Chemical Society* 131: 5018-5019.
- RASNIK I, MCKINNEY SA AND HA T. 2006. Nonblinking and long-lasting single-molecule fluorescence imaging. *Nature methods* 3: 891-893.



## **CHAPTER 4**

# **Is there Excitation Energy Transfer between Different Layers of Stacked Photosystem-II-containing Thylakoid membranes?**

based on:

Farooq, S., J. Chmeliov, G. Trinkunas, L. Valkunas and H. van Amerongen (2016). "Is There Excitation Energy Transfer between Different Layers of Stacked Photosystem-II-Containing Thylakoid Membranes?" *The Journal of Physical Chemistry Letters* 7(7): 1406-1410.

## **Abstract**

We have compared picosecond fluorescence decay kinetics for stacked and unstacked photosystem II membranes in order to evaluate the efficiency of excitation energy transfer between the neighboring layers. The measured kinetics were analyzed in terms of a recently developed fluctuating antenna model that provides information about the dimensionality of the studied system. Independently of the stacking state, all preparations exhibited virtually the same value of the apparent dimensionality,  $d = 1.6$ . Thus, we conclude that membrane stacking does not affect the efficiency of the delivery of excitation energy towards the reaction centers but ensures a more compact organization of the thylakoid membranes within the chloroplast and separation of photosystems I and II.

## **Introduction**

In oxygenic photosynthesis, two photosystems of different types work in series to convert the energy of solar irradiation into storable energy of chemical bonds. Photosystems I (PSI) and II (PSII) are both large pigment–protein supercomplexes containing hundreds of pigments—chlorophyll (Chl) and carotenoid molecules. Excitation energy arising from light absorption by the light-harvesting antenna is transferred on a timescale of several tens to several hundreds of ps to the reaction centers (RCs) of PSI and PSII, where it leads to charge separation (Blankenship 2002, Van Amerongen et al. 2000). In green plants and algae, the photosystems occupy a large part of the thylakoid membranes, an extensive system of internal membranes found within the chloroplasts, where light reactions of photosynthesis take place. Whereas PSI is mainly present in the unstacked stroma lamellae, PSII is almost exclusively located in the disc-like grana with both diameter and height being of the order of several hundreds of nanometers. These grana consist of stacked thylakoid membranes. It is still not clear whether excitation energy transfer (EET) in the grana occurs only in two dimensions—within the membranes—or whether also effective inter-layer energy transfer takes place. Almost three decades ago, photovoltage measurements were conducted on stacked thylakoids that provided some evidence for inter-membrane exciton transfer (Trissl et al. 1987). However, in a later study (Kirchhoff et al. 2004) it was found that unstacking of the membranes by cation depletion (Izawa et al. 1966) does not lead to a decrease of the connectivity in PSII, indicating that no significant inter-layer EET occurs and therefore excitation migrates through the membrane mainly in a lateral fashion. This result was then further supported by time-resolved fluorescence measurements of stacked and unstacked thylakoid membranes in the presence of variable amounts of additional excitation quenchers (Lambrev et al. 2011).

However, it should be kept in mind that unstacking of the thylakoid membrane by  $\text{MgCl}_2$  depletion can also cause some intermixing of the protein complexes (Kirchhoff et al. 2007, Staehelin 1976). Moreover, some spillover from PSII to PSI has been observed (Briantais et al. 1984, van der Weij-de Wit et al. 2007), which may also influence the apparent connectivity within the thylakoid membrane (Kirchhoff et al. 2007, Lambrev et al. 2011).

Recently, we proposed a new method to describe and analyze the multi-exponential fluorescence decay kinetics in various photosynthetic complexes and membranes (Chmeliov et al. 2014). Dealing with simple excitation diffusion in a continuous medium, our fluctuating antenna model accounted for both the fluctuating nature of the light-harvesting antenna, resulting in the varying connectivity between the pigment-protein complexes, and the non-uniform distribution of these complexes around the reaction centers. That was achieved by introducing an effective *fractal* dimensionality  $d$  of the mentioned continuous medium under consideration. As a result, fluorescence decay kinetics, arising from variably sized PSII, stacked PSII-enriched membranes (so-called BBY particles), aggregates of major light-harvesting complexes (LHCII), or even the whole photosynthetic membranes, were successfully described using just 2 major fitting parameters, the dimensionality  $d$  being one of them (Chmeliov et al. 2014, Chmeliov et al. 2016b). In particular, the kinetics of 4 different purified PSII supercomplexes of various sizes were all readily described using a value of  $d$  ranging from 1.5 to 1.7 (Chmeliov et al. 2014, Chmeliov et al. 2016b), which indicated the existence of some distortions in the planar distribution of the light-harvesting complexes in PSII. On the other hand, a value of  $d = 2.2$  was obtained for the stacked BBY particles. As a result, it was proposed that the latter value, being larger than 2, might indicate EET between different layers of the grana, in contrast to the PSII supercomplexes, where such transfer cannot take place, thus resulting in  $d < 2$ . In order to study this in more detail, we now performed picosecond fluorescence measurements to study both stacked and unstacked PSII-enriched membranes. By applying our fluctuating antenna model (Chmeliov et al. 2014, Chmeliov et al. 2016b) to analyze the obtained excitation decay kinetics we are able to compare the functional organization of the BBY particles of both types in terms of the dimensionality  $d$  of the stacked and unstacked membranes. Based on these results, the efficiency of the inter-layer excitation energy transfer can be evaluated.

## **Materials and Methods**

Thylakoid membranes were isolated from dark-adapted spinach leaves from the local market by utilizing two different procedures. In the first method, the spinach leaves were depetiolated, de-midribbed and homogenized in a blender in an ice-cold buffer containing 20 mM Tricine (pH 7.5), 5 mM MgCl<sub>2</sub> and 0.4 M Sorbitol, washed in a buffer containing Tricine (pH 7.5), 5 mM MgCl<sub>2</sub> and 0.15 M Sorbitol, and then again washed and diluted in a buffer containing 20 mM MES (pH 6.5), 15 mM NaCl and 5 mM MgCl<sub>2</sub>.

PSII-enriched grana membranes (BBY) were isolated from the stacked thylakoid membranes (Berthold et al. 1981) with a slight modification (Caffarri et al. 2009), and the chlorophyll concentration was adjusted to 2.5 mg/ml (Porra et al. 1989). Unstacked BBY membranes were prepared in a similar manner as above, but MgCl<sub>2</sub> was replaced by 5 mM EDTA in all buffers. We also prepared a set of unstacked BBYs, where EDTA was omitted in the last step *i.e.* no EDTA in storage buffer in order to lower the risk of Mn and Fe depletion.

The second set of BBY membranes was prepared by using the method described in *Methods in molecular biology* (Carpentier 2004). For unstacking the BBYs, MgCl<sub>2</sub> was replaced by EDTA in all buffers. As for reason mentioned in first preparation method, we also made a set of unstacked BBY sample, where EDTA was omitted from storage buffer (*i.e.* no EDTA).

Steady-state fluorescence spectra were recorded with a Fluorolog FL-3.22 spectrofluorimeter (Horiba Jobin Yvon, Edison, NJ) at room temperature. The excitation wavelength was 412 nm, and a 2-nm bandwidth was used both for excitation and emission. The measurements were corrected for wavelength-dependent detection sensitivity as well as for fluctuations in the lamp output.

Time-correlated single photon counting (TCSPC) measurements were performed at magic angle (54.7°) polarization with a home-built setup, as described previously (Burri et al. 2005). The excitation wavelength used was 412 nm with a pulse duration of 0.2 ps at a repetition rate of 3.8 MHz. The excitation spot diameter was about 2 mm. The samples were placed in a 3 mL cuvette with an optical path length of 10 mm. For the measurement, each BBY sample (stacked and un-stacked) was diluted to an optical density (OD) of 0.1 per cm in the Q<sub>y</sub> band to minimize re-absorption. To keep the reaction centers in the open state (for nearly 100%), 0.3 mM ferrocyanide was used in combination with low excitation intensity. The samples were continuously stirred in a temperature-controlled sample holder at 20°C. The

instrument response function (IRF) of 60 ps (FWHM) was obtained with 6 ps decay of pinacyanol iodide in methanol (van Oort et al. 2008b, van Oort et al. 2007). Fluorescence was detected at 679 nm. Each measurement was repeated at least three times on the same sample and at least twice for different samples from the same batch, and they always gave (nearly) identical results. Data analysis was performed using a home-built computer program (Digris et al. 1999, Novikov et al. 1999). The data was fitted to a multi-exponential decay function with amplitudes  $A_i$  and fluorescence decay times  $\tau_i$ .

For several decades, such multi-exponential fluorescence decay kinetics, observed in various photosynthetic systems, were attributed to the reversible charge separation occurring in the reaction centers. Recently, we have proposed that the origin of this multi-exponentiality can be related to the fluctuating properties of the light-harvesting antenna, manifesting itself via the varying connectivity between the pigment-protein complexes and, as a result, varying mean times needed for the excitation to reach the RC (Chmeliov et al. 2014, Chmeliov et al. 2016b). Dealing with just simple excitation diffusion in a continuous medium, this model has proven to reasonably reproduce the multi-exponential excitation kinetics in various systems, provide some information on their structural organization as well as to naturally explain some puzzles that could not be fully understood in terms of earlier models. In this study, we used this model to describe non-exponential fluorescence decay kinetics in the large fluctuating antenna of PSII (see  $F_{\text{PSII}}(t)$  term in Eq. 1). By accounting for the small (the relative amplitude  $1-A$ ) long-lived fluorescence signal coming from free Chls or separated LHClI trimers, we obtained the total excitation decay kinetics, which was then convolved with the IRF and fitted to the experimentally observed fluorescence kinetics using the standard least-squares-based algorithm.

## Results and discussion

The fluorescence decay kinetics, measured in stacked and unstacked PSII-enriched grana membranes (BBYs) with open RCs, are shown in Fig. 1. For a good fit, at least four exponential decay components are needed in both cases. The contribution of the long components with 2–3 ns lifetimes is very small, only about ~0.2%, and arises probably due to some free Chls, disconnected antenna complexes and/or closed RCs (Broess et al. 2006). Other obtained lifetime components are as follows: 95 ps (38.2%), 278 ps (33.5%), and 458 ps (27.8%) for the stacked membranes and 100 ps (44%), 299 ps (45.2%), and 513 ps (12.4%) for the unstacked ones, corresponding to average lifetimes of 258 ps and 238 ps, respectively. The same measurements were repeated several times with different samples and also

## **EET between different layers of stacked PSII-containing Thylakoid membranes**

using different procedures to obtain stacked and unstacked BBYs (see Experimental Methods). In all cases, the measured average lifetimes are considerably longer than the 120–150 ps, recently reported for BBYs (Broess et al. 2006, Gibasiewicz et al. 2015), which were similar to the mean excitation lifetimes of PSII supercomplexes (Caffarri et al. 2011). On the other hand, they are notably shorter than average lifetimes reported for PSII in thylakoid membranes, ranging from 220 to 320 ps (van Oort et al. 2010, Wientjes et al. 2013). This range of the mean excitation lifetimes in PSII is in line with the results obtained by Veerman *et al.* (Veerman et al. 2007), who implemented different isolation methods and varied the detergent treatment. We also observed a shortening of lifetimes upon prolonged treatment with the detergent Triton X-100, but since this led to sample instabilities, we have limited the incubation time to 10 minutes for our experiments, leading to relatively long average lifetimes.

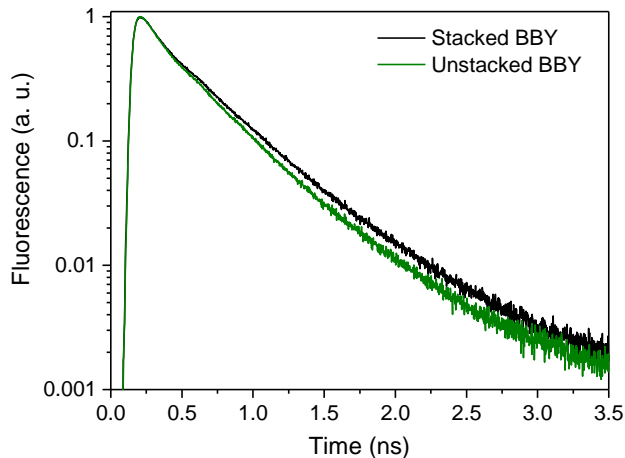


Figure 1. Fluorescence decay kinetics in stacked and unstacked BBY preparations with the PSII RCs being in the open state. Both samples were excited at 412 nm and fluorescence was detected at 679 nm.

The fact that the average lifetime in the unstacked membranes is somewhat shorter than that in the stacked ones might seem unexpected at first glance. The disruption of EET between different layers upon unstacking should lead to an increase of the average lifetime, whereas the complete absence of EET between different layers in stacked membranes would leave the lifetime unchanged (Chmeliov et al. 2014). However, the observed increase of the fluorescence decay rate can arise due to reorganization upon unstacking (Stoitchkova et al. 2006) which might result in the enhanced energy transfer from LHCII to PSI (Kouril et al. 2005, van der Weij-de Wit et al. 2007). Alternatively, the unstacking procedure can also lead to some



aggregation of antenna complexes, which in turn could cause some shortening of excitation lifetimes (van Oort et al. 2007).

In order to discriminate between a change in dimensionality and other effects, we analyzed the measured fluorescence decay kinetics in terms of the fluctuating antenna model (Chmeliov et al. 2014), depending on just two major parameters that have the strongest effect on the excitation decay kinetics on a sub-ns timescale: the dimensionality of the system,  $d$ , and the simple product,  $Dc^2/d$ , where  $D$  is the mean excitation diffusion rate and  $c$  is the mean concentration of the excitation traps (open RCs) in PSII. To expand our analysis to the ns time region, we have additionally accounted for the intrinsic linear excitation dissipation rate not related to the charge separation by the RC,  $k_{\text{dis}}$ , as well as the presence of free Chls and/or disconnected LHCII complexes that are responsible for the ns-lifetime component ( $\tau_{\text{ns}}$ ) discussed above:

$$F(t) = A \cdot F_{\text{PSII}}\left(t; d, Dc^2/d, k_{\text{dis}}\right) + (1 - A)e^{-\frac{t}{\tau_{\text{ns}}}}, \quad (1)$$

where  $F_{\text{PSII}}(t)$  is the multi-exponential fluorescence decay kinetics originating from PSII, the second term describes slow exponential fluorescence decay, and  $A$  is the amplitude reflecting the relative influences of both components to the overall fluorescence decay kinetics. The  $F_{\text{PSII}}(t)$  term, containing three parameters ( $d$ ,  $Dc^2/d$ , and  $k_{\text{dis}}$ ), was calculated according to the fluctuating antenna model by assuming excitation diffusion in a continuous fractal medium (see Methods and (Chmeliov et al. 2014, Chmeliov et al. 2016b) for details).

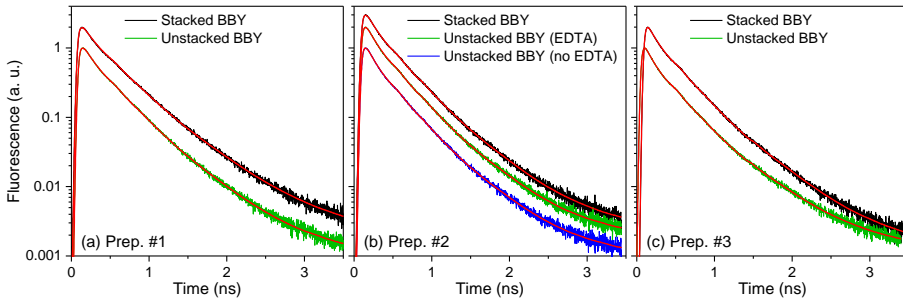


Figure 2. Experimental (black, green, and blue lines) and fitted (red lines) fluorescence kinetics in various BBY preparations, presented on a semi-logarithmic scale. The fitted kinetics were calculated according to Eq. 1 using the parameters listed in Table 1. For visual clarity, the different kinetics are normalized to 1, 2 and 3.

The obtained fitting results for the various BBY preparations are presented in Fig. 2 while the corresponding model parameters are summarized in Table 1. As

### **EET between different layers of stacked PSII-containing Thylakoid membranes**

expected, the relative amplitude of the ns time component originating from free Chls or separated LHCII complexes, 1-A, was just about 0.1–0.2%, indicating high sample purity. Since the fitting results did not exhibit any pronounced dependence on  $\tau_{\text{ns}}$  with such a negligible amplitude, we fixed it to  $\tau_{\text{ns}} = 4$  ns in all cases for simplicity. From Table 1 we see that, independently of the sample preparation, there is no significant variation of the dimensionality  $d$  upon membrane unstacking: of intra-membrane excitation energy transfer pathways in all the preparations. the obtained mean value, averaged over all the samples, is  $d = 1.59 \pm 0.05$ . This result indicates that there is no substantial transverse EET across the neighboring layers of the stacked photosynthetic membrane, so that ordinary intra-layer excitation diffusion dominates in all our samples.

**Table 1.** Model parameters,<sup>a</sup> obtained by fitting the fluorescence decay kinetics in different BBY preparations according to Eq. 1.

Preparation	BBY <sup>b</sup>	$d$	$[Dc^{2/d}]^{-1}$ (ns)	$k_{\text{dis}}^{-1}$ (ns)	$A$
#1	Stacked BBY	1.59	5.26(20)	0.85	99.86(1) %
	Unstacked BBY (EDTA)	1.52	4.63(24)	0.74	99.88(1) %
#2	Stacked BBY	1.54	3.88(25)	0.74	99.91(1) %
	Unstacked BBY (EDTA)	1.52	3.40(24)	0.75	99.89(1) %
	Unstacked BBY (no EDTA)	1.42	3.10(29)	0.70	99.89(1) %
#3	Stacked BBY	1.75	3.95(19)	0.94	99.91(1) %
	Unstacked BBY (EDTA)	1.77	3.33(17)	1.19	99.82(1) %

<sup>a</sup> The parameter  $\tau_{\text{ns}} = 4$  ns was fixed in all the cases. Numbers in parentheses represent the uncertainties of the obtained model parameters corresponding to 95% confidence interval.

<sup>b</sup> Unstacked BBYs were prepared by using either EDTA in the storage buffer (indicated with (EDTA)) or no EDTA in the storage buffer (indicated with (no EDTA)), as explained in the Methods section.

The obtained dimensionality  $d$  is smaller than 2, which reflects the presence of void regions and/or the lack of connectivity at some antenna points. Moreover, similar values of  $d$ , obtained for the stacked and unstacked membranes, suggest rather similar patterns. Since  $d$  remains virtually the same in all our samples, the observed differences in the fluorescence decay kinetics in the stacked and unstacked BBY preparations arise entirely from the variations of the other model parameter,  $Dc^{2/d}$  (cf. Table 1), which relates the excitation transfer rate through the light-harvesting antenna to the mean antenna size (Chmeliov et al. 2014, Chmeliov et al. 2016b):

$$[Dc^{2/d}]^{-1} \cong 2d\tau_h N^{2/d}, \quad (2)$$

here  $\tau_h$  is the mean inter-complex excitation hopping time and  $N$  is the average number of the pigment-protein complexes per RC. The interdependence between  $N$  and  $\tau_h$ , calculated for various BBY preparations and yielding the same parameters  $Dc^{2/d}$  as listed in Table 1, is shown in Fig. 3.

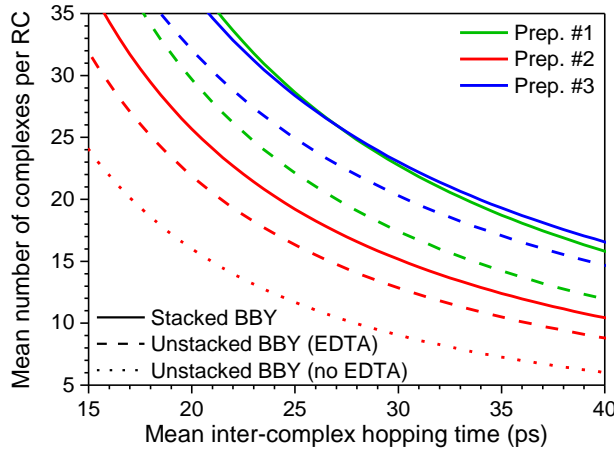


Figure 3. The relationship between the mean number of antenna complexes per RC and the mean inter-complex hopping time, calculated from the obtained  $Dc^{2/d}$  parameter for variously prepared BBY membranes. Solid, dashed, and dotted lines correspond to the stacked and two unstacked BBY samples, respectively, while different colors represent different BBY preparations.

We see that for all preparations, the observed faster kinetics in the unstacked BBY can be explained either by better inter-complex connectivity, leading to the faster

### **EET between different layers of stacked PSII-containing Thylakoid membranes**

EET to the RC, or by a reduced antenna size (*e.g.*, due to separation of some LHCII trimers during the unstacking procedure). The occurrence of the latter process is indirectly supported by the slightly reduced amplitude  $A$  of the relative influence of PSII to the measured fluorescence kinetics, obtained for the majority of the unstacked membranes (see Eq. 1 and Table 1).

Interestingly, Fig. 3 also reveals that the properties of the isolated BBY particles are very sensitive to the preparation procedure. For example, if we assume an average inter-complex excitation hopping time of 25 ps for all the samples, the PSII antenna size can be evaluated as 29 complexes per RC for the stacked BBY from the preparations (#1 and #3) and just 19 complexes for the preparation #2 (corresponding to  $\sim 7.5$  and 4.5 LHCII trimers per RC, respectively). The unstacked BBY particles then contain 1–2 LHCII trimers per RC less. Such sensitivity to the sample preparation method might explain somewhat faster fluorescence kinetics observed in previous studies (Broess et al. 2006), for which the dimensionality  $d = 2.2$  was obtained (Chmeliov et al. 2014, Chmeliov et al. 2016b).

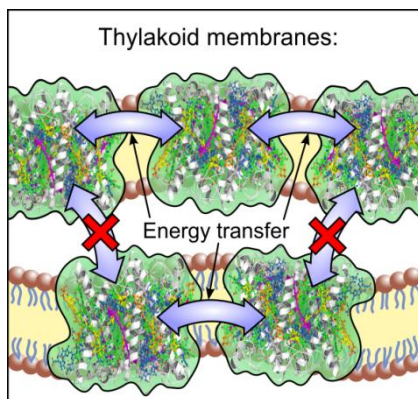


Figure 4. Schematic diagram of thylakoid membrane showing no transverse inter-layer excitation energy transfer (EET) between the neighboring layers.

Another important result of our simulations is the rather fast intrinsic excitation decay,  $k_{\text{dis}}^{-1} = 0.7\text{--}1.1$  ns, far below the typical value of  $\sim 4$  ns observed in separate LHCII trimers. Contrarily, the obtained values are more similar to the mean excitation lifetimes in LHCII aggregates (van Oort et al. 2010, van Oort et al. 2007). This result might indicate the formation of a relatively large LHCII clusters across the thylakoid membrane between the RCs of different PSIIs, resulting in the random generation of additional slow quenching centers that lead to the faster excitation decay kinetics (Belgio et al. 2014a). Indeed, somewhat similar fluorescence quenching, reducing the mean excitation lifetime to  $\sim 2$  ns, was

observed recently in the RC-deficient thylakoid membranes from plants treated with lincomycin, inhibiting the synthesis of reaction centers (Belgio et al. 2012).

## **Conclusion**

To summarize, in this work we have compared fluorescence decay kinetics for stacked and unstacked BBY complexes. In order to evaluate the efficiency of the excitation energy transfer between the neighboring layers of the photosynthetic membrane, we analyzed the measured kinetics in terms of the recently developed fluctuating antenna model that provides information about the dimensionality of the studied system (Chmeliov et al. 2014). We found that, independently of the stacking state of the thylakoid membranes, all our BBY preparations exhibited virtually the same value of  $d = 1.6$ , indicating the absence of any transverse inter-layer EET, in agreement with the conclusions of Lambrev *et al.* (Kirchhoff et al. 2007, Lambrev et al. 2011) and Kirchhoff *et al.* (Kirchhoff et al. 2007, Lambrev et al. 2011), but in contrast to the earlier work by Trissl *et al.* (Trissl et al. 1987). Thus, we can conclude that stacking of the grana lamellae does not affect the efficiency of the delivery of excitation energy towards the reaction centers but probably just ensures a more compact organization of the thylakoid membranes within the chloroplast and efficient separation of photosystems I and II (Garab 2015, Lambrev et al. 2011).

## **Acknowledgment**

The authors thank Arjen Bader for technical help with the measurements, Cor Wolfs and Alonso Zavafer for their initial help with BBY sample preparation. This work is funded by the Foundation for Fundamental Research on Matter (FOM), which is part of the Netherlands Organization for Scientific Research (NWO), and the Research Council of Lithuania (LMT grant no. MIP-080/2015).

## **References**

- BELGIO E, JOHNSON MP, JURIC S AND RUBAN AV. 2012. Higher plant photosystem II light-harvesting antenna, not the reaction center, determines the excited-state lifetime-both the maximum and the nonphotochemically quenched. *Biophysical journal* 102: 2761-2771.
- BELGIO E, KAPITONOVA E, CHMELIOV J, DUFFY CD, UNGERER P, VALKUNAS L AND RUBAN AV. 2014. Economic photoprotection in photosystem II that retains a complete light-harvesting system with slow energy traps. *Nature communications* 5: 4433.
- BERTHOLD DA, BABCOCK GT AND YOCUM CF. 1981. A highly resolved, oxygen-evolving photosystem II preparation from spinach thylakoid membranes. *FEBS Letters* 134: 231-234.
- BLANKENSHIP RE 2002. *Molecular Mechanisms of Photosynthesis*. Oxford, United Kingdom: Blackwell Science.
- BRIANTAIS JM, VERNOTTE C, OLIVE J AND WOLLMAN FA. 1984. Kinetics of cation-induced changes of photosystem II fluorescence and of lateral distribution of the two photosystems in the thylakoid membranes of pea chloroplasts. *Biochim Biophys Acta* 766: 1-8.
- BROESS K, TRINKUNAS G, VAN DER WEIJ-DE WIT CD, DEKKER JP, VAN HOEK A AND VAN AMERONGEN H. 2006. Excitation energy transfer and charge separation in photosystem II membranes revisited. *Biophysical journal* 91: 3776-3786.
- BURRI H, SUNTHORN H, SOMSEN A AND ZAZA SF, E.; SHAH, D.; RIGHETTI, A. 2005. Optimizing sequential biventricular pacing using radionuclide ventriculography. *Heart rhythm : the official journal of the Heart Rhythm Society* 2: 960-965.
- CAFFARRI S, BROESS K, CROCE R AND VAN AMERONGEN H. 2011. Excitation energy transfer and trapping in higher plant Photosystem II complexes with different antenna sizes. *Biophysical journal* 100: 2094-2103.
- CAFFARRI S, KOURIL R, KEREICHE S, BOEKEMA EJ AND CROCE R. 2009. Functional architecture of higher plant photosystem II supercomplexes. *The EMBO journal* 28: 3052-3063.
- CARPENTIER R 2004. *Photosynthesis Research Protocols*. Methods in molecular biology, U.S: Humana Press.
- CHMELIOV J, TRINKUNAS G, VAN AMERONGEN H AND VALKUNAS L. 2014. Light harvesting in a fluctuating antenna. *Journal of the American Chemical Society* 136: 8963-8972.

- CHMELIOV J, TRINKUNAS G, VAN AMERONGEN H AND VALKUNAS L. 2016. Excitation migration in fluctuating light-harvesting antenna systems. *Photosynthesis research* 127: 49-60.
- DIGRIS AV, SKAKOUN VV, NOVIKOV EG, VAN HOEK A, CLAIBORNE A AND VISSER AJ. 1999. Thermal stability of a flavoprotein assessed from associative analysis of polarized time-resolved fluorescence spectroscopy. *European biophysics journal* : EBJ 28: 526-531.
- GARAB G. 2015. Self-assembly and structural-functional flexibility of oxygenic photosynthetic machineries: personal perspectives. *Photosynthesis research*.
- GIBASIEWICZ K ET AL. 2015. Monte Carlo simulations of excitation and electron transfer in grana membranes. *Biochim Biophys Acta* 1847: 314-327.
- IZAWA S, WINGET GD AND GOOD NE. 1966. Phlorizin, a specific inhibitor of photophosphorylation and phosphorylation-coupled electron transport in chloroplasts. *Biochemical and biophysical research communications* 22: 223-226.
- KIRCHHOFF H, BORINSKI M, LENHERT S, CHI L AND BUCHEL C. 2004. Transversal and lateral exciton energy transfer in grana thylakoids of spinach. *Biochemistry* 43: 14508-14516.
- KIRCHHOFF H, HAASE W, HAFERKAMP S, SCHOTT T, BORINSKI M, KUBITSCHKE U AND ROGNER M. 2007. Structural and functional self-organization of Photosystem II in grana thylakoids. *Biochim Biophys Acta* 1767: 1180-1188.
- KOURIL R, ZYGADLO A, ARTENI AA, DE WIT CD, DEKKER JP, JENSEN PE, SCHELLER HV AND BOEKEMA EJ. 2005. Structural characterization of a complex of photosystem I and light-harvesting complex II of *Arabidopsis thaliana*. *Biochemistry* 44: 10935-10940.
- LAMBREV PH, SCHMITT FJ, KUSSIN S, SCHOENGEN M, VARKONYI Z, EICHLER HJ, GARAB G AND RENGIER G. 2011. Functional domain size in aggregates of light-harvesting complex II and thylakoid membranes. *Biochim Biophys Acta* 1807: 1022-1031.
- NOVIKOV EG, VAN HOEK A, VISSER AJ AND HOFSTRAAT JW. 1999. Linear algorithms for stretched exponential decay analysis. *Opt Commun* 166: 189-198.
- PORRA RJ, THOMPSON WA AND KRIEDEMANN PE. 1989. Determination of accurate extinction coefficients and simultaneous equations for assaying chlorophylls a and b extracted with four different solvents: verification of the concentration of chlorophyll standards by atomic absorption spectrometry. *Biochem Biophys Acta* 975: 384-394.
- STAEHELIN LA. 1976. Reversible particle movements associated with unstacking and restacking of chloroplast membranes in vitro. *The Journal of cell biology* 71: 136-158.
- STOITCHKOVA K, BUSHEVA M, APOSTOLOVA E AND ANDREEVA A. 2006. Changes in the energy distribution in mutant thylakoid membranes of pea with modified pigment content. II. Changes due to magnesium ions concentration. *Journal of photochemistry and photobiology B, Biology* 83: 11-20.
- TRISSEL HW, BRETON J, DEPREEZ J AND LEIBL W. 1987. Primary Electrogenic Reactions of Photosystem-II as Probed by the Light-Gradient Method. *Biochim Biophys Acta* 893: 305-319.
- VAN AMERONGEN H, VALKUNAS L AND VAN GRONDELLE R. 2000. *Photosynthetic excitons*. Singapore: World Scientific.
- VAN DER WEIJ-DE WIT CD, IHALAINEN JA, VAN GRONDELLE R AND DEKKER JP. 2007. Excitation energy transfer in native and unstacked thylakoid membranes studied by low

***EET between different layers of stacked PSII-containing Thylakoid membranes***

temperature and ultrafast fluorescence spectroscopy. *Photosynthesis research* 93: 173-182.

VAN OORT B, ALBERTS M, DE BIANCHI S, DALL'OSTO L, BASSI R, TRINKUNAS G, CROCE R AND VAN AMERONGEN H. 2010. Effect of antenna-depletion in Photosystem II on excitation energy transfer in *Arabidopsis thaliana*. *Biophysical journal* 98: 922-931.

VAN OORT B, AMUNTS A, BORST JW, VAN HOEK A, NELSON N, VAN AMERONGEN H AND CROCE R. 2008. Picosecond fluorescence of intact and dissolved PSI-LHCI crystals. *Biophysical journal* 95: 5851-5861.

VAN OORT B, VAN HOEK A, RUBAN AV AND VAN AMERONGEN H. 2007. Aggregation of light-harvesting complex II leads to formation of efficient excitation energy traps in monomeric and trimeric complexes. *FEBS Lett* 581: 3528-3532.

VEERMAN J, MCCONNELL MD, VASIL'EV S, MAMEDOV F, STYRING S AND BRUCE D. 2007. Functional heterogeneity of photosystem II in domain specific regions of the thylakoid membrane of spinach (*Spinacia oleracea* L.). *Biochemistry* 46: 3443-3453.

WIJNTJES E, VAN AMERONGEN H AND CROCE R. 2013. LHCII is an antenna of both photosystems after long-term acclimation. *Biochim Biophys Acta* 1827: 420-426.



## **CHAPTER 5**

# **Monitoring non-photochemical quenching in leaves with ultrafast fluorescence measurements**

based on:

Farooq, S., Wientjes, E., Koehorst, R., and H. van Amerongen. "Monitoring non-photochemical quenching in leaves with ultrafast fluorescence measurements."

### **Abstract**

In this work we have applied ultrafast fluorescence spectroscopy to study the picosecond kinetics of photosystems I (PSI) and II (PSII) in spinach leaves using a streak-camera setup. The leaves were measured in 4 different conditions: with all PSII reaction centers (RCs) either in the open state ( $F_o$ ) or in the closed state ( $F_{max}$ ) while being dark-adapted, or after the photoprotective mechanism of nonphotochemical quenching (NPQ) had been induced by high light illumination. Over excitation of PSII RCs can lead to charge recombination in closed RCs accompanied by chlorophyll triplet formation, which leads to the formation of harmful singlet oxygen. The process of NPQ leads to dissipation of excess excitations by producing harmless heat. Surprisingly it is found that the rate of NPQ is higher in the case of closed RCs than in the case of open RCs, which from a functional point of view can be considered as an ideal situation because closed RCs are prevented from causing singlet oxygen formation while the open RCs can continue to function. However, at the moment we do not have a good explanation at the molecular level for this remarkable observation and further research will be needed to validate our results and to come up with an explanation for the experimental results.

### **Introduction**

When plants are exposed to excess light, more excitations are created than the reaction centers (RCs) in the thylakoid membranes can handle. Especially when the RCs of photosystem II are overloaded, photodamage can occur. To protect themselves from this photodamage, plants utilize a set of photoprotective mechanisms and regulatory responses, in which excess absorbed light energy is dissipated as heat and which can be measured as the non-photochemical quenching (NPQ) of chlorophyll (Chl) fluorescence (Avenson et al. 2004, Barber and Andersson 1992, de Bianchi et al. 2010, Horton et al. 1996, Krause and Jahns 2004, Niyogi 1999, Ruban et al. 2012). These mechanisms are often shortly called NPQ and the dominant and fastest reversible component of NPQ is known as energy-dependent quenching (qE) (Horton et al. 1996, Kulheim et al. 2002, Li et al. 2002). It switches on and off in seconds to minutes upon strongly increased/decreased illumination, allowing plants to respond to high light intensities in a reversible way (Kulheim et al. 2002, Li et al. 2002). By thermally deactivating the Chl excited-state energy it efficiently removes excitations from the system (Demmig-Adams and Adams 1996). The molecular mechanisms behind NPQ are still not fully clear, but it is known that the activation of qE requires a low pH at the luminal side (Jahns et al. 2002, Macko et al. 2002, Müller et al. 2001), the

presence and protonation of the PsbS protein (Li et al. 2000, Li et al. 2004), the conversion of the xanthophyll violaxanthin (Vx) into zeaxanthin (Zx) by the violaxanthin de-epoxidase (VDE) (Demmig-Adams 1990, Horton et al. 2000, Niyogi et al. 1998) and PSII antenna complexes (Belgio et al. 2013, Belgio et al. 2012, Horton et al. 2005, Kalituho et al. 2006, Ruban and Horton 1994, Ruban et al. 1996). The pH regulation of qE allows rapid switching of the PSII antenna function between light harvesting and energy dissipation. The PsbS protein of PSII acts as one of the sensors of the lumenal pH (Horton et al. 2008, Li et al. 2000, Li et al. 2004) and possibly even as the site for energy dissipation (Niyogi et al. 2005). Different models have been proposed for both the site and mechanism of qE (Avenson et al. 2008, Holt et al. 2005, Miloslavina et al. 2008, Ruban et al. 2007). Most of the models have in common that the pH and PsbS dependent conformation change of PSII antenna proteins control qE (Horton et al. 2005). Instead the role of Zx is debated: Zx is either directly involved in the quenching process according to some researchers (Ahn et al. 2008, Avenson et al. 2008, Holt et al. 2005), whereas others suggest an allosteric role in qE inducing a conformational change in the light-harvesting antenna which mediates quenching (Pascal et al. 2005). A recent study, which showed that Zx-dependent quenching is active in isolated thylakoid membranes, but not in isolated PSII supercomplexes, supports the idea of a mediating role of Zx in NPQ (Xu et al. 2015). It has also been suggested, based on time-resolved fluorescence measurements, that the PsbS dependent and Zx-dependent quenching mechanism occur at different sites and contribute to NPQ with different temporal components (Holzwarth et al. 2009, Lambrev et al. 2012, Lambrev et al. 2010, Miloslavina et al. 2009).

Changes in the chlorophyll fluorescence yield are mostly used to measure the amount of NPQ. These measurements are typically done by using the pulse amplitude modulated (PAM) chlorophyll fluorometer. PAM measurements have revealed the different time-scales on which NPQ occurs and in combination with chemical treatments and mutant studies the role of pH and several proteins (Johnson and Ruban 2011, Johnson et al. 2012, Ruban et al. 2012, Li et al. 2004). A disadvantage of the PAM method is that it can only measure the amount of fluorescence, but not the fluorescence quantum yield. As a result chloroplast movement and photobleaching, which change the amount of light absorption cannot be distinguished from a change in the Chl fluorescence yield (Baker 2008). Furthermore, the method does not give information about the rates of photosynthetic charge separation ( $k_{CS}$ ) and NPQ ( $k_{NPQ}$ ). To overcome these shortcomings we have studied NPQ with time-resolved picosecond/nanosecond fluorescence measurements (Holzwarth et al. 2009, Lambrev et al. 2012, Lambrev et al. 2010, Miloslavina et al. 2009, Sylak-Glassman et al. 2016). Such measurements

## **Monitoring NPQ in leaves with ultrafast fluorescence measurements**

are not sensitive to photobleaching and chloroplast movement, and in addition, can be used to reveal the rates of qE both in the presence of open and closed RCs. Moreover, they can provide spectral information of Chl emission in all conditions. Since it is known that qE to a large extent turns off within (tens of) seconds after switching off high-intensity actinic light, we followed the qE relaxation by using ps-ns fluorescence decay measurements, for different periods of time (10, 30 and 60 sec) in order to obtain differences in the quenching rates and spectral signatures for the fast and slow parts of qE.

To determine the kinetics of the early steps in photosynthesis and the photoprotective mechanisms, we have used non-invasive picosecond fluorescence measurements on intact spinach leaves. We have studied the excited-state kinetics of photosystems I (PSI) and II (PSII) both for open and closed RCs in the leaves *in vivo*, both in the presence and absence of NPQ-inducing actinic light of 1300  $\mu\text{E}/\text{m}^2/\text{sec}$  intensity.

## **Materials & Methods**

### **Streak-camera measurements:**

To perform time-resolved picosecond fluorescence measurements, a streak camera system was used as previously described in (van Oort et al. 2008a, van Oort et al. 2009, van Stokkum et al. 2006). The advantage of using a streak camera instead of a more common time-correlated single photon counting setup is that it provides entire spectra with a high temporal resolution. A disadvantage is the lower S/N ratio. Measurements were performed on fresh spinach leaves from the local market. Intact leaves were placed in a home-built, circular cuvette with a diameter of 7 cm. The cuvette rotates around its center and simultaneously moves sideways over a 4 cm distance by using a horizontal displacer. The samples were rotated at 1500 rpm for closed RCs and 1000 rpm for open RCs and moved horizontally at 50 rpm under both conditions. As a result, the leaves were illuminated by a Lissajous pattern. The fluorescence kinetics were measured by focusing the frequency-doubled output of a Ti: sapphire laser (400 nm) on the sample with a 7 cm focal length achromatic lens assembly; the height of the excitation spot was approximately 1 cm below the rotation **axis** of the cell. To avoid back reflections, the sample rotator was placed at an angle of  $\sim 80$  degrees with respect to the excitation beam. The upper surface of the leaf was facing the excitation light, on the rear of the leaves a piece of wet tissue was placed to prevent them from dehydration and overheating (for detached leaves without access to water qE is significantly reduced (Sylak-Glassman et al. 2016)). Laser powers of 100 nW or

1mW were used to keep the reaction centers in either the open or closed state, respectively. The diameter of the excitation spot was  $\sim 100\ \mu\text{m}$ , and the laser repetition rate was 4 MHz. The fluorescence emission was collected from the upper surface of the leave using front-face detection, and the excitation and emission light were separated by a dichroic mirror (405LP). The fluorescence light was focused on the entrance slit of the spectrograph, which projected a spectrum on the photocathode of the streak camera. A time window of 2ns was used for all measurements. For data acquisition, the photon counting mode was selected. In this mode, the maximum microchannel plate (MCP) gain is applied, and individual photons are detected. Each detected photon creates a peak in the streak image, which is fitted with a 2D Gaussian function. The peak coordinates of all photons are combined in a 2D histogram (photon counting image) that can be analyzed in the same way as a streak image. The number of photons detected in each camera frame should be kept low to prevent overlap between two or more photon peaks. In experiments on open reaction centers, the number of detected photons was  $\sim 500\ \text{s}^{-1}$ . For closed reaction centers, the fluorescence was suppressed by gray filters (in total 0.01% transmission) so that the number of detected photons was also  $\sim 500\ \text{s}^{-1}$ . All experiments were performed at room temperature in the dark. Experiments were repeated with three different sets of leaves.

## PAM measurements

A pulse-amplitude-modulated fluorometer (PAM 101, Walz, Germany) was used to measure  $F_v/F_m$  and NPQ of spinach leaves under *in vivo* conditions at room temperature. The stem of each leaf was wrapped in wet tissue throughout the experiment. The leaves were dark-adapted for 1 hr prior to the measurement. Briefly after switching on the weak modulated measuring light, resulting in a fluorescence signal with intensity  $F_0$ , a saturating light pulse of  $4500\ \mu\text{mol photons m}^{-2}\ \text{s}^{-1}$  with duration 0.8s (KL1500 LCD halogen lamp (Schott, UK)) was applied to obtain the  $F_v/F_m$  value. The average  $F_v/F_m$  value for the leaves was 0.80 which is a typical value for healthy leaves. For the induction of NPQ, leaves were illuminated with an actinic light source for up to 25 min at a light intensity of  $1050\ \mu\text{mol photons m}^{-2}\ \text{s}^{-1}$ . Then the actinic light was switched off, and the relaxation of NPQ was followed during complete darkness for up to 45 min (only the first 20 min are shown in supplementary Fig 1). To monitor the induction of NPQ, saturating white light pulses ( $4500\ \mu\text{mol photons m}^{-2}\ \text{s}^{-1}$ , duration 0.6s) were applied every 5 mins during the period of actinic illumination. For the determination of the relaxation of NPQ in the dark, the first saturating light pulse was applied 10 sec after switching off the actinic light source, the 2<sup>nd</sup> one after 50 sec and after that 9 flashes were given with periods of several minutes in between.

### **Data Analysis**

The streak camera images were background and shading corrected and subsequently binned every 5nm along the wavelength axis. The streak camera data was globally analyzed with the TIMP package for R language (Mullen and Van Stokkum 2007) and Glotaran, the graphical user interface of the R package TIMP (Snellenburg et al. 2012). By global analysis, the data was fitted to a sum of exponential decays convolved with a Gaussian-shaped instrument response function (IRF) and the amplitude of each decay component was determined as a function of wavelength, leading to Decay Associated Spectra (DAS). To estimate the lifetimes of long-lived components (i.e. components whose lifetime is longer than the time-window) more precisely, the back-sweep of the streak camera was also considered in the fitting (van Stokkum et al. 2004, Van Stokkum et al. 2008).

### **Measurement of time-resolved fluorescence after dark and light adaptation**

The lifetime measurements on intact leaves were performed under four different conditions: (i) to measure the dark-adapted  $F_o$ , (unquenched state) spinach leaves were kept in the dark for 1 hr. Measurements were done with a very low laser intensity of 100nW to keep PSII RCs in the open state. (ii) To measure the maximal fluorescence ( $F_{max}$ , unquenched state), spinach leaves were dark adapted for 1hour prior to the measurements. To bring and keep the PSII RCs in the closed state a high laser light intensity of 1mW (RCs 'close' as the acceptor,  $Q_A$ , becomes reduced) was used during the measurements. (iii) To measure the high-light adapted  $F_{NPQ}$  quenched state, the leaves were illuminated with an actinic light intensity of  $1300\mu\text{mol.m}^{-2}.\text{sec}^{-1}$  for about 30 min to stabilize NPQ. To measure the fluorescence lifetime in the presence of NPQ, the actinic light was blocked, and the shutters in front of the laser and detector were immediately opened to measure for a period  $\Delta T$  of 10 sec. After data collection, the laser and detector shutters were blocked, and the sample was again illuminated by actinic light for 1 min to re-stabilize NPQ before measuring the fluorescence decay for another  $\Delta T=10$  sec. The procedure was repeated many times until a good signal-to-noise ratio (SNR) was achieved. Because the energy-dependent qE component of NPQ relaxes on a timescale of seconds to minutes (Kulheim et al. 2002, Li et al. 2002), data was not only collected with  $\Delta T=10$  sec but also with  $\Delta T=30$  and 60 sec in order to track the changes in the fluorescence decay profile. To measure  $F_{NPQ}$  with either open or closed reaction centers low and high laser intensities of 100nW and 1mW were used, respectively. Note that some of these measurements last for 2 hours. (iv) 45

min after switching off the quenching light (recovered state) the samples were measured again.

## Results

To measure the fluorescence kinetics of PSII in intact NPQ-induced leaves, a low laser intensity of 100nW was used to measure fluorescence ( $F$ ) with open RCs ( $F_o$ ), while a 1mW intensity was used to close the RCs ( $F_{max}$ ). The kinetics of dark-adapted leaves were then compared to the kinetics of NPQ-induced leaves (30 min,  $1300 \mu\text{mol.m}^{-2}.\text{sec}^{-1}$  illumination) in both cases. The fast qE component of NPQ relaxes within seconds to minutes, as shown in Supplementary Fig.1. Measurements were performed on sample leaves which are exposed to the measuring laser light for  $\Delta T = 10, 30$  and  $60$  sec. These measuring periods were followed by periods of  $1$  min with  $1300 \mu\text{mol.m}^{-2}.\text{sec}^{-1}$  to re-induce NPQ (as mentioned in Materials & Methods).

As can be seen in Supplementary Fig.1, during the first 10 sec the amount of NPQ drops by around 40%, whereas the average drop during these 10 sec is around 20%. The average drop during the first 30 sec is estimated to be  $\sim 35\%$  whereas for 60 sec it is close to 45%.

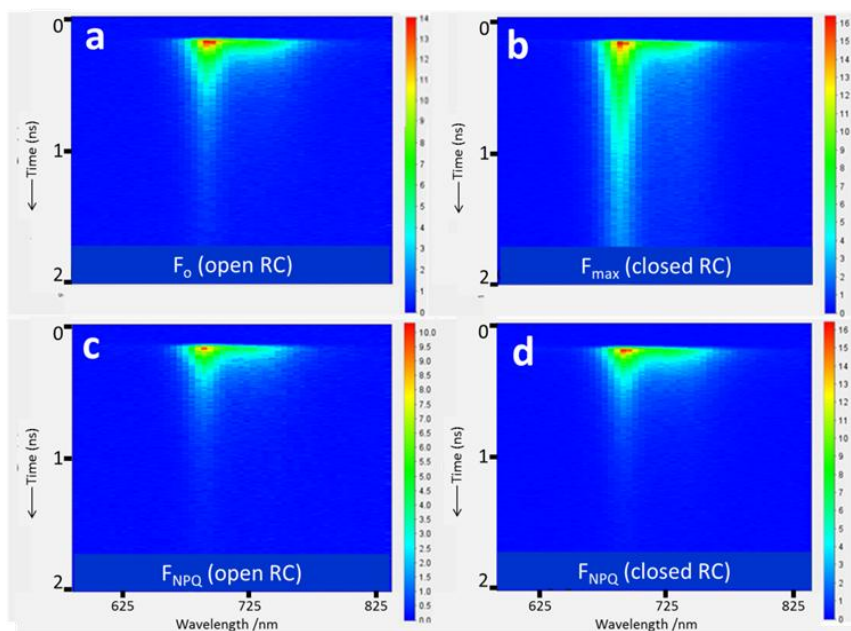


Figure 1: Streak-camera images of intact leaves under different conditions: (a)  $F_o$ , (b)  $F_{max}$ , (c)  $F_{NPQ,Open}$  (d)  $F_{NPQ,Closed}$ . A comparison of Fig 1a) and c) in case of open RCs and Fig 2b)

## Monitoring NPQ in leaves with ultrafast fluorescence measurements

and d) in case of closed RCs shows that there is a significant amount of quenching occurring in both cases after intense actinic light illuminates the leaves.

Fig.1 shows the difference in fluorescence kinetics of open and closed RCs for  $F_o$ ,  $F_{max}$  and  $F_{NPQ}$  (open/closed RC for 10 sec measurements after switching off the actinic light). For intact leaves with open RCs ( $F_o$  condition), a much faster decay was observed as compared to leaves with closed RCs ( $F_{max}$  condition). After NPQ was induced, we observed much faster fluorescence decay in case of  $F_{NPQ}$  (closed RCs) than for  $F_{max}$ . In case of  $F_o$  and  $F_{NPQ}$  (open RC), the difference due to quenching is indeed visible, but it is far less prominent.

After 45 min of recovery (Supplementary Fig.2) in the dark, the leaves showed almost identical fluorescence decay curves as before quenching, indicating that the amount of photoinhibition was very limited. In case of closed RCs we observed a decrease of about 5 to 8 % in average lifetime after 45 min recovery whereas, in case of open RC there was an increase of about 4 to 8 % ps after the recovery period

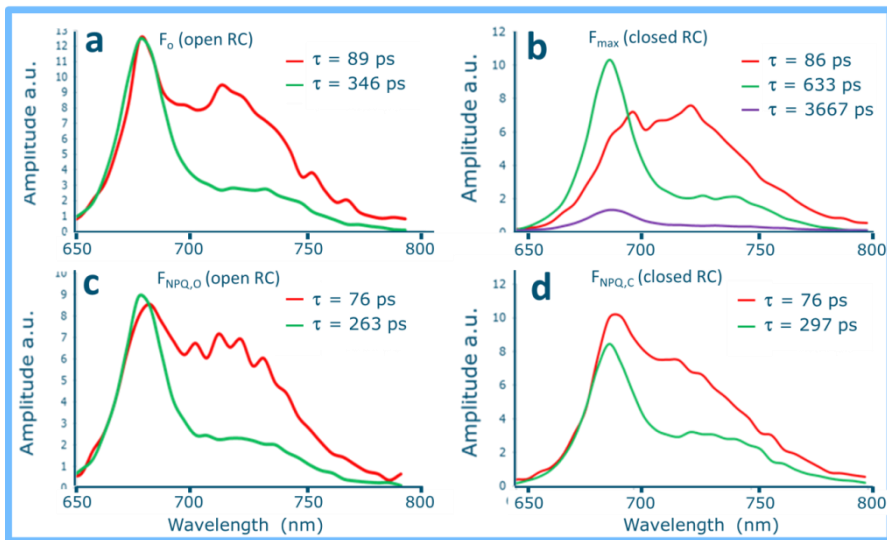


Figure 2: The decay associated spectra (DAS) of intact leaves for different light conditions. For NPQ the measurements were performed in 10 sec intervals immediately after the NPQ-inducing light was switched off. (a)  $F_o$ , (b)  $F_{max}$ , (c)  $F_{NPQ}$  (open RCs), (d)  $F_{NPQ}$  (closed RCs). Corresponding lifetimes are indicated in the figure.

The decay-associated spectra (DAS) for open and closed RCs in both quenched and unquenched states are shown in Fig. 2. A fit with 3 lifetimes for closed RCs in the  $F_{max}$  unquenched state was needed for a satisfactory description of the data, whereas 2 lifetimes were sufficient at all wavelengths for the three other states, i.e.



$F_o$  and  $F_{NPQ}$  (open/closed RCs). A  $\sim 10$  ps energy transfer component is required to obtain the best fit in all cases, but this lifetime is omitted below because the lifetime is almost equal to the 12 ps width of the IRF and moreover it is not needed to quantify NPQ.

The 85-90 ps DAS for the  $F_o$  and  $F_{max}$  unquenched state and the  $\sim 75$  ps DAS for the  $F_{NPQ}$  (open/closed RCs) quenched state correspond mostly to PSI and only partly to PSII (Broess et al. 2006, van Oort et al. 2010, Wientjes et al. 2013). On the other hand, the 2<sup>nd</sup> DAS (250ps to 350ps for  $F_o$ ,  $F_{NPQ, open}$  and  $F_{NPQ, closed}$  and 600-630ps for  $F_{max}$ ) and 3<sup>rd</sup> DAS (2ns to 3.5ns) for  $F_{max}$  correspond almost entirely to PSII. The fitted PSII lifetimes are shown in Table 1 where the contribution of PSI to the 1st DAS has been removed as explained in (van Oort et al. 2010).

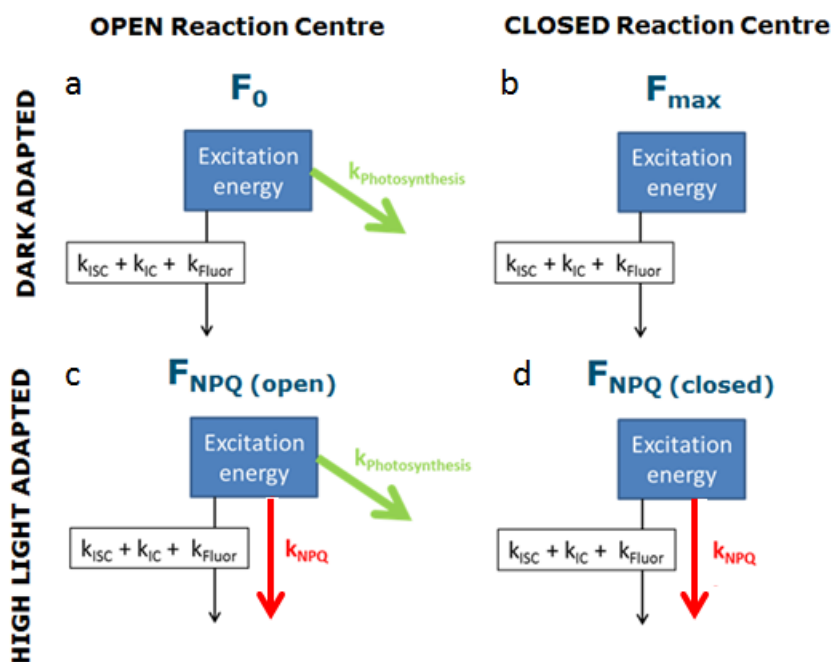


Figure 3: Schematic overview of the different pathways for chlorophyll de-excitation for the different measuring conditions: (a)  $F_o$ , (b)  $F_{max}$ , unquenched state, dark adapted leaves were measured with a very low/high laser intensity of 100nW/1mW to keep PSII RCs in the open/closed state. (c)  $F_{NPQ, Open}$  (d)  $F_{NPQ, Closed}$ , quenched state, leaves were illuminated with an actinic light intensity of  $1300\mu\text{mol}\cdot\text{m}^{-2}\cdot\text{sec}^{-1}$  for about 30 min to stabilize NPQ and were then probed with a very low/high laser intensity of 100nW/1mW, respectively. Note that the rate of nonphotochemical quenching  $k_{NPQ}$  is not necessarily the same for open and closed RCs. Please see text for further explanation.

## Monitoring NPQ in leaves with ultrafast fluorescence measurements

At the maximum fluorescence level  $F_{\max}$ , the average lifetime for closed PSII RCs for intact leaves is found to be  $\sim 890 \pm 90$  ps (see Table 1). This falls within the range of values reported in earlier work, ranging from 611 ps (Lukins et al. 2005) to 1.7 ns (Holub et al. 2000). The average lifetime for the  $F_0$  unquenched state is found to be  $235 \pm 19$  ps, which is in between the lifetimes obtained by (Miloslavina et al. 2011) of 210 ps in WT Arabidopsis leaves and (Iermak et al. 2016) who obtained values of around 280 ps on the adaxial side of the leaves and 340 ps on the abaxial side of WT Arabidopsis leaves.

$F_{\text{NPQ}}$  (open RCs) shows a decrease in average lifetime as compared to  $F_0$ . By measuring the sample for 10, 30 and 60 sec after the 30 min illumination, the average lifetime in case of  $F_{\text{NPQ}}$  (open RCs) is found to be 173, 183 and 190 ps (for  $F_0$  value of 220 ps, respectively (see Table 1), whereas in case of  $F_{\text{NPQ}}$  (closed RCs), it is found to be 215, 270 and 315 ps, respectively.

The obtained average lifetimes were used to estimate the average rate of NPQ for both the open and closed states. For isolated chlorophylls the excited-state lifetime  $\tau'$  depends on the radiative transition with rate constant  $k_F$ , internal conversion (IC) and intersystem crossing (ISC) with rate constants  $k_{IC}$  and  $k_{ISC}$ , respectively, according to:

$$\tau' = \frac{1}{k} = \frac{1}{k_F + k_{IC} + k_{ISC}},$$

*In vivo* two more processes can contribute to chlorophyll de-excitation and thus to a shortening of the excited-state lifetime, namely photochemical quenching ( $k_{CS}$ ), due to charge separation in the reaction centres and nonphotochemical quenching ( $k_{\text{NPQ}}$ ) leading to the following equation if all processes take place:

$$\tau = \frac{1}{k} = \frac{1}{k_F + k_{IC} + k_{ISC} + k_{CS} + k_{\text{NPQ}}},$$

If we assume that for the open state, all the processes that contribute to chlorophyll de-excitation including the rate of charge separation do not change when NPQ is induced, the rate of non-photochemical quenching  $k_{\text{NPQ}}$  can be determined by using

$$\tau_{\text{open}} = \frac{1}{k_F + k_{IC} + k_{ISC} + k_{CS}},$$
$$\tau_{\text{NPQ,open}} = \frac{1}{k_F + k_{IC} + k_{ISC} + k_{CS} + k_{\text{NPQ}}},$$

$$k_{NPQ,open} = \frac{1}{\tau_{NPQ,open}} - \frac{1}{\tau_{open}},$$

For the closed RCs one gets

$$k_{NPQ,closed} = \frac{1}{\tau_{NPQ,closed}} - \frac{1}{\tau_{closed}},$$

The obtained rates of NPQ with closed RCs for measuring periods of 10, 30 and 60 sec are found to be 3.5, 2.5 and 2.0 ns<sup>-1</sup>, respectively. In the case of open RCs,  $k_{NPQ,open}$  is found to be 1.2, 0.92 and 0.72 ns<sup>-1</sup>, respectively. In all cases the apparent rate of NPQ with open RCs,  $k_{NPQ,open}$ , is 2.7 times slower than for closed RCs,  $k_{NPQ,closed}$ .

The NPQ values for closed RCs were then calculated from the obtained average lifetimes of PSII according to the following equation:

$$NPQ_{avg,closed} = \frac{\tau_{max,avg} - \tau_{NPQ}}{\tau_{NPQ}}$$

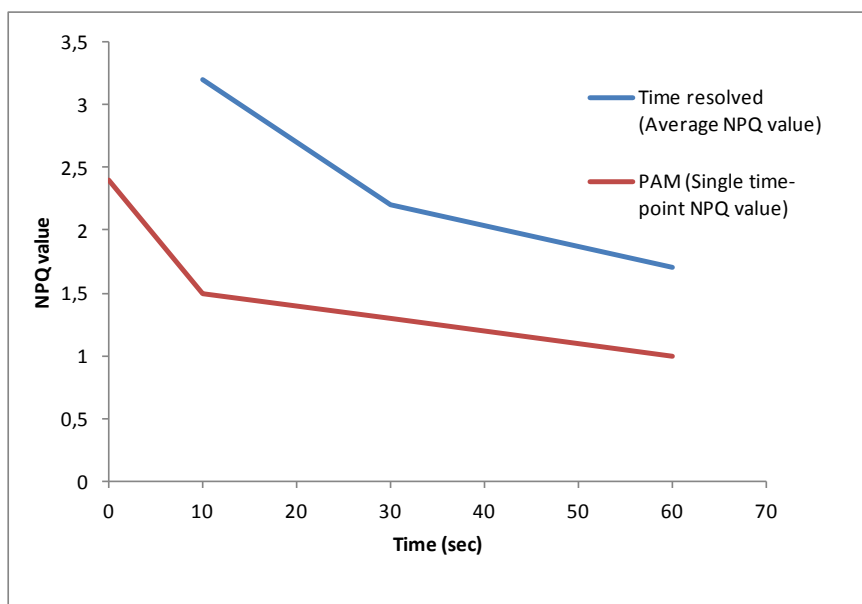


Figure 4: The average NPQ values as obtained by time-resolved measurements after 30 min of illumination with 1300  $\mu\text{mol} \cdot \text{m}^{-2} \cdot \text{sec}^{-1}$  light is plotted as a function of the measuring time (blue points, connected by blue lines). Note that the 10 sec point corresponds to averaging over the first 10 sec. Therefore a direct comparison

## ***Monitoring NPQ in leaves with ultrafast fluorescence measurements***

with the PAM values (red points) is not possible because they reflect the amount of NPQ 0, 10 and 60 sec after switching off the actinic light.

The average NPQ values obtained for measuring time periods of 10, 30 and 60 sec, respectively are  $3.2 \pm 0.3$ ,  $2.1 \pm 0.3$  and  $1.7 \pm 0.2$ . These average NPQ value as calculated from the time-resolved measurements in case of closed RCs (given in Table 1) are compared with the ones obtained from the PAM analysis in Fig. 4. The obtained values in the case of time-resolved measurements are higher, because PSI fluorescence is contributing to the PAM results, and lower actinic light intensities were used from the PAM experiments. We can also not fully rule out that some of the RCs were still open during the time-resolved measurements. On the other hand the average drop in NPQ as obtained from the PAM and the time-resolved fluorescence measurements show a similar trend.

## **Discussion**

The time-resolved fluorescence measurements on spinach leaves in the absence of NPQ lead to results that are similar to previous results on Arabidopsis leaves and/or thylakoid membranes, both for open and closed RCs. As always there is a spread in the obtained average PSII lifetimes for different leaves measured on different days: 8 different datasets obtained on different days lead to  $\sim 890 \pm 90$  ps and  $\sim 235 \pm 19$  ps for closed and open PSII RCs, respectively. Note that these numbers have already been corrected for the contributions of PSI (see above). Because of the variation of the fluorescence kinetics for different leaves it is important to make the comparison of the kinetics in the presence and absence of NPQ for the same leaves. From Table 1 it is clear that despite the leaf-to-leaf variation of the fluorescence kinetics, the calculated rate constants  $k_{\text{NPQ}}$  are very reproducible. For instance, in case of closed RCs the obtained rates are  $3.50 \pm 0.21$  ns<sup>-1</sup>,  $3.58 \pm 0.27$  ns<sup>-1</sup>, and  $3.51 \pm 0.17$  ns<sup>-1</sup>, when measuring during 10 seconds after switching off the actinic light. It should be realized that our approach to calculate average quenching constants is strictly speaking only correct if the fluorescence decay is mono-exponential in all cases, which is not the case. Instead we use the inverse of the average lifetime to calculate an average rate in all cases. Therefore, the obtained results are only approximate. Detailed future modeling will be required to take into account the non-exponentiality but for the discussion below the current approximation is sufficient.

It is well-known that NPQ consists of different contributions, disappearing with different time constants after switching off the actinic light as can for instance be seen in Supplementary Fig. 1 where the NPQ parameter  $((F_m - F_m') / F_m')$  drops from

2.4 to 1.5 in 10s after switching off the NPQ-inducing actinic light. Therefore, the rate of quenching that is obtained during the first 10s is already substantially lower than the rate in the presence of actinic light. The rate of NPQ is decreasing further afterwards as is also clear from the rates that were determined with 30s and 60s measuring times after switching off the light. The corresponding rates are  $2.51\text{ns}^{-1}$  and  $1.97\text{ns}^{-1}$ , respectively, as compared to the value of  $3.53\text{ns}^{-1}$  for the first 10s. These 3 rates correspond to NPQ values of 3.2, 2.2, and 1.7, respectively. These numbers are higher than those obtained with the PAM measurements on similar leaves. This can partly be explained by the lower light intensity used to induce NPQ ( $1050\mu\text{mol.m}^{-2}.\text{sec}^{-1}$  vs.  $1300\mu\text{mol.m}^{-2}.\text{sec}^{-1}$ ) in the PAM measurements. The main difference is that based on the fluorescence lifetime data the real PSII NPQ value can be calculated, while in the PAM data the fluorescence from PSI interferes. While the contribution of PSI to the total fluorescence intensity at  $F_{\text{max}}$  is very small, its contribution is significant for  $F_{\text{M}}'$  when NPQ is induced which strongly reduces the fluorescence quantum yield (QY) of PSII ( $\text{PSII}_{\text{QY}} = 1.1\%$  based on 220 ps average lifetime and  $k_{\text{rad}}$  of 0.05/ns), but not of PSI ( $\text{PSI}_{\text{QY}} = 0.4\%$  based on 80 ps average lifetime found in this work). This effect is enhanced by the fact that in most PAM instrument the fluorescence is detected through a 710 nm long-pass filter, thus selecting for PSI emission.

Also the rate of NPQ,  $k_{\text{NPQ}}$ , for open RCs appears to be very reproducible with values of  $1.23 \pm 0.20 \text{ ns}^{-1}$ ,  $1.24 \pm 0.18 \text{ ns}^{-1}$ , and  $1.22 \pm 0.15 \text{ ns}^{-1}$ , obtained during 10s after switching off the actinic light, despite the variations in average fluorescence lifetimes. However, this rate is a factor of 2.7 smaller than the rate obtained for closed RCs, which is  $3.5\text{ns}^{-1}$ . Also this rate decreases further as a function of time and the obtained rate averaged over the first 30s and 60s are  $0.92\text{ns}^{-1}$  and  $0.73\text{ns}^{-1}$ , respectively. These values are also a factor of  $\sim 2.7$  lower than the rates of NPQ,  $2.51\text{ns}^{-1}$  and  $1.97\text{ns}^{-1}$ , obtained for closed RCs. Apparently, the quenching is more effective in case of closed RCs although the underlying origin of the quenching must be the same in both cases, considering the way in which the amount of quenching is disappearing during the first minute after switching off the actinic light (see also Fig. 5). Although it is not possible to determine directly how much the amount of NPQ drops during the first 10 seconds, it seems safe to conclude that the relative change in quenching rate is the same for open and closed RCs. For closed RCs NPQ drops from 2.4 to 1.5 during the first 10s (results from PAM measurements), which implies a drop in  $k_{\text{NPQ}} \sim 35\%$  and most likely the drop is very similar in case of open RCs.

There is one effect that may influence the apparent value of  $k_{\text{NPQ}}$  in case of open RCs and which has been ignored so far. When the actinic light is switched off not

### ***Monitoring NPQ in leaves with ultrafast fluorescence measurements***

all RCs are immediately in the open state again, leading to more fluorescence as compared to the fully open case and thus to an apparent decrease in quenching. However, the consequence of this effect is relatively small. After switching off the actinic light it takes at most 4.5s for all RCs to be open again (Supplementary Fig. 3) and the corresponding time constant is less than 2s, but to calculate an absolute upper limit we simply assume it is 2s. This means that during the first 10s of measuring at most 20% of the RCs would on average still be closed if they were all closed with the actinic light on, implying that the obtained average lifetime of 187ps is at most for 20% due to quenched closed RCs with an average lifetime of 216ps. This means that the real average lifetime would have been 180ps instead of 187ps, corresponding to  $k_{\text{NPQ}} = 1.45\text{ns}^{-1}$  instead of  $1.24\text{ns}^{-1}$ . As already pointed out, this is an absolute upper limit but it is still far smaller than the value of  $3.2\text{ns}^{-1}$  for closed RCs.

It was recently reported that the efficiency of NPQ is smaller than the efficiency of charge separation in case of open reaction centers (Belgio et al. 2014b) and it was concluded that NPQ therefore works efficiently for closed rather than for open RCs. This is exactly what is needed to optimize NPQ, and therefore it was termed economic photoprotection. Here we demonstrate that the photoprotection is even more economic than was realized before. In fact the rate of NPQ is changing dependent on whether the RCs are open or closed. After NPQ has been induced its rate in the presence of closed RCs can be even higher than that of photochemical quenching (charge separation) in the case of open RCs. On the other hand, when the RCs open again in the presence of NPQ, the rate of NPQ seems to slow down instantaneously, thereby lowering the unwanted loss of useful excitations. Remarkably, this seems to be the case both for the fast phase (disappearing in (tens of) seconds and the slower one, which is decreasing on a time scale of minutes).

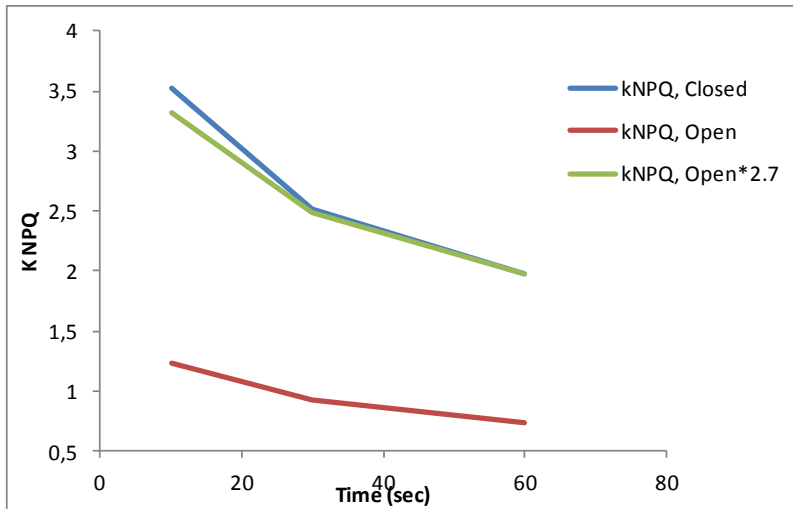


Figure5: Average rates of nonphotochemical quenching,  $k_{NPQ}$ , as determined for leaves with the RCs in the open and closed state. In order to demonstrate the similarity between the time dependence of  $k_{NPQ}$  for open and closed RCs, the rates for open RCs were also multiplied by a factor of 2.7.

What can be the molecular nature of the nonphotochemical quenching mechanism that seems to be able to sense the state of the RCs, open or closed? In case one RC is closed while a neighbouring RC is open, the excitation should preferably only be quenched when it is in the direct neighbourhood of the closed RC, where it could lead to the creation of a Chl triplet and thus to the formation of singlet oxygen. Chl triplets are produced by intersystem crossing from singlet excited Chls in the light-harvesting antenna complex of PSII or in the PSII RCs by charge recombination processes. Since antenna Chls are in close contact with carotenoids, which rapidly quench the Chl triplet states, no major photodamage is caused by the Chl triplet state that is produced in the light harvesting antenna complex of PSII (Peterman et al. 1995, Peterman et al. 1997, van Amerongen and Croce 2008). On the other hand the PSII RC Chls do form triplet states by subsequent triplet charge recombination at a rate much faster than the intersystem crossing from the singlet excited Chl states, when the PSII RCs are closed (Müller et al. 1996, Vass 2011). However, the organization of PSII in the thylakoid membranes seems to be such that excitations can easily move around in a well-connected network of light-harvesting complexes in which many reaction centers are embedded. When NPQ would occur in one or several of the antenna complexes, which is the consensus picture in the NPQ literature, then NPQ would not be selective. Our current results demonstrate that the quenching is dependent on the state of the RCs, which can be very efficient as is argued above. However, it would only be effective if the fast quenching would

### ***Monitoring NPQ in leaves with ultrafast fluorescence measurements***

occur in the direct environment of the closed RC, which is in disagreement with all existent models.

At the moment we can only speculate about the underlying physical mechanism of NPQ which appears to be dependant on the state of the RC: The plant light-harvesting complexes are all in a poised state (Ruban et al. 2007), meaning that they are all close to be being quenched and inducing small changes in their structure/conformation can make the difference between being quenched or not. The balance between these two situations or the equilibrium can be shifted by NPQ via the protonation of PsbS or the conversion of violaxanthin into zeaxanthin, shifting the equilibrium of the entire antenna system from a partially quenched one (lifetimes are 1-2 ns, not 4 ns as for isolated complexes) (Chmeliov et al. 2016a). In such a delicate system any perturbation in the direct environment might have an immediate consequence for the equilibrium and the creation of a closed RC with its inherent local charges within the membrane might lead to conformational changes. However, this is only speculation at the moment and further research is needed to sort this out further.



**Table 1: Average PSII lifetimes in absence and presence of NPQ for open and closed RCs**

Measurement Time (sec)	Open Reaction Centre			Closed Reaction Centre			
	$F_0$ $T_{0.avg}$ (ps)	$F_{NPQ}$ open $T_{NPQavg}$ (ps)	$k_{NPQ\ open}$ (ns <sup>-1</sup> )	$F_{max}$ $T_{max.avg}$ (ps)	$F_{NPQ}$ closed $T_{NPQavg}$ (ps)	$k_{NPQ\ closed}$ (ns <sup>-1</sup> )	Average NPQ value  $NPQ_{avg.closed}$
10	220 (~+/-5)	173 (~+/-3)	1.23 (~+/-0.20)	975 (~+/-25)	221 (~+/-9)	3.50 (~+/-0.21)	3.4
	240 (~+/-4)	185 (~+/-4)	1.24 (~+/-0.18)	975 (~+/-25)	217 (~+/-11)	3.58 (~+/-0.27)	3.5
	270 (~+/-4)	203 (~+/-4)	1.22 (~+/-0.15)	802 (~+/-19)	210 (~+/-6)	3.51 (~+/-0.17)	2.8
30	220 (~+/-5)	183 (~+/-4)	0.92 (~+/-0.22)	927 (~+/-24)	276 (~+/-11)	2.54 (~+/-0.18)	2.3
	240 (~+/-4)	197 (~+/-4)	0.91 (~+/-0.17)	731 (~+/-18)	257 (~+/-8)	2.52 (~+/-0.14)	1.8
	257 (~+/-3)	207 (~+/-2)	0.94 (~+/-0.09)	971 (~+/-23)	285 (~+/-9)	2.48 (~+/-0.14)	2.4
60	220 (~+/-5)	190 (~+/-3)	0.72 (~+/-0.18)	912 (~+/-23)	324 (~+/-16)	1.99 (~+/-0.18)	1.8
	215 (~+/-5)	186 (~+/-5)	0.73 (~+/-0.25)	789 (~+/-20)	311 (~+/-12)	1.95 (~+/-0.17)	1.5

## **Acknowledgment**

This work is funded by the Foundation for Fundamental Research on Matter (FOM), which is part of the Netherlands Organization for Scientific Research (NWO).

## **References**

- AHN TK, AVENSON TJ, BALLOTTARI M, CHENG Y-C, NIYOGI KK, BASSI R AND FLEMING GR. 2008. Architecture of a Charge-Transfer State Regulating Light Harvesting in a Plant Antenna Protein. *Science* 320: 794-797.
- AVENSON TJ, AHN TK, ZIGMANTAS D, NIYOGI KK, LI Z, BALLOTTARI M, BASSI R AND FLEMING GR. 2008. Zeaxanthin Radical Cation Formation in Minor Light-harvesting Complexes of Higher Plant Antenna. *Journal of Biological Chemistry* 283: 3550-3558.
- AVENSON TJ, CRUZ JA AND KRAMER DM. 2004. Modulation of energy-dependent quenching of excitons in antennae of higher plants. *Proceedings of the National Academy of Sciences of the United States of America* 101: 5530-5535.
- BAKER NR. 2008. Chlorophyll fluorescence: a probe of photosynthesis in vivo. *Annual review of plant biology* 59: 89-113.
- BARBER J AND ANDERSSON B. 1992. Too much of a good thing: light can be bad for photosynthesis. *Trends in biochemical sciences* 17: 61-66.
- BELGIO E, DUFFY CD AND RUBAN AV. 2013. Switching light harvesting complex II into photoprotective state involves the lumen-facing apoprotein loop. *Physical chemistry chemical physics : PCCP* 15: 12253-12261.
- BELGIO E, JOHNSON MP, JURIC S AND RUBAN AV. 2012. Higher plant photosystem II light-harvesting antenna, not the reaction center, determines the excited-state lifetime-both the maximum and the nonphotochemically quenched. *Biophysical journal* 102: 2761-2771.
- BELGIO E, KAPITONOVA E, CHMELIOV J, DUFFY CDP, UNGERER P, VALKUNAS L AND RUBAN AV. 2014. Economic photoprotection in photosystem II that retains a complete light-harvesting system with slow energy traps. 5.
- BROESS K, TRINKUNAS G, VAN DER WEIJ-DE WIT CD, DEKKER JP, VAN HOEK A AND VAN AMERONGEN H. 2006. Excitation energy transfer and charge separation in photosystem II membranes revisited. *Biophysical journal* 91: 3776-3786.
- CHMELIOV J, GELZINIS A, SONGAILA E, AUGULIS R, DUFFY CDP, RUBAN AV AND VALKUNAS L. 2016. The nature of self-regulation in photosynthetic light-harvesting antenna. 2: 16045.
- DE BIANCHI S, BALLOTTARI M, DALL'OSTO L AND BASSI R. 2010. Regulation of plant light harvesting by thermal dissipation of excess energy. *Biochemical Society transactions* 38: 651-660.
- DEMMIG-ADAMS B. 1990. Carotenoids and photoprotection in plants: A role for the xanthophyll zeaxanthin. *Biochimica et Biophysica Acta (BBA) - Bioenergetics* 1020: 1-24.
- DEMMIG-ADAMS B AND ADAMS WW. 1996. The role of xanthophyll cycle carotenoids in the protection of photosynthesis. *Trends in plant science* 1: 21-26.

- HOLT NE, ZIGMANTAS D, VALKUNAS L, LI X-P, NIYOGI KK AND FLEMING GR. 2005. Carotenoid Cation Formation and the Regulation of Photosynthetic Light Harvesting. *Science* 307: 433-436.
- HOLUB O, SEUFFERHELD MJ, GOHLKE C, GOVINDJEE AND CLEGG RM. 2000. Fluorescence Lifetime Imaging (FLI) in Real-Time - a New Technique in Photosynthesis Research. *Photosynthetica* 38: 581-599.
- HOLZWARTH AR, MILOSLAVINA Y, NILKENS M AND JAHNS P. 2009. Identification of two quenching sites active in the regulation of photosynthetic light-harvesting studied by time-resolved fluorescence. *Chemical Physics Letters* 483: 262-267.
- HORTON P, JOHNSON MP, PEREZ-BUENO ML, KISS AZ AND RUBAN AV. 2008. Photosynthetic acclimation: does the dynamic structure and macro-organisation of photosystem II in higher plant grana membranes regulate light harvesting states? *The FEBS journal* 275: 1069-1079.
- HORTON P, RUBAN AV AND WALTERS RG. 1996. Regulation of Light Harvesting in Green Plants. *Annual review of plant physiology and plant molecular biology* 47: 655-684.
- HORTON P, RUBAN AV AND WENTWORTH M. 2000. Allosteric regulation of the light-harvesting system of photosystem II. *Philosophical transactions of the Royal Society of London Series B, Biological sciences* 355: 1361-1370.
- HORTON P, WENTWORTH M AND RUBAN A. 2005. Control of the light harvesting function of chloroplast membranes: the LHCII-aggregation model for non-photochemical quenching. *FEBS Lett* 579: 4201-4206.
- IERMAK I, VINK J, BADER AN, WIENTJES E AND VAN AMERONGEN H. 2016. Visualizing heterogeneity of photosynthetic properties of plant leaves with two-photon fluorescence lifetime imaging microscopy. *Biochim Biophys Acta* 1857: 1473-1478.
- JAHNS P, GRAF M, MUNEKAGE Y AND SHIKANAI T. 2002. Single point mutation in the Rieske iron-sulfur subunit of cytochrome b6/f leads to an altered pH dependence of plastoquinol oxidation in Arabidopsis. *FEBS Lett* 519: 99-102.
- JOHNSON MP AND RUBAN AV. 2011. Restoration of Rapidly Reversible Photoprotective Energy Dissipation in the Absence of PsbS Protein by Enhanced ΔpH. *The Journal of biological chemistry* 286: 19973-19981.
- JOHNSON MP, ZIA A AND RUBAN AV. 2012. Elevated DeltapH restores rapidly reversible photoprotective energy dissipation in Arabidopsis chloroplasts deficient in lutein and xanthophyll cycle activity. *Planta* 235: 193-204.
- KALITUHO L, GRASSES T, GRAF M, RECH J AND JAHNS P. 2006. Characterization of a nonphotochemical quenching-deficient Arabidopsis mutant possessing an intact PsbS protein, xanthophyll cycle and lumen acidification. *Planta* 223: 532-541.
- KRAUSE GH AND JAHNS P 2004. Non-photochemical Energy Dissipation Determined by Chlorophyll Fluorescence Quenching: Characterization and Function. In: PAPAGEORGIOU, GC AND GOVINDJEE (Eds.) *Chlorophyll a Fluorescence: A Signature of Photosynthesis*, Dordrecht: Springer Netherlands, p. 463-495.
- KULHEIM C, AGREN J AND JANSSON S. 2002. Rapid regulation of light harvesting and plant fitness in the field. *Science* 297: 91-93.
- LAMBREV PH, MILOSLAVINA Y, JAHNS P AND HOLZWARTH AR. 2012. On the relationship between non-photochemical quenching and photoprotection of Photosystem II. *Biochim Biophys Acta* 1817: 760-769.

## ***Monitoring NPQ in leaves with ultrafast fluorescence measurements***

- LAMBREV PH, NILKENS M, MILOSLAVINA Y, JAHNS P AND HOLZWARTH AR. 2010. Kinetic and spectral resolution of multiple nonphotochemical quenching components in Arabidopsis leaves. *Plant physiology* 152: 1611-1624.
- LI XP, BJORKMAN O, SHIH C, GROSSMAN AR, ROSENQUIST M, JANSSON S AND NIYOGI KK. 2000. A pigment-binding protein essential for regulation of photosynthetic light harvesting. *Nature* 403: 391-395.
- LI XP, GILMORE AM, CAFFARRI S, BASSI R, GOLAN T, KRAMER D AND NIYOGI KK. 2004. Regulation of photosynthetic light harvesting involves intrathylakoid lumen pH sensing by the PsbS protein. *The Journal of biological chemistry* 279: 22866-22874.
- LI XP, MULLER-MOULE P, GILMORE AM AND NIYOGI KK. 2002. PsbS-dependent enhancement of feedback de-excitation protects photosystem II from photoinhibition. *Proceedings of the National Academy of Sciences of the United States of America* 99: 15222-15227.
- LUKINS PB, REHMAN S, STEVENS GB AND GEORGE D. 2005. Time-resolved spectroscopic fluorescence imaging, transient absorption and vibrational spectroscopy of intact and photo-inhibited photosynthetic tissue. *Luminescence : the journal of biological and chemical luminescence* 20: 143-151.
- MACKO S, WEHNER A AND JAHNS P. 2002. Comparison of violaxanthin de-epoxidation from the stroma and lumen sides of isolated thylakoid membranes from Arabidopsis: implications for the mechanism of de-epoxidation. *Planta* 216: 309-314.
- MILOSLAVINA Y, DE BIANCHI S, DALL'OSTO L, BASSI R AND HOLZWARTH AR. 2011. Quenching in Arabidopsis thaliana Mutants Lacking Monomeric Antenna Proteins of Photosystem II. *Journal of Biological Chemistry* 286: 36830-36840.
- MILOSLAVINA Y, GROUNOVA I, LAMBREV PH, LEPETIT B, GOSS R, WILHELM C AND HOLZWARTH AR. 2009. Ultrafast fluorescence study on the location and mechanism of non-photochemical quenching in diatoms. *Biochimica et Biophysica Acta (BBA) - Bioenergetics* 1787: 1189-1197.
- MILOSLAVINA Y, WEHNER A, LAMBREV PH, WIENTJES E, REUS M, GARAB G, CROCE R AND HOLZWARTH AR. 2008. Far-red fluorescence: A direct spectroscopic marker for LHCII oligomer formation in non-photochemical quenching. *FEBS Letters* 582: 3625-3631.
- MULLEN KM AND VAN STOKKUM IH. 2007. TIMP: an R package for modeling multi-way spectroscopic measurements. *Journal of Statistical Software* 18: 1-46.
- MÜLLER P, BIESER G, HARTWICH G, LANGENBACHER T, LOSSAU H, OGRONIK A AND MICHEL-BEYERLE M-E. 1996. The internal conversion rate of the primary donor in reaction centers of Rhodospirillum rubrum. *Berichte der Bunsengesellschaft für physikalische Chemie* 100: 1967-1973.
- MÜLLER P, LI X-P AND NIYOGI KK. 2001. Non-Photochemical Quenching. A Response to Excess Light Energy. *Plant physiology* 125: 1558-1566.
- NIYOGI KK. 1999. PHOTOPROTECTION REVISITED: Genetic and Molecular Approaches. *Annual review of plant physiology and plant molecular biology* 50: 333-359.
- NIYOGI KK, GROSSMAN AR AND BJORKMAN O. 1998. Arabidopsis mutants define a central role for the xanthophyll cycle in the regulation of photosynthetic energy conversion. *The Plant cell* 10: 1121-1134.

- NIYOGI KK, LI X-P, ROSENBERG V AND JUNG H-S. 2005. Is PsbS the site of non-photochemical quenching in photosynthesis? *Journal of experimental botany* 56: 375-382.
- PASCAL AA, LIU Z, BROESS K, VAN OORT B, VAN AMERONGEN H, WANG C, HORTON P, ROBERT B, CHANG W AND RUBAN A. 2005. Molecular basis of photoprotection and control of photosynthetic light-harvesting. 436: 134-137.
- PETERMAN EJ, DUKKER FM, VAN GRONDELLE R AND VAN AMERONGEN H. 1995. Chlorophyll a and carotenoid triplet states in light-harvesting complex II of higher plants. *Biophysical journal* 69: 2670-2678.
- PETERMAN EJC, GRADINARU CC, CALKOEN F, BORST JC, VAN GRONDELLE R AND VAN AMERONGEN H. 1997. Xanthophylls in Light-Harvesting Complex II of Higher Plants: Light Harvesting and Triplet Quenching. *Biochemistry* 36: 12208-12215.
- RUBAN AV, BERERA R, ILIOAIA C, VAN STOKKUM IHM, KENNIS JTM, PASCAL AA, VAN AMERONGEN H, ROBERT B, HORTON P AND VAN GRONDELLE R. 2007. Identification of a mechanism of photoprotective energy dissipation in higher plants. 450: 575-578.
- RUBAN AV AND HORTON P. 1994. Spectroscopy of non-photochemical and photochemical quenching of chlorophyll fluorescence in leaves; evidence for a role of the light harvesting complex of Photosystem II in the regulation of energy dissipation. *Photosynthesis research* 40: 181-190.
- RUBAN AV, JOHNSON MP AND DUFFY CD. 2012. The photoprotective molecular switch in the photosystem II antenna. *Biochim Biophys Acta* 1817: 167-181.
- RUBAN AV, YOUNG AJ AND HORTON P. 1996. Dynamic properties of the minor chlorophyll a/b binding proteins of photosystem II, an in vitro model for photoprotective energy dissipation in the photosynthetic membrane of green plants. *Biochemistry* 35: 674-678.
- SNELLENBURG J, LAPTENOK S, SEGER R, MULLEN K AND VAN STOKKUM I. 2012. Glotaran: a Java-based graphical user interface for the R package TIMP. *Journal of Statistical Software* 49: -.
- SYLAK-GLASSMAN EJ, ZAKS J, AMARNATH K, LEUENBERGER M AND FLEMING GR. 2016. Characterizing non-photochemical quenching in leaves through fluorescence lifetime snapshots. *Photosynthesis research* 127: 69-76.
- VAN AMERONGEN H AND CROCE R 2008. Chapter 8 Structure and Function of Photosystem II Light-Harvesting Proteins (Lhcb) of Higher Plants. *Primary Processes of Photosynthesis, Part 1: Principles and Apparatus: The Royal Society of Chemistry*, p. 329-367.
- VAN OORT B, ALBERTS M, DE BIANCHI S, DALL'OSTO L, BASSI R, TRINKUNAS G, CROCE R AND VAN AMERONGEN H. 2010. Effect of antenna-depletion in Photosystem II on excitation energy transfer in *Arabidopsis thaliana*. *Biophysical journal* 98: 922-931.
- VAN OORT B, AMUNTS A, BORST JW, VAN HOEK A, NELSON N, VAN AMERONGEN H AND CROCE R. 2008. Picosecond Fluorescence of Intact and Dissolved PSI-LHCI Crystals. *Biophysical journal* 95: 5851-5861.
- VAN OORT B, MURALI S, WIENTJES E, KOEHORST RBM, SPRUIJT RB, VAN HOEK A, CROCE R AND VAN AMERONGEN H. 2009. Ultrafast resonance energy transfer from a site-specifically attached fluorescent chromophore reveals the folding of the N-terminal domain of CP29. *Chemical Physics* 357: 113-119.
- VAN STOKKUM IHM, GOBETS B, GENSCH T, MOURIK F, HELLINGWERF KJ, GRONDELLE R AND KENNIS JTM. 2006. (Sub)-Picosecond Spectral Evolution of Fluorescence in

### ***Monitoring NPQ in leaves with ultrafast fluorescence measurements***

Photoactive Proteins Studied with a Synchroscan Streak Camera System. Photochemistry and photobiology 82: 380-388.

VAN STOKKUM IHM, LARSEN DS AND VAN GRONDELLE R. 2004. Global and target analysis of time-resolved spectra. Biochimica et Biophysica Acta (BBA) - Bioenergetics 1657: 82-104.

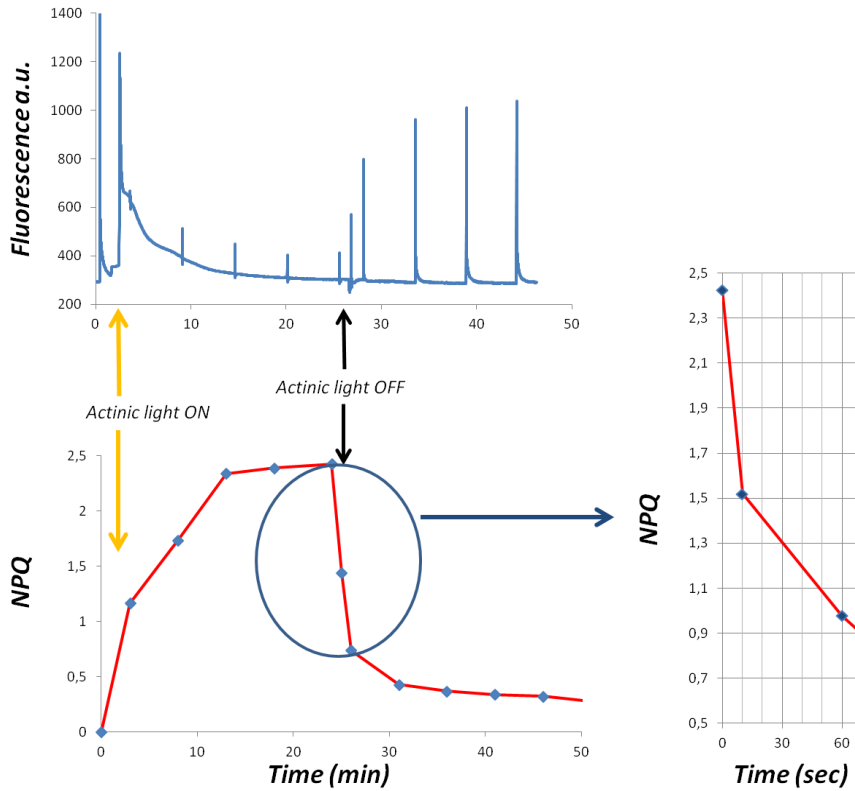
VAN STOKKUM IHM, VAN OORT B, VAN MOURIK F, GOBETS B AND VAN AMERONGEN H 2008. (Sub)-Picosecond Spectral Evolution of Fluorescence Studied with a Synchroscan Streak-Camera System and Target Analysis. In: AARTSMA, TJ AND MATYSIK, J (Eds.) Biophysical Techniques in Photosynthesis, Dordrecht: Springer Netherlands, p. 223-240.

VASS I. 2011. Role of charge recombination processes in photodamage and photoprotection of the photosystem II complex. Physiologia plantarum 142: 6-16.

WIENTJES E, VAN AMERONGEN H AND CROCE R. 2013. LHCII is an antenna of both photosystems after long-term acclimation. Biochim Biophys Acta 1827: 420-426.

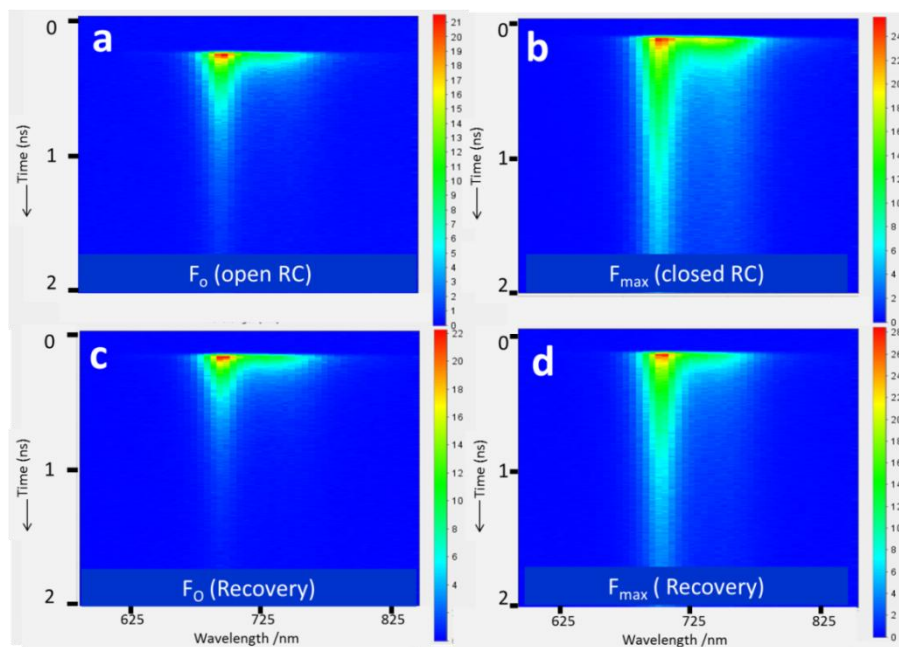
XU P, TIAN L, KLOZ M AND CROCE R. 2015. Molecular insights into Zeaxanthin-dependent quenching in higher plants. 5: 13679.

## SUPPLEMENTARY MATERIAL

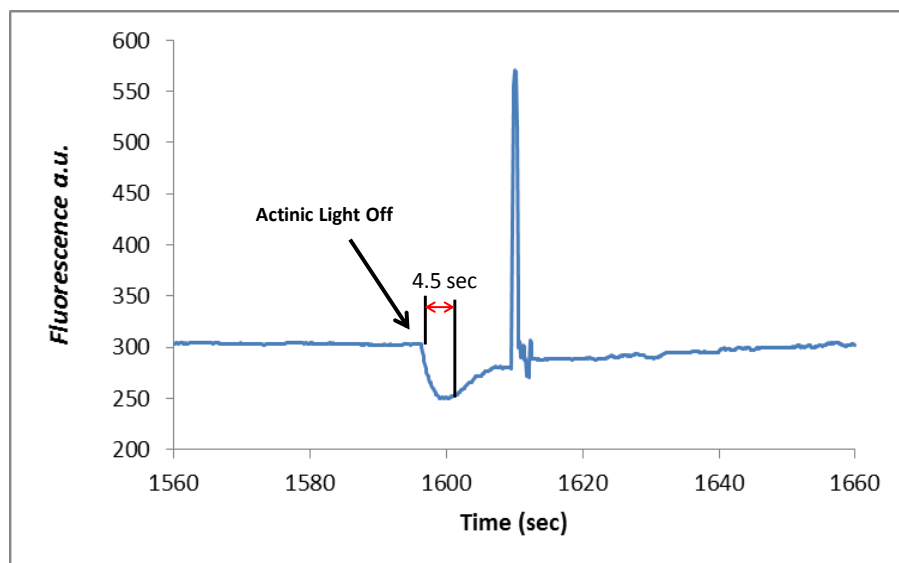


Supplementary Figure1: NPQ as a function of time. In approximately 10sec after switching off the actinic light, the NPQ value drops by 40%, whereas after 60 sec the drop is 60%, respectively.

## Monitoring NPQ in leaves with ultrafast fluorescence measurements



Supplementary Figure2: After 45 min of relaxation in the dark, the leaves in both cases i.e. (a)  $F_o$ , (b)  $F_{max}$ , showed nearly identical fluorescence kinetics as before quenching i.e. (c)  $F_o$ , Recovery, (d)  $F_{max}$ , Recovery.



Supplementary Figure 3: PAM measurement showing that after switching off the actinic light it takes at most 4.5s for all RCs to be open again.



# **CHAPTER 6**

## **General Discussion**

### **General discussion**

Recent developments in the field of fluorescence are speeding up the pace of research and development in the area of bioengineering, medical diagnoses and industrial microbiology. These techniques are widely used to address fundamental and applied questions in the field of basic and applied life sciences, as they can provide direct information on molecular structure and dynamics of (bio)molecular systems (Valeur 2001). They are also used in industry for quantitative analysis of chemical compositions, particle size and velocities. A significant advantage of fluorescence techniques is that they can often be non-invasive and measurements can be performed in real time.

The work presented in this thesis is devoted to two different matters: The first part aims at improving the smFRET technique for the analysis of DNA dynamics and other fast conformational changes. This improvement is made by combining and developing instrumentation and data evaluation tools. The second part is the continuous development of time-resolved fluorescence spectroscopy methods, as well their application in the field of photosynthesis to study ultrafast processes in thylakoid membranes and leaves. The two fluorescence techniques are technically and conceptually very different, but they are both designed for analysis of biomolecular systems. In this thesis, the techniques are applied to study energy transfer and dynamical changes in DNAs, thylakoid membranes and leaves.

#### **Part 1:**

### **Single-molecule Förster Resonance Energy Transfer (smFRET)**

Combining cell biology and photophysics techniques is a major step towards identifying and quantifying biological processes in their natural environment. In particular, single molecule Förster-Resonance-Energy-Transfer (smFRET) can provide quantitative information on distances (2-10 nm), which are far below the diffraction limit of the light ( $\lambda/2$ ). It is a widely used technique for monitoring interaction and dynamics between and within biological complexes with suitable donor-acceptor pairs. In FRET, energy from a donor fluorophore is transferred non-radiatively to an acceptor chromophore at close distance (2-10 nm) via a weak dipole-dipole coupling (Förster 1948). **Chapter 2** in this thesis contains a general description of the detection of sm-FRET to study biological and chemical processes at the molecular level. The two standard detection schemes for smFRET (Walter et al. 2008): diffusion-based confocal microscopy and image-based total internal reflection fluorescence (TIRF) microscopy (Axelrod et al. 1984, Holden et al. 2010)

are discussed in great depth, along with recent developments in sm-FRET based applications. The theoretical framework presented in this chapter forms the background for understanding the basics of the studied doubly labeled DNA hairpin and the experimental and calculational methods used to investigate in Chapter 3.

## Conformational dynamics of DNA hairpins

As discussed in chapter 2, smFRET has become a powerful tool to study dynamics and interactions of biological entities at the nanometer scale. Recently, there has been a growing interest in applying this technique to study conformational dynamics of individual molecules under equilibrium conditions and even to monitor the conformational changes of DNA polymerases during DNA synthesis (Christian et al. 2009b). Taken together, these applications often would benefit from data acquisition at higher time resolution. However, the currently available standard schemes for smFRET detection (Walter et al. 2008), i.e. diffusion-based confocal microscopy and camera based total internal reflection fluorescence (TIRF) microscopy (Axelrod et al. 1984, Holden et al. 2010), are limited in their ability to combine parallel detection of many molecules with obtaining data at sufficiently high time resolution (<15 ms).

In Chapter 3 we therefore experimentally demonstrate significant improvement in the time resolution achievable for image-based TIRF microscopy which is limited by the achievable frame rate of the camera (currently around 60 Hz corresponding to a time resolution of 15 ms). To improve the time resolution of camera-based smFRET, we combined the concept of *alternating-laser excitation (ALEX)* (Hohlbein et al. 2014b, Kapanidis et al. 2004, Laurence et al. 2005, Lee et al. 2005, Muller et al. 2005) with *stroboscopic illumination* (Blumberg et al. 2005, Elf et al. 2007, Flors et al. 2007) i.e. we only excite the sample for short time intervals (e.g., 3 ms), rather than exciting the sample for the full duration of a camera frame. The potential of stroboscopic alternating-laser excitation (sALEX) is then experimentally demonstrated by studying the dynamic system of an interconverting, doubly labeled DNA hairpin at different salt concentrations (0-1 M). The DNA hairpin is excited for 50 ms i.e. the full camera frame duration for ALEX measurements, whereas for sALEX measurements the sample is only excited for a short interval of time (i.e. 3 ms). Conformational dynamics of a DNA hairpin is then studied by comparing standard ALEX with sALEX E'S histograms. We observe from the FRET value histogram that sALEX can detect fluctuations in the low millisecond time range, while they are averaged out in the conventional detection scheme (Fig.1). Our results for opening and closing rates i.e.  $k_{oc} = (117 \pm$

## General Discussion

4)  $s^{-1}$  and  $k_{co} = (188 \pm 6) s^{-1}$  at a salt concentration of 300 mM NaCl (fig.4 Chapt.3) is comparable with the results obtained by Tsukanov et al. (Tsukanov et al. 2013b) who obtained opening and closing rates of  $\sim 200 s^{-1}$  for a similar stem sequence of six complementary bases (5' TGG ATT) but using time consuming diffusion-based confocal microscopy. The differences in the rates can be due to the different donor fluorophore (Cy3B instead of ATTO 550) and different labeling positions as both can have a substantial influence on the conformational rates of DNA hairpins (Hartmann et al. 2014, Kugel et al. 2012). The main advantage of our imaging-based implementation is that it allows us to observe a molecule for extended periods of time without sacrificing the highly parallelized detection of total internal reflection fluorescence (TIRF) microscopy as shown in Fig.1. Compared to confocal microscopy, the sALEX scheme increases the throughput by a factor of at least 1000.

One must remember that by reducing the duration of the excitation time (i.e. 3 ms) below the camera frame time which is required to read and write the data, we lose information about the species during periods of no excitation as they are hidden and cannot be monitored. This information is often not relevant especially in cases in which the species are in a conformational equilibrium but has to be considered in cases where reactions such as DNA synthesis are studied (Christian et al. 2009b).

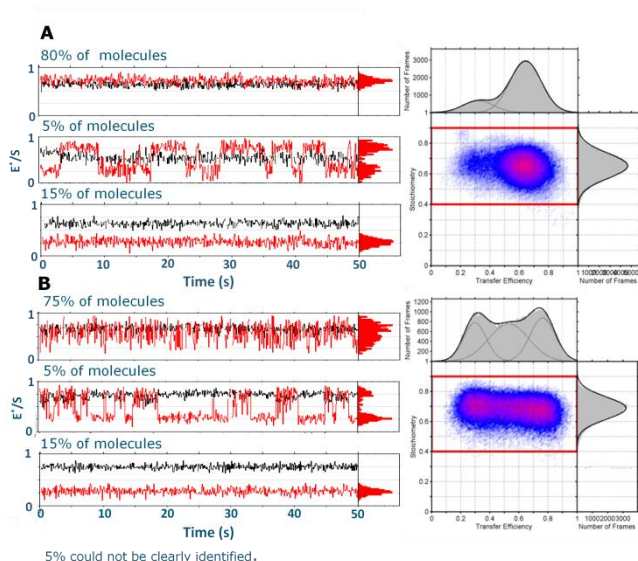


**Figure1.** An example of single molecule time traces and FRET histogram of DNA hairpin by applying (A) standard ALEX technique and (B) sALEX technique.

Another crucial point in the extraction of information about protein interactions from FRET data is advanced and robust data analysis. The brief snapshots acquired by using sALEX are comparable to the data obtained from diffusion-based confocal microscopy. Therefore, we adapted dynamic probability distribution analysis (dPDA) (Antonik et al. 2006, Kalinin et al. 2007, Kalinin et al. 2010a, Nir et al. 2006, Santoso et al. 2010b), a concept known from diffusion-based confocal microscopy, to analyse dynamics which are faster than the corresponding frame rates of the camera. The shape and width of these distributions are influenced by the potential presence of static FRET species as well as by species dynamically interconverting between two or more conformations.

The main experimental limitation which we faced was the limited laser power of the green laser (<50 mW before entering the TIRF objective) and photobleaching, which prevented us from increasing the time resolution while keeping the number of detected photons per excitation constant. For future work a more powerful laser might help to improve the time resolution. Whereas, recent developments in photoprotection mechanisms such as oxygen scavengers in combination with triplet state quencher or “self-healing” dyes (Ha and Tinnefeld 2012, van der Velde et al. 2013, Zheng et al. 2014) will help to further push the number of photons detectable from single emitters. Thus, we expect by using sALEX and dPDA in combination, it will be possible to resolve dynamic conformational states with a lifetime in the order of a few milliseconds.

## Part II:

Photosynthesis is the process that converts light energy into chemical energy in many living organisms for e.g. plants, algae and cyanobacteria (Blankenship 2002, Van Amerongen et al. 2000). In oxygenic photosynthesis, two types of reactions occur in chloroplasts, the *light reactions*: that mainly take place inside the thylakoid membrane and lead to the production of NADPH and ATP which are later used in the *dark reactions* which are responsible for the reduction of CO<sub>2</sub> into sugar (Arnon 1971, Calvin and Benson 1948, Raven et al. 2005). Despite a significant amount of progress in this field, there are still many aspects which need to be understood. One of the most remarkable advances made in this area is that crystal structures of many photosynthetic complexes have been resolved (Guskov et al. 2009, Liu et al. 2004, Wei et al. 2016, Yan et al. 2007). Many of these complexes have been investigated in depth by using ultrafast spectroscopic techniques which allow us to study the fundamental processes such as excitation energy transfer (EET) and charge separation (CS), after the absorption of a photon.

## General Discussion

The second part of this thesis is focused on understanding part of the underlying molecular mechanisms and to determine the photosynthetic efficiencies. To do so, picosecond time-resolved fluorescence spectroscopy was used to study ultrafast processes such as excitation energy transfer (EET) and non-photochemical quenching (NPQ) in thylakoid membrane and intact spinach leaves.

### EET between granum layers

In the first steps of photosynthesis, light is harvested by two main pigment-protein complexes PSI and PSII, which are embedded in the thylakoid membrane (Blankenship 2014). Both photosystems contain pigments that harvest light and efficiently transfer excitation energy to the reaction centers (RCs) of PSI and PSII, where charge separation occurs. In green plants and algae, the thylakoid membranes are found in the chloroplasts, where the light reactions of photosynthesis take place. The thylakoid consists of stacked and unstacked regions, known as *grana* and *stroma lamellae*, respectively. In the thylakoid membranes, the pigment-protein complexes are distributed unevenly. PSI and ATP synthase reside mainly in the stroma lamellae whereas PSII is found in the stacked grana, and the *cyt b<sub>6</sub>f* complex is suggested to be located both in grana and stroma lamellae (Albertsson 2001, Dekker and Boekema 2005, Nelson and Ben-Shem 2004, Staehelin 2003).

In **Chapter 4** the long-standing question regarding whether excitation energy transfer (EET) in the grana occurs only in two dimensions (i.e. within the membranes) or whether efficient inter-layer energy transfer takes place within the membrane has been studied. To evaluate the efficiency of the excitation energy transfer between the neighboring layers of the photosynthetic membranes in the grana, we compared picosecond fluorescence decay kinetics for stacked and unstacked PSII enriched grana membranes. The measured excitation decay kinetics was analyzed by applying the fluctuating antenna model/method (Chmeliov et al. 2014). This model describes excitation energy diffusion in a continuous medium and accounts for both the fluctuating nature of the light-harvesting antenna and the non-uniform distribution of these complexes around the reaction centers. The method used can describe the fluorescence decay kinetics, arising from variable sized PSII, stacked PSII-enriched membranes (so-called BBY particles), aggregates of major light-harvesting complexes (LHCII), or even the whole photosynthetic membranes, by using just 2 major fitting parameters, instead of the many decay times and amplitudes required in standard analysis procedures. The method is also able to provide valuable information on the structural organization of the photosynthetic antenna, like the stacked structure of BBY complexes with the

existing channels for the interlayer excitation energy transfer (Chmeliov et al. 2014, Chmeliov et al. 2016b). In our work, we used this model to compare the functional organization of PSII enriched grana membranes regarding the dimensionality  $d$  of the stacked and the unstacked membranes.

Our results shows that there is no significant variation of the functional dimensionality  $d$  upon membrane unstacking, all our PSII enriched grana membranes preparations exhibited virtually the same value of  $d = 1.6$ , indicating the absence of any substantial transverse inter-layer EET, in agreement with the conclusions of Lambrev *et al.* and Kirchhoff *et al.* (Kirchhoff et al. 2007, Lambrev et al. 2011), but in contrast to the earlier work by Trissl *et al.* (Trissl et al. 1987). The obtained dimensionality  $d$  is smaller than 2, which shows the presence of void regions and/or the lack of connectivity at some antenna points. We conclude from our results that stacking of the membranes in the grana does not affect the efficiency of the delivery of excitation energy towards the reaction centers but probably just ensures a more compact organization of the thylakoid membranes within the chloroplast and efficient separation of photosystems I and II.

## **NPQ mechanism in plants**

Too much light can be damaging for photosynthetic organisms. When plants are exposed to excess light, more excitations are created than the reaction centers (RCs) in the thylakoid membranes can handle. To protect themselves plants utilize a set of photoprotective mechanisms, in which excess absorbed light energy is dissipated as heat and which can be measured as the non-photochemical quenching (NPQ) of chlorophyll (Chl) fluorescence (Barber and Andersson 1992, Horton et al. 1996, Krause and Jahns 2004, Niyogi 1999, Ruban et al. 2012).

In **Chapter 5**, we have used non-invasive picosecond fluorescence measurements on intact spinach leaves using a streak camera setup to study the kinetics of the early steps in photosynthesis and the photoprotective mechanisms. The main advantage of time-resolved picosecond fluorescence measurements is that these measurements are less sensitive to photobleaching and chloroplast movement, and in addition, can be used to reveal the rates of qE (energy dependent component). Moreover, they can provide spectral information of Chl emission in all conditions. However, the experiments are complicated by the fact that the high concentration of chloroplasts found in leaves leads to re-absorption and re-emission of fluorescence. This may sometimes have a large impact on the leaf's emission spectrum.

## **General Discussion**

The lifetime measurements on intact leaves were performed under four different conditions, with all PSII reaction centers (RCs) either in the open state ( $F_0$ ) or in the closed state ( $F_{\max}$ ) while being dark-adapted, and after photoprotective mechanism of nonphotochemical quenching (NPQ) had been induced by high light illumination. Our results from time-resolved fluorescence measurements on leaves in the absence of NPQ are similar to previously obtained results on Arabidopsis leaves and/or thylakoid membranes, both for open and closed RCs (Holub et al. 2000, Iermak et al. 2016, Lukins et al. 2005, Miloslavina et al. 2011). Whereas, after inducing NPQ we see a clear decrease in average lifetime as compared to  $F_0$  and  $F_{\max}$  respectively. The average lifetimes were then used to estimate the average rate of NPQ for both the open and closed states. But these rates are much higher than those obtained with the PAM measurements on similar leaves. This could be due to the fact that we use lower light intensity to induce NPQ ( $1050\mu\text{mol.m}^{-2}.\text{sec}^{-1}$  vs.  $1300\mu\text{mol.m}^{-2}.\text{sec}^{-1}$ ) in the PAM measurements, but also that from the fluorescence lifetime data, real PSII NPQ value can be calculated, while in the PAM data the fluorescence from PSI interferes.

The calculated rate constants  $k_{\text{NPQ}}$  are very reproducible in both open and closed states. However, we have observed that the rate of NPQ is higher by the factor of 2.7 times in case of closed RCs compared to open RCs. Which from a functional point of view can be considered as an ideal situation because closed RCs are prevented from causing singlet oxygen formation while the open RCs can continue to function. Our current results demonstrate that the quenching is dependent on the state of the RCs. However, it would only be effective if the fast quenching would occur in the direct environment of the closed RC, which is in disagreement with all existent models. At the moment we do not have a good explanation for this observation at the molecular level and further research will be needed to validate and explain results. One outstanding problem with these measurements is that they can only be performed on detached leaves at the moment. Although this is already a significant improvement compared to measurements on isolated chloroplasts and thylakoid membranes, it would be desirable to design and build a setup that can be used for non-invasive measurements on real plants.

## **Future Outlook:**

In this thesis, we have discussed fluorescence spectroscopic techniques to study biological complexes, especially the photosynthetic systems. In particular, these studies explore the photophysical processes such as energy transfer (functional heterogeneity) and conformational dynamics (structural heterogeneity) in biomolecular complexes. As demonstrated in this thesis, single-molecule and time-



resolved fluorescence spectroscopic techniques have made significant progress, yet still many challenges remain in technological, biological and application area.

Since the primary electron and energy transfer in photosynthesis occur on pico- or sub-picosecond time scale, early steps of photosynthesis are mostly studied by ultrafast spectroscopy at the ensemble level. As outlook, we expect that using ultrafast temporal resolution and time-correlated single photon counting at the single-molecule level will further broaden our understanding of the heterogeneity in energy transfer dynamics in individual pigment-protein complexes. We also point out that potential slow conformational changes occurring in photosynthetic systems could be probed using smFRET and the improvements described in this thesis.

Another challenge in terms of biology is to perform experiments under near physiological sample conditions to improve the reliability and relevance of the results. In Chapter 5 we developed a time resolved spectroscopic technique, in which fluorescence snapshots at different time intervals during the relaxation process of leaves are recorded allowing us to investigate the physical mechanism of quenching and their relative timescale of disappearance upon recovery from quenched state. However, these experiments are complicated by the fact that the sample under investigations carries significant scattering problems and further improvements are needed.

Furthermore, due to the ever-growing energy demand on our planet, many bio-inspired artificial systems for solar energy applications are being developed (Odobel et al. 2013, Scholes et al. 2011). While we here focused on natural photosynthetic systems, single-molecule and ultrafast spectroscopic experiments could also be used to understand the functionality of these artificial systems, which in turn, can aid in the optimization of artificial light-harvesting devices (Choi et al. 2004, Gust et al. 2009).

## References

- ALBERTSSON P-Å. 2001. A quantitative model of the domain structure of the photosynthetic membrane. *Trends in plant science* 6: 349-354.
- ANTONIK M, FELEKYAN S, GAIDUK A AND SEIDEL CA. 2006. Separating structural heterogeneities from stochastic variations in fluorescence resonance energy transfer distributions via photon distribution analysis. *The journal of physical chemistry B* 110: 6970-6978.
- ARNON DI. 1971. The Light Reactions of Photosynthesis. *Proceedings of the National Academy of Sciences* 68: 2883-2892.
- AXELROD D, BURGHARDT TP AND THOMPSON NL. 1984. Total internal reflection fluorescence. *Annual review of biophysics and bioengineering* 13: 247-268.
- BARBER J AND ANDERSSON B. 1992. Too much of a good thing: light can be bad for photosynthesis. *Trends in biochemical sciences* 17: 61-66.
- BLANKENSHIP RE 2002. *Molecular mechanisms of photosynthesis*. Oxford Blackwell Science.
- BLANKENSHIP RE 2014. *Molecular mechanisms of photosynthesis*. Second edition. ed, Chichester, West Sussex: Wiley Blackwell, xv, 296 pages p.
- BLUMBERG S, GAJRAJ A, PENNINGTON MW AND MEINERS JC. 2005. Three-dimensional characterization of tethered microspheres by total internal reflection fluorescence microscopy. *Biophysical journal* 89: 1272-1281.
- CALVIN M AND BENSON AA. 1948. The Path of Carbon in Photosynthesis. *Science* 107: 476-480.
- CHMELIOV J, TRINKUNAS G, VAN AMERONGEN H AND VALKUNAS L. 2014. Light harvesting in a fluctuating antenna. *Journal of the American Chemical Society* 136: 8963-8972.
- CHMELIOV J, TRINKUNAS G, VAN AMERONGEN H AND VALKUNAS L. 2016. Excitation migration in fluctuating light-harvesting antenna systems. *Photosynthesis research* 127: 49-60.
- CHOI MS, YAMAZAKI T, YAMAZAKI I AND AIDA T. 2004. Bioinspired molecular design of light-harvesting multiporphyrin arrays. *Angewandte Chemie (International ed in English)* 43: 150-158.
- CHRISTIAN TD, ROMANO LJ AND RUEDA D. 2009. Single-molecule measurements of synthesis by DNA polymerase with base-pair resolution. *Proceedings of the National Academy of Sciences of the United States of America* 106: 21109-21114.
- DEKKER JP AND BOEKEMA EJ. 2005. Supramolecular organization of thylakoid membrane proteins in green plants. *Bba-Bioenergetics* 1706: 12-39.
- ELF J, LI GW AND XIE XS. 2007. Probing transcription factor dynamics at the single-molecule level in a living cell. *Science* 316: 1191-1194.
- FLORS C, HOTTA J, UJI-I H, DEDECKER P, ANDO R, MIZUNO H, MIYAWAKI A AND HOFKENS J. 2007. A stroboscopic approach for fast photoactivation-localization microscopy with Dronpa mutants. *Journal of the American Chemical Society* 129: 13970-13977.

- FÖRSTER T. 1948. Zwischenmolekulare Energiewanderung und Fluoreszenz. *Ann Phys* 437: 55-75.
- GUSKOV A, KERN J, GABDULKHAKOV A, BROSER M, ZOUNI A AND SAENGER W. 2009. Cyanobacterial photosystem II at 2.9-Å resolution and the role of quinones, lipids, channels and chloride. *Nat Struct Mol Biol* 16: 334-342.
- GUST D, MOORE TA AND MOORE AL. 2009. Solar Fuels via Artificial Photosynthesis. *Accounts of Chemical Research* 42: 1890-1898.
- HA T AND TINNEFELD P. 2012. Photophysics of fluorescent probes for single-molecule biophysics and super-resolution imaging. *Annual review of physical chemistry* 63: 595-617.
- HARTMANN A, KRAINER G AND SCHLIERF M. 2014. Different fluorophore labeling strategies and designs affect millisecond kinetics of DNA hairpins. *Molecules (Basel, Switzerland)* 19: 13735-13754.
- HOHLBEIN J, CRAGGS TD AND CORDES T. 2014. Alternating-laser excitation: single-molecule FRET and beyond. *Chemical Society reviews* 43: 1156-1171.
- HOLDEN SJ, UPHOFF S, HOHLBEIN J, YADIN D, LE RESTE L, BRITTON OJ AND KAPANIDIS AN. 2010. Defining the limits of single-molecule FRET resolution in TIRF microscopy. *Biophysical journal* 99: 3102-3111.
- HOLUB O, SEUFFERHELD MJ, GOHLKE C, GOVINDJEE AND CLEGG RM. 2000. Fluorescence Lifetime Imaging (FLI) in Real-Time - a New Technique in Photosynthesis Research. *Photosynthetica* 38: 581-599.
- HORTON P, RUBAN AV AND WALTERS RG. 1996. Regulation of Light Harvesting in Green Plants. *Annual review of plant physiology and plant molecular biology* 47: 655-684.
- IERMAK I, VINK J, BADER AN, WIENTJES E AND VAN AMERONGEN H. 2016. Visualizing heterogeneity of photosynthetic properties of plant leaves with two-photon fluorescence lifetime imaging microscopy. *Biochim Biophys Acta* 1857: 1473-1478.
- KALININ S, FELEKYAN S, ANTONIK M AND SEIDEL CA. 2007. Probability distribution analysis of single-molecule fluorescence anisotropy and resonance energy transfer. *The journal of physical chemistry B* 111: 10253-10262.
- KALININ S, SISAMAKIS E, MAGENNIS SW, FELEKYAN S AND SEIDEL CA. 2010. On the origin of broadening of single-molecule FRET efficiency distributions beyond shot noise limits. *The journal of physical chemistry B* 114: 6197-6206.
- KAPANIDIS AN, LEE NK, LAURENCE TA, DOOSE S, MARGEAT E AND WEISS S. 2004. Fluorescence-aided molecule sorting: analysis of structure and interactions by alternating-laser excitation of single molecules. *Proceedings of the National Academy of Sciences of the United States of America* 101: 8936-8941.
- KIRCHHOFF H, HAASE W, HAFERKAMP S, SCHOTT T, BORINSKI M, KUBITSCHKE U AND ROGNER M. 2007. Structural and functional self-organization of Photosystem II in grana thylakoids. *Biochim Biophys Acta* 1767: 1180-1188.
- KRAUSE GH AND JAHNS P. 2004. Non-photochemical Energy Dissipation Determined by Chlorophyll Fluorescence Quenching: Characterization and Function. In: PAPAGEORGIOU, GC AND GOVINDJEE (Eds.) *Chlorophyll a Fluorescence: A Signature of Photosynthesis*, Dordrecht: Springer Netherlands, p. 463-495.
- KUGEL W, MUSCHIELOK A AND MICHAELIS J. 2012. Bayesian-inference-based fluorescence correlation spectroscopy and single-molecule burst analysis reveal the influence of dye

## General Discussion

- selection on DNA hairpin dynamics. *Chemphyschem : a European journal of chemical physics and physical chemistry* 13: 1013-1022.
- LAMBREV PH, SCHMITT FJ, KUSSIN S, SCHOENGEM M, VARKONYI Z, EICHLER HJ, GARAB G AND RENGIER G. 2011. Functional domain size in aggregates of light-harvesting complex II and thylakoid membranes. *Biochim Biophys Acta* 1807: 1022-1031.
- LAURENCE TA, KONG X, JAGER M AND WEISS S. 2005. Probing structural heterogeneities and fluctuations of nucleic acids and denatured proteins. *Proceedings of the National Academy of Sciences of the United States of America* 102: 17348-17353.
- LEE NK, KAPANIDIS AN, WANG Y, MICHALET X, MUKHOPADHYAY J, EBRIGHT RH AND WEISS S. 2005. Accurate FRET measurements within single diffusing biomolecules using alternating-laser excitation. *Biophysical journal* 88: 2939-2953.
- LIU Z, YAN H, WANG K, KUANG T, ZHANG J, GUI L, AN X AND CHANG W. 2004. Crystal structure of spinach major light-harvesting complex at 2.72 Å resolution. *Nature* 428: 287-292.
- LUKINS PB, REHMAN S, STEVENS GB AND GEORGE D. 2005. Time-resolved spectroscopic fluorescence imaging, transient absorption and vibrational spectroscopy of intact and photo-inhibited photosynthetic tissue. *Luminescence : the journal of biological and chemical luminescence* 20: 143-151.
- MILOSLAVINA Y, DE BIANCHI S, DALL'OSTO L, BASSI R AND HOLZWARTH AR. 2011. Quenching in *Arabidopsis thaliana* Mutants Lacking Monomeric Antenna Proteins of Photosystem II. *Journal of Biological Chemistry* 286: 36830-36840.
- MULLER BK, ZAYCHIKOV E, BRAUCHLE C AND LAMB DC. 2005. Pulsed interleaved excitation. *Biophysical journal* 89: 3508-3522.
- NELSON N AND BEN-SHEM A. 2004. The complex architecture of oxygenic photosynthesis. 5: 971-982.
- NIR E, MICHALET X, HAMADANI KM, LAURENCE TA, NEUHAUSER D, KOVCHEGOV Y AND WEISS S. 2006. Shot-noise limited single-molecule FRET histograms: comparison between theory and experiments. *The journal of physical chemistry B* 110: 22103-22124.
- NIYOGI KK. 1999. PHOTOPROTECTION REVISITED: Genetic and Molecular Approaches. *Annual review of plant physiology and plant molecular biology* 50: 333-359.
- ODOBEL F, PELLEGRIN Y AND WARNAN J. 2013. Bio-inspired artificial light-harvesting antennas for enhancement of solar energy capture in dye-sensitized solar cells. *Energy & Environmental Science* 6: 2041-2052.
- RAVEN PH, EVERT RF AND EICHHORN SE 2005. *Biology of Plants*. W. H. Freeman.
- RUBAN AV, JOHNSON MP AND DUFFY CD. 2012. The photoprotective molecular switch in the photosystem II antenna. *Biochim Biophys Acta* 1817: 167-181.
- SANTOSO Y, TORELLA JP AND KAPANIDIS AN. 2010. Characterizing single-molecule FRET dynamics with probability distribution analysis. *Chemphyschem : a European journal of chemical physics and physical chemistry* 11: 2209-2219.
- SCHOLES GD, FLEMING GR, OLAYA-CASTRO A AND VAN GRONDELLE R. 2011. Lessons from nature about solar light harvesting. 3: 763-774.
- STAEHELIN LA. 2003. Chloroplast structure: from chlorophyll granules to supra-molecular architecture of thylakoid membranes. *Photosynthesis research* 76: 185-196.

- TRISSEL HW, BRETON J, DEPREZ J AND LEIBL W. 1987. Primary Electrogenic Reactions of Photosystem-II as Probed by the Light-Gradient Method. *Biochim Biophys Acta* 893: 305-319.
- TSUKANOV R, TOMOV TE, MASOUD R, DRORY H, PLAVNER N, LIBER M AND NIR E. 2013. Detailed study of DNA hairpin dynamics using single-molecule fluorescence assisted by DNA origami. *The journal of physical chemistry B* 117: 11932-11942.
- VALEUR B 2001. *Molecular Fluorescence: Principles and Applications*. 1 ed: Wiley-VCH.
- VAN AMERONGEN H, VALKUNAS L AND VAN GRONDELLE R 2000. *Photosynthetic excitons*. Singapore: World Scientific.
- VAN DER VELDE JH, PLOETZ E, HIERMAIER M, OELERICH J, DE VRIES JW, ROELFES G AND CORDES T. 2013. Mechanism of intramolecular photostabilization in self-healing cyanine fluorophores. *Chemphyschem : a European journal of chemical physics and physical chemistry* 14: 4084-4093.
- WALTER NG, HUANG CY, MANZO AJ AND SOBHY MA. 2008. Do-it-yourself guide: how to use the modern single-molecule toolkit. *Nature methods* 5: 475-489.
- WEI X, SU X, CAO P, LIU X, CHANG W, LI M, ZHANG X AND LIU Z. 2016. Structure of spinach photosystem II-LHCII supercomplex at 3.2 Å resolution. *534*: 69-74.
- YAN H, ZHANG P, WANG C, LIU Z AND CHANG W. 2007. Two lutein molecules in LHCII have different conformations and functions: Insights into the molecular mechanism of thermal dissipation in plants. *Biochemical and biophysical research communications* 355: 457-463.
- ZHENG Q, JUETTE MF, JOCKUSCH S, WASSERMAN MR, ZHOU Z, ALTMAN RB AND BLANCHARD SC. 2014. Ultra-stable organic fluorophores for single-molecule research. *Chemical Society reviews* 43: 1044-1056.



# **CHAPTER 7**

## **Summary**

## Summary

In this thesis, I have focused on the application and development of fluorescence spectroscopy techniques to study two important biological processes: (1) DNA dynamics and (2) plant photosynthesis.

**Chapter 2** in this thesis provides a general description of the detection of smFRET to study biological and chemical processes at the molecular level. Two standard detection schemes for smFRET, diffusion-based confocal microscopy and imaged-based total internal reflection fluorescence (TIRF) microscopy are discussed in depth, along with recent development in sm-FRET based applications.

In **Chapter 3** we demonstrated both by simulations and experiments using doubly labelled DNA hairpin that significant improvement in time resolution for camera based sm-FRET detection method can be achieved. We presented two methods (1) by combining alternating laser excitation (ALEX) technique with stroboscopic illumination and (2) by adapting dynamic probability distribution analysis (dPDA) for TIRF microscopy to show that it is possible to resolve conformational dynamic states in the milli-seconds time range.

In **Chapter 4** we compared picosecond fluorescence decay kinetics for stacked and unstacked photosystem II membranes to evaluate the efficiency of excitation energy transfer between the neighboring layers. The measured kinetics were analyzed in terms of a recently developed fluctuating antenna model that provides information about the dimensionality of the studied system. Independently of the stacking state, all preparations exhibited virtually the same value of the apparent dimensionality i.e.  $d = 1.6$ . We conclude from our results that membrane stacking does not affect the efficiency of the delivery of excitation energy towards the reaction centers but ensures a more compact organization of the thylakoid membranes within the chloroplast and separation of photosystems I and II.

In **Chapter 5** we have applied ultrafast fluorescence spectroscopy to study the picosecond kinetics of photosystems I (PSI) and II (PSII) in spinach leaves using a streak camera setup. The leaves were measured in 4 different conditions: (1)  $F_o$ , (2)  $F_{max}$ , unquenched state, dark adapted leaves were measured with a very low/high laser intensity of 100nW/1mW to keep PSII RCs in the open/closed state. (3)  $F_{NPQ, Open}$  (4)  $F_{NPQ, Closed}$ , quenched state, leaves were illuminated with an actinic light intensity of  $1300\mu\text{mol.m}^{-2}.\text{sec}^{-1}$  for about 30 min to stabilize NPQ. We found that the rate of NPQ is 2.7 times higher in the case of closed RCs than in the case of open RCs, which from a functional point of view can be considered as an ideal situation because closed RCs are prevented from causing singlet oxygen formation while the open RCs can continue to function. However, at the moment we do not have a good explanation for this remarkable observation at the molecular level and



further research will be needed to validate our results and to come up with an explanation for the experimental results.

## ***Summary***

## Acknowledgements

It has truly been a privilege to be a PhD student at the Laboratory of Biophysics, and having a possibility to work in the border zone between physics and biology. I would like to express my gratitude to all the people who have made my work with this thesis easier, better and more fun.

First of all I would like to thank my supervisor, prof. Herbert van Amerongen for the dedication and guidance through the years and for always lending me an ear when things have gone bad. He is not only helpful but also amazingly patient as a supervisor. I am also grateful to my co-supervisor Dr. Johannes Hohlbein, who has taught me a lot about the fascinating world of single molecules and DNAs. I would like to thank Rob for helping me designing the experiments and all the helpful discussion. I also want to thank Arjen for all great technical support in the laser lab. It has been a pleasure to work closely together with these people who with their skills, enthusiasm and hard work have buildup a very strong lab with a friendly and informal atmosphere.

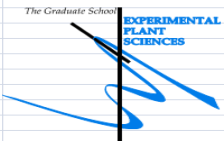
I would especially like to say thanks to Evgenia for always being there for me, and also for providing me with all the chocolates. Carel you are an amazing friend thanks for helping me with PEGslides and for making the cakes for our group dinners.

Caner, Olga, Lijin, Shanti, Alena, Daan, Mattia, Ana, Alena, Fugui, Yasher and Koen it was a great pleasure to work with you guys, thank you very much for all the help you had provided and all the great time we spent together. Netty I would like to say thank you for all the help you had given me.

The rest of my friends are fortunately too many to mention by name and too good to blame me for not doing so. Thank you!

I am especially grateful to my parents and family. With your massive support behind me everything seems possible.

## ***Acknowledgements***

Education Statement of the Graduate School Experimental Plant Sciences			
<b>Issued to:</b>	<b>Shazia Farooq</b>		
<b>Date:</b>	<b>14 March 2017</b>		
<b>Group:</b>	<b>Laboratory of Biophysics</b>		
<b>University:</b>	<b>Wageningen University &amp; Research</b>		
<b>1) Start-up phase</b>		<u>date</u>	
► <b>First presentation of your project</b>			
<i>Title:</i> Time resolve absorption and scattering spectroscopy in turbid media			26 Jun 2012
► <b>Writing or rewriting a project proposal</b>			
► <b>Writing a review or book chapter</b>			
Studying DNA-protein interactions with single-molecule Förster resonance energy transfer, <i>Protoplasma</i> , 2013, SPECIAL ISSUE: NEW/EMERGING TECHNIQUES IN BIOLOGICAL MICROSCOPY, DOI 10.1007/s00709-013-0596-6			09 Dec 2013
► <b>MSc courses</b>			
► <b>Laboratory use of isotopes</b>			
<i>Subtotal Start-up Phase</i>			<i>7.5 credits*</i>
<b>2) Scientific Exposure</b>		<u>date</u>	
► <b>EPS PhD student days</b>			
EPS PhD student day, Leiden, NL			29 Nov 2013
EPS PhD student day, Soest, NL			29-30 Jan 2015
► <b>EPS theme symposia</b>			
EPS Theme 3 Symposium: 'Metabolism and Adaptation' Wageningen University			11 Mar 2014
EPS Theme 4 Symposium: 'Genome Biology', Wageningen University			16 Dec 2016
► <b>Lunteren days and other National Platforms</b>			
Dutch meeting on molecular and cellular biophysics, Veldhoven			01-02 Oct 2012
Dutch meeting 'Chemistry in Relation to Physics and Materials Sciences, Veldhoven			04-05 Mar 2013
Dutch meeting on molecular and cellular biophysics, Veldhoven			30 Sep-01 Oct 2013
Dutch meeting on molecular and cellular biophysics, Veldhoven			29-30 Sep 2014
Dutch Physics @FOM meeting, Veldhoven			20-21 Jan 2015
Dutch meeting on molecular and cellular biophysics, Veldhoven			03-04 Oct 2016
► <b>Seminars (series), workshops and symposia</b>			
Invited lecture by Claudiu Gradinaru			23 Aug 2012
Invited seminar Prof. Jan van Hest			07 Jan 2014
Invited seminar by Dr. Ilja Voets			21 Jan 2014
Invited seminar by Dr. C. Ottmann			28 Jan 2014
Measuring the Photosynthetic phenotype, Wageningen University			07-09 Jul 2014
FOM symposium for women in science			19 Sept 2014
COST PHOTOTECH international workshop, Szeged, Hungary			22-23 Oct 2014
Invited seminar by Alonso Zavaleta Fernandez de Cordova			28 Oct 2014
Invited seminar by Dr. thoben Cordes			03 Dec 2014
The Caner Ünlü Fluctuation and Regulation Symposium			19 May 2015
FOM young scientist day			10 Dec 2015
Invited seminar by Dr. Martin Jinek			02 Jun 2015
FOM valorisation workshop			04-05 Jun 2015
Lecture: "Rewriting our genes?"			30 Sep 2016
► <b>Seminar plus</b>			
► <b>International symposia and congresses</b>			
International conference on the Biophysics of Photosynthesis, Roma Italy (poster)			28-30 Oct 2013
Quantitative Bio-Imaging conference, Delft, NL (poster)			13-15 Jan 2016
Light-Harvesting satellite meeting Egmond aan Zee, NL			04-06 Aug 2016
17th International Congress on Photosynthesis Research, Maastricht, NL			07-12 Aug 2016
► <b>Presentations</b>			
<i>Talk:</i> FOM meeting, Vrije University Amsterdam			29 Oct 2012
<i>Poster:</i> Dutch meeting 'Chemistry in Relation to Physics and Materials Sciences, Veldhoven			04-05 Mar 2013
<i>Talk:</i> FOM meeting, Wageningen University			07 Mar 2013
<i>Talk:</i> FOM meeting, Vrije University Amsterdam			20 Jun 2013
<i>Poster:</i> Dutch meeting on molecular and cellular biophysics, Veldhoven			30 Sep-01 Oct 2013
<i>Poster:</i> Dutch meeting on molecular and cellular biophysics, Veldhoven			29-30 Sep 2014
<i>Talk:</i> COST PHOTOTECH international workshop, Szeged, Hungary			22-23 Oct 2014
<i>Talk:</i> The Caner Ünlü Fluctuation and Regulation Symposium			19 May 2015
<i>Poster:</i> Quantitative Bio-Imaging conference, Delft, NL (won poster prize)			13-15 Jan 2016
<i>Poster:</i> 17th International Congress on Photosynthesis Research, Maastricht, NL			7-12 Aug 2016
► <b>IAB interview</b>			
► <b>Excursions</b>			
AlgePARC Wageningen			31 Aug 2012
ASML, Veldhoven			11 Jun 2015
<i>Subtotal Scientific Exposure</i>			<i>22.9 credits*</i>
<b>3) In-Depth Studies</b>		<u>date</u>	
► <b>EPS courses or other PhD courses</b>			
COST PHOTOTECH training school, Szeged, Hungary			18-21 Oct 2014
Nyenrode Business Orientation Program			22-27 Nov 2015
► <b>Journal club</b>			
► <b>Individual research training</b>			
<i>Subtotal In-Depth Studies</i>			<i>3.0 credits*</i>
<b>4) Personal development</b>		<u>date</u>	
► <b>Skill training courses</b>			
Taking Charge of your PhD project (FOM)			03 & 17 Oct 2012
Dutch language course (FOM)			29 Nov-03 Dec 2012
Art of presenting science (FOM)			24 May, 07Jun & 21 Jun 2013
FOM Scientific Writing (FOM)			19 Sep, 03 & 24 Oct 2013
Career Planning			22.29 May & 12.9,26 Jun 2016
► <b>Organisation of PhD students day, course or conference</b>			
► <b>Membership of Board, Committee or PhD council</b>			
<i>Subtotal Personal Development</i>			<i>5.4 credits*</i>
<b>TOTAL NUMBER OF CREDIT POINTS*</b>			<b>38,8</b>
Herewith the Graduate School declares that the PhD candidate has complied with the educational requirements set by the Educational Committee of EPS which comprises of a minimum total of 30 ECTS			
* A credit represents a normative study load of 28 hours of study.			